Table des matières

Liste des figures

Nomenclature

Symboles	Description	Unités de mesures S.I.
A_{germe}	Surface du germe	m^2
c	Capacité calorifique massique	$J.kg^{-1}.K^{-1}$
CR	Vitesse de refroidissement	$K.s^{-1}$
G	Enthalpie libre	J
H	Enthalpie	J
k	Conductivité thermique	$W.m^{-1}.K^{-1}$
L	Chaleur latente de fusion	$J.kg^{-1}$
l_f	Chaleur molaire de fusion	$J.mol^{-1}$
m	Masse	kg
Nm	Nombre de moles	mol
M, N	Nombre des mailles	-
P	Pression	Pa
Q	Quantité d'énergie	J
r	Rayon	m
S_v	Densité volumique d'une source thermique	$W.m^{-3}$
t	Temps	s
T	Température	K
T_m	Température d'équilibre de fusion	K
T^*	Température moyenne de la cristallisation	K
V_m	Volume molaire	$m^3.mol^{-1}$
ΔT	Degré de surfusion	K
Δt	Intervalle de temps	s
Δx	Longueur de la maille	m
Δy	Largeur de la maille	m

Lettres Grecque	Description	Unités de mesures S.I.
α	Diffusivité thermique	$m^2.s^{-1}$
ε	Epaisseur de la maille	m
$\emptyset$	Flux thermique	W
γ	Tension superficielle	$N.m^{-1}$
μ	Potentiel chimique	$J.mol^{-1}$
Φ	Orientation	rd
ρ	Masse volumique	$Kg.m^{-3}$

Indices	Description
l	Liquide
s	Solide
N	Nucléation

c	Critique
i	initial
D	Droite
G	Gauche
H	Haut
B	Bas

Abréviations

ÉTS	École de Technologie Supérieure
LaTEP	Laboratoire de thermique, énergétique, et procédés
MCP	Matériaux à Changement de Phase
T3e	Groupe de recherche industrielle en technologie de l'énergie et en efficacité énergétique

Introduction

Contexte et objectifs

Le stockage de l'énergie est au cœur des enjeux actuels. En effet, il constitue un besoin technique en forte croissance en raison des sources d'énergies renouvelables intermittentes de plus en plus présentes et de la consommation énergétique parfois en déphasage par rapport à la production. Ainsi, il représente depuis quelques années un levier économique dont la prépondérance augmentera au fil du temps. Le stockage de l'énergie sert principalement à ajuster la production à la consommation de l'énergie.

Parmi les techniques du stockage de l'énergie, le stockage d'énergie thermique est de plus en plus envisagé (Paksoy, H.O., 2007). Plus particulièrement, le stockage de l'énergie thermique par chaleur latente attire l'attention des communautés scientifiques et industrielles, car il ne nécessite ni des grands volumes ni des variations significatives de température, et est un bon compromis entre la densité énergétique et la maturité technologique. Cette technique est utilisée dans des nombreuses applications industrielles et commerciales (Zanganeh, G. et al., 2014 ; Cai, Y., et al., 2014 ; Khalifa, A., et al., 2014), par l'intermédiaire des Matériaux à Changement de Phase solide-liquide, notés généralement MCP.

La connaissance et la compréhension des mécanismes de solidification des MCP s'avèrent indispensables afin d'optimiser le fonctionnement de systèmes dans lesquels les changements d'états liquide-solide ont lieu.

Plusieurs MCP sont largement utilisés dans les applications de stockage d'énergie du fait de leurs avantages thermiques, économiques, et environnementaux, comme par exemple l'eau. En effet, l'eau se trouve presque partout sur la terre, elle n'est pas chère, ne pose aucun problème de pollution, et sa chaleur latente lors de la cristallisation ou la fusion est élevée. Malgré ces avantages, l'utilisation de l'eau et de certains autres MCP présente quelques inconvénients. Un des problèmes sérieux concerne le phénomène de surfusion, i.e. un retard du changement de phase liquide-solide. Ces matériaux, en effet, ne se solidifient pas toujours à leur température d'équilibre liquide-solide T_m mais à une température inférieure T_N. L'écart de température $\Delta T = T_m - T_N$ qui caractérise ce phénomène est appelé degré de surfusion. Dans ce cas, le liquide est en état métastable, et est appelé liquide surfondu.

Lors de la rupture de surfusion, suite à la nucléation provoquant le début de la solidification, des cristaux commencent à croître au sein des régions surfondues du liquide. Le type ainsi que le comportement de la croissance de ces cristaux dépendent particulièrement du degré de surfusion correspondant. Pour un degré de surfusion suffisamment important, une croissance de forme dendritique est dominante. Ce type de croissance est dû à l'interaction complexe de nombreux mécanismes physiques associés à l'interface. Durant cette phase, la chaleur latente évacuée à l'interface liquide-solide se

propageant dans le liquide surfondu lui permet de revenir à sa température d'équilibre liquide-solide T_m (température de fusion), avant de poursuivre la solidification complète de l'échantillon (voir figure 0-1).

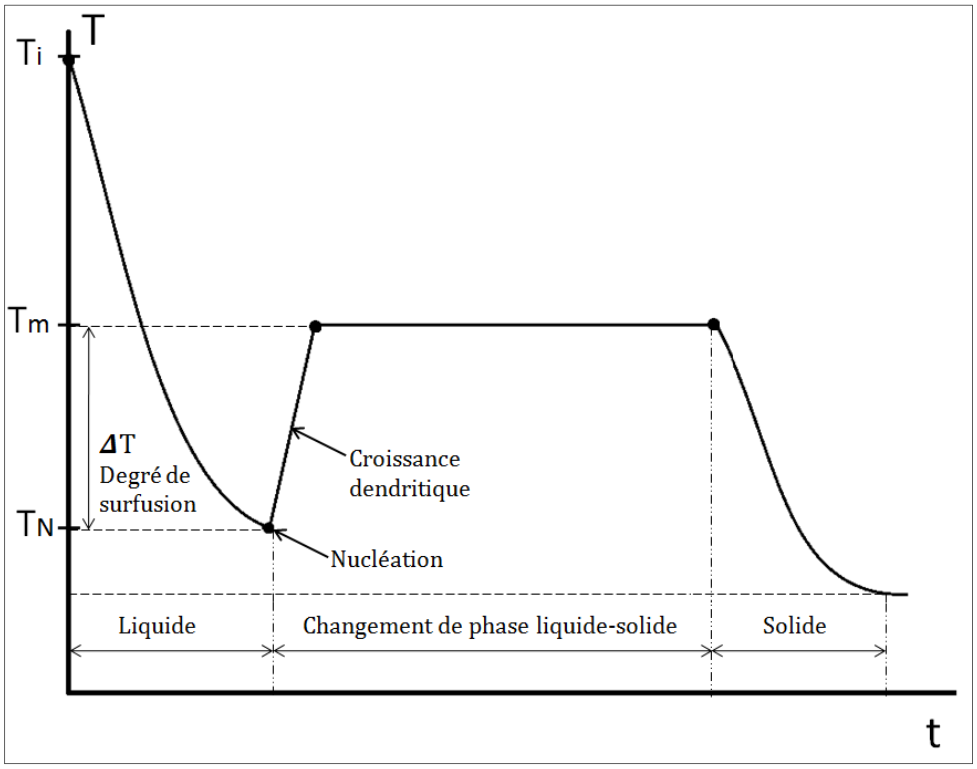

Figure 0-1 : Variation de la température (au centre d'un échantillon) en fonction du temps, durant le processus de solidification d'un liquide surfondu.

La phase de la croissance dendritique est un sujet très étudié dans différents secteurs, grâce à ses intérêts scientifiques et industriels dans les domaines de la métallurgie (Glicksman, M.E., 2011) et le stockage thermique par chaleur latente (Braga S.L., Milon, J.J., 2012). Malgré la bibliographie conséquente, ce phénomène n'est pas encore parfaitement compris. En effet, les théories mathématiques et les investigations numériques ne sont qu'en accord limité avec les études expérimentales. Cela est dû à la complexité de l'interaction des mécanismes physiques associés à l'évolution de l'interface liquide-solide et à la difficulté de mener des campagnes expérimentales adaptées. Par conséquent, même si les lois physiques élémentaires sont assez bien connues et si de nombreux travaux numériques et/ou expérimentaux ont été menés, plusieurs questions restent sans réponse claire lorsqu'on aborde le problème dans sa globalité. Par exemple, quels sont les paramètres qui guident la propagation dendritique ? Le hasard a probablement une part de responsabilité (au moins dans les tous premiers instants), mais quelle est l'influence réelle de la thermique ?

Dans ce contexte, un projet de recherche a débuté dont les enjeux principaux sont d'étudier les mécanismes physiques influençant l'évolution de l'interface liquide-solide lors de la croissance dendritique et de contribuer à la progression de la compréhension

d'un tel problème complexe et instable pour différents matériaux à changements de phase. Pour atteindre ces objectifs, ce projet comprend globalement deux parties complémentaires : l'une numérique de modélisation et l'autre expérimentale de visualisation.

L'étude numérique consiste à résoudre le problème de la croissance dendritique d'un germe solide au cours du processus de solidification des MCP surfondus, en modélisant l'évolution de l'interface liquide-solide durant cette phase complexe. Le modèle proposé doit tenir compte de tous les mécanismes physiques associés à la propagation de l'interface liquide-solide. Pour cela une compréhension suffisante, une bonne formulation mathématique ainsi que des techniques numériques appropriées sont requises. Les buts de ce volet numérique sont (1) de réaliser un modèle capable de produire des microstructures dendritiques réelles, et (2) d'étudier l'influence des différents paramètres sur le comportement ainsi que le développement des dendrites.

D'autre part, l'étude expérimentale consiste à visualiser *in-situ* le processus de la transformation liquide-solide du MCP, en se focalisant particulièrement sur la phase de la croissance dendritique. Le banc d'essai expérimental, avec la visualisation en temps réel de la croissance dendritique, a plusieurs objectifs. Premièrement, une meilleure compréhension des phénomènes physiques qui contrôlent la formation et le développement des dendrites est attendue. Deuxièmement, les résultats expérimentaux serviront à valider le modèle numérique proposé ainsi que les résultats obtenus via ce modèle. Enfin, le banc d'essai permettra l'identification des hypothèses géométriques et thermiques sur lesquelles le modèle numérique doit se baser.

Depuis longtemps, le laboratoire de thermique, énergétique, et procédés (LaTEP) de l'Université de Pau et des Pays de l'Adour (France), étudie les phénomènes de surfusion (Lafargue, 1952 ; Babin, 1966 ; Monge, 1968 ; Xans, 1970 ; Lere-Porte, 1970 ; Lemercier, 1975 ; Dumas, 1976 ; Broto, 1979 ; Combes, 1982 ; Clausse, 1983 ; Sifrini, 1983 ; Aguerd, 1984 ; Bédécarrats, 1993 ; Gibout, 2001 ; Ribeiro, 2007). Ces nombreux travaux lui ont permis d'acquérir une forte connaissance de ces phénomènes.

Le groupe de recherche industrielle en technologie de l'énergie et en efficacité énergétique (t3e), de l'École de Technologie Supérieure de Montréal (Canada) porte ses activités sur le solaire, le stockage d'énergie, et la bio-énergie. Il s'intéresse en particulier au stockage de l'énergie en utilisant les MCP depuis 2011 (Dutil et al. 2011).

C'est pourquoi, il a été décidé d'effectuer cette thèse de doctorat dans le cadre d'une collaboration internationale entre le laboratoire français LaTEP et le groupe canadien t3e. Ce travail de doctorat, présenté dans ce mémoire, constitue la première étape du projet de recherche engagé entre les deux équipes. Bien qu'il comprenne deux aspects, le premier numérique et l'autre expérimental, la majorité du travail s'est focalisée sur l'étude numérique et le volet expérimental s'est limité à la conception et au montage d'un banc d'essai par manque de temps.

Méthodologies

La thèse de doctorat a démarré en octobre 2013 à Pau (France). Dans cette première phase, la conception et le montage du banc d'essai ont été réalisés au LaTEP. Ensuite, un séjour d'un an et trois mois (de juin 2014 à août 2015) a été fait à Montréal (ÉTS). Durant cette période, l'introduction de la partie numérique ainsi que les premières étapes du développement du code ont été menées. Un examen doctoral à l'ÉTS comportant trois étapes (pendant un an) a été également validé. Au retour à Pau (septembre 2015), le doctorat s'est focalisé seulement le volet numérique du projet.

L'aspect expérimental est donc consacré à la conception et au montage d'un banc d'essai expérimental, au LaTEP en France, capable de visualiser la phase dendritique dans différentes conditions géométriques et thermiques tout en mesurant les champs de température dans les deux phases liquide et solide. Pour atteindre cet objectif, le dispositif est conçu de sorte que, d'une part, l'épaisseur de matériau à étudier (MCP) soit modifiable, et d'autre part, le gradient thermique initial crée au sein du liquide surfondu par le système de refroidissement soit contrôlé. Des faibles épaisseurs de MCP, par exemple, empêchent la convection naturelle au sein du liquide.

Aucun résultat expérimental significatif n'a été obtenu par manque du temps. Bien que la conception et le montage du banc d'essai aient permis l'identification des hypothèses sur lesquelles se base le modèle numérique, la validation expérimentale des résultats numériques reste une perspective principale dans les prochaines étapes du projet.

Le volet numérique est consacré au développement d'un code général traitant les processus de solidification instables du liquide surfondu des corps purs sous différentes conditions thermiques et géométriques. Plus spécifiquement, il modélise l'évolution bidimensionnelle dynamique de l'interface liquide-solide durant la croissance dendritique tenant compte de tous les effets associés à l'interface dans des conditions suffisamment instables. Le modèle néglige la variation de la masse volumique avec la température et au cours de changement de phase, la convection naturelle dans le fluide n'est donc pas prise en compte. Par conséquent, le problème consiste alors à résoudre l'équation de conduction dans les deux phases liquide et solide afin d'obtenir les champs de température. Outre les conditions aux limites imposées aux frontières, les équations sont couplées avec deux conditions à l'interface mobile : la condition de Gibbs-Thomson, et l'équation de bilan de l'énergie. La difficulté principale dans ce type de problèmes réside dans le fait que l'interface de solidification constitue à la fois une des inconnus de problème et une des limites où des conditions doivent être satisfaites. La méthode à double maillage proposée dans cette étude se base sur une approche de suivi d'interface (*Front-Tracking method*). Cette méthode est couplée, d'une part, avec une méthode de volumes finis d'ordre zéro, pour la discrétisation spatiale du système, et d'autre part, avec une méthode d'Euler explicite pour la résolution temporelle.

Plan

Ce mémoire se compose de cinq chapitres et deux annexes.

Le premier chapitre rappelle les principes et les avantages du stockage de l'énergie par chaleur latente par l'intermédiaire des matériaux à changement de phase. Cette partie correspond au contexte initial de la thèse.

Le second chapitre aborde le phénomène de surfusion, les paramètres influençant ce phénomène, ainsi que les théories associées à sa rupture. Ces informations permettent d'avoir tous les éléments sur la surfusion afin de concevoir au mieux le banc d'essai mais aussi pour une éventuelle modélisation de ce phénomène.

Le troisième chapitre introduit la phase de la croissance dendritique, et ses potentiels scientifiques et industriels. Il décrit les théories, la formulation mathématique, et les revues de la littérature expérimentale de visualisation et numérique de modélisation de cette phase. Les travaux numériques sont présentés sous forme d'un article de revue rédigé en anglais qui a été soumis à la revue « *Renewable and Sustainable Energy Reviews* ».

Ensuite, le quatrième chapitre est consacré à la description du modèle numérique réalisé et à la présentation de différents résultats de simulation permettant de le valider. Il comporte deux sections présentées sous forme de deux articles rédigés en anglais soumis à des journaux scientifiques avec comité de lecture. Dans le premier article, la méthode numérique ainsi que son implémentation sont détaillées. Des résultats numériques ainsi que des études paramétriques concernant la croissance dendritique sont également présentés montrant la capacité du code numérique proposé à traiter la phase dendritique réelle. Dans le deuxième article, l'effet des conditions thermiques, résultant un champ de température non-homogène au sein du liquide surfondu, sur l'évolution et le comportement de l'interface liquide-solide durant la phase dendritique est étudié.

Enfin, le dernier chapitre apporte une conclusion générale ainsi que quelques perspectives.

En plus, deux annexes sont ajoutées à la fin de ce mémoire. L'annexe A fournit la description du banc d'essai expérimental, monté au LaTEP, ainsi que la procédure expérimentale prévue. Enfin, l'annexe B discute des résultats numériques préliminaires testant le code à traiter le transfert thermique par conduction avec et sans une source de chaleur.

Avertissements :

Certains chapitres présentent des articles soumis à des journaux scientifiques avec comité de lecture. Ils contiennent leur bibliographie et leur nomenclature spécifiques.

Pour le reste du texte, les références bibliographiques citées sont regroupées à la fin de ce document après les annexes. Les articles sont indiqués par les noms d'auteurs suivis de l'année de parution. Si le nombre d'auteurs est supérieur ou égal à trois, la mention « et al. » est employée.

I. Stockage thermique par chaleur latente

I.1. Introduction

La demande énergétique humaine est en hausse continue, et la plupart des ressources énergétiques renouvelables sont intermittentes (énergie éolienne ou énergie solaire par exemple). La croissance de ces sources à intensité variable dans les réseaux de distribution d'énergie menace l'équilibre offre/demande. Pour cette raison, les communautés scientifique et industrielle font des efforts conséquents pour trouver des stratégies qui peuvent améliorer l'efficacité énergétique mondiale.

Le stockage de l'énergie est l'une des solutions pour cette situation. Il s'agit d'optimiser les ressources énergétiques ou d'en favoriser l'accès, en permettant principalement d'ajuster la « production » à la « consommation » d'énergie en limitant les pertes.

Le principe du stockage de l'énergie consiste à préserver une quantité d'énergie produite à un moment donné pour une utilisation ultérieure et qui autrement serait parfois irrémédiablement perdue. Les formes principales de stockage de l'énergie sont les suivantes :

- Mécanique (Stys, Z.S. ,1980 ; Yot, P.G. et al., 2016) : cette catégorie inclut les volants d'inertie, les accumulateurs hydrauliques, et généralement tout type de stockage d'énergie potentielle ou cinétique.
- Electrochimique (Kordesch, K. , 1980 ; Li, X., et al. 2016) : ce type de stockage consiste à stocker l'énergie sous forme électrochimique dans les batteries. Les batteries sont destinées à des applications portables et quotidiennes.
- Electromagnétique (Haririe, A. et al., 1973 ; Zhao, J.M. et al., 2015) : cette catégorie consiste à créer, grâce à l'électricité, un champ magnétique dans une bobine. L'électricité peut ensuite être récupérée dans un laps de temps très court.
- Thermique (Paksoy, H.O., 2007) : de nombreuses solutions de stockage de froid (glace, liquides cryogéniques) et de chaud (sels fondus, accumulateurs de vapeur, graviers ou capsules à changement de phase…) existent et permettent de stocker l'énergie sous forme thermique (chaleur latente, chaleur sensible, thermochimique) avant de la restituer, le plus souvent directement sous forme de chaleur ou de froid.

Le mémoire se concentre sur la dernière forme de stockage ci-haut mentionnée : le stockage de l'énergie sous forme thermique, en se limitant au cas latent.

I.2. Stockage de l'énergie sous forme thermique

En général, le stockage d'énergie thermique consiste à emmagasiner l'énergie thermique pendant une période où elle est abondante ou moins coûteuse pour l'utiliser pendant une période durant laquelle elle est indisponible ou plus chère.

Le stockage de l'énergie sous forme thermique est de trois types :

- Stockage thermique par chaleur sensible (Fernandez, Al. et al., 2010) : il consiste par exemple à réchauffer un corps à haute température et à le mettre ultérieurement en contact avec le système d'utilisation à température plus basse. En effet, si on fournit l'énergie Q à un corps de masse m qui fait élever sa température de T_1 à T_2, lorsque le corps revient à T_1, il restitue cette même énergie, donnée par l'équation suivante :

$$Q = \int_{T_1}^{T_2} m\, c(T)\, dT \qquad \text{(I-1)}$$

  Où $c(T)$ est la capacité calorifique massique du corps, qui peut dépendre de la température (voire de la pression).
- Stockage thermique par chaleur latente (Dumas J.P., 2002) : Pour ce type de stockage, l'énergie est échangée à température constante lors du changement de phase d'un corps pur. L'énergie Q mise en jeu dans ce cas est exprimée par le produit de la masse m du corps et sa chaleur latente massique L,

$$Q = mL \qquad \text{(I-2)}$$

  Ce type de stockage thermique est décrit en détail dans la section ci-après.
- Stockage thermochimique (Mugnier, D., et Goetz, V., 2001 ; Istria, S. et al., 1996 ; Bales, C. et al., 2008) : Ce dernier type de stockage thermique utilise une réaction chimique réversible d'un matériau : apport de la chaleur dans un sens (endothermique) et dégagement de la chaleur dans le sens opposé (exothermique).

Ces types de stockage se différencient de part leur densité énergétique mais aussi de part leur maturité technologique. Le stockage sensible est la technologie la plus développée mais est celle ayant la densité énergétique la moins élevée. Le stockage thermochimique a la meilleure densité énergétique mais reste encore au stade de la recherche et développement. Le stockage latent se situe entre les deux avec une densité énergétique intéressante et une maturité technologique déjà avérée dans certains domaines comme celui du froid et du conditionnement d'air.

Après ce bref rappel des types de stockage thermique, la section suivante est consacrée au stockage thermique par chaleur latente. Elle rappelle le principe de stockage par chaleur latente et ses avantages, ainsi que les critères de choix d'un MCP.

I.3. Stockage par chaleur latente

Le stockage thermique par chaleur latente, tel que spécifié antérieurement, est basé sur l'énergie (chaleur) mise en jeu lorsqu'un matériau change de phase. Les transformations liquide-solide sont les plus communément utilisées en ingénierie

(Viskanta, R. et al., 1983 ; Benmansour, A. et Hamdan, M.A. , 2001). Mais d'autres transformations donnent des résultats intéressants, comme par exemple les transformations solide-solide (Font, J. et al., 1986) et liquide-gaz. Les transformations où intervient le phénomène de croissance dendritique (objet de l'étude) sont les transformations gaz-solide et liquide-solide. Ce projet spécifique de doctorat est limité aux transformations liquide-solide que l'on retrouve avec les MCP.

I.3.1. Principe et avantages

Supposons que le constituant, de masse m, servant au stockage par chaleur latente soit, à une température initiale T_1, un solide pur ayant une température de fusion T_m, telle que $T_1<T_m<T_2$. L'énergie emmagasinée lors du chauffage à pression constante jusqu'à une température T_2 est alors donnée par la relation de la variation d'enthalpie suivante :

$$Q = H_2 - H_1 = \int_{T_1}^{T_m} m\, c_s(T)\, dT + mL + \int_{T_m}^{T_2} m\, c_l(T)\, dT \qquad \text{(I-3)}$$

$c_s(T)$ et $c_l(T)$ sont respectivement les capacités calorifiques massiques du solide et du liquide, et L représente la chaleur latente massique de fusion. Pour la plupart des substances le terme (mL) est, en général, plus important que les autres termes. En effet, à masse égale, l'énergie stockée par chaleur latente est plus grande que celle stockée par chaleur sensible. D'où l'avantage principal de ce type de stockage : on peut stocker de plus grandes quantités d'énergie pour une masse donnée. Cet avantage se traduit concrètement par une diminution du coût des infrastructures requises pour le stockage (dans le bâtiment (Soares N., et al. 2013), par exemple). Il permet en outre de stocker ou restituer de grandes quantités d'énergie dans des endroits restreints (micro-électronique).

De plus, la variation de la température est très faible lors du stockage latent, au contraire du stockage sensible, qui nécessite, par principe, une variation significative de température.

La performance du procédé de stockage thermique dépend fortement des propriétés du MCP utilisé. La section suivante présente les critères de choix d'un MCP.

I.3.2. Critères de choix d'un MCP

Le premier critère de choix d'un MCP est bien sa température d'équilibre de changement de phase puisqu'elle doit être adaptée au procédé. Parmi tous les produits ayant une température d'équilibre de fusion acceptable, pour que le stockage soit le plus efficace possible, il est plus judicieux énergétiquement de choisir celui qui a la plus grande chaleur latente. La chaleur latente est alors le deuxième critère de choix d'un MCP. D'autres propriétés très importantes dans le choix des MCP sont encore à considérer :

- Bonne conduction thermique : pour être en mesure d'obtenir des cinétiques de stockage adaptées;
- Abondance et faible coût (pour des raisons économiques) ;
- Une grande masse volumique : un corps plus dense demande un volume de stockage plus restreint ;
- Faible variation de masse volumique au changement de phase : pour limiter les contraintes physiques sur les réservoirs de stockage ;
- Peu ou pas de surfusion : ce retard du changement de phase liquide-solide compromet la viabilité des installations, sujet traité au chapitre (II) ci-après ;
- Non dangereux et non polluant ;
- Stabilité dans le temps ou au cours de cycles fusion-cristallisation : pour une durée de vie du MCP la plus longue possible ;
- Compatible avec les matériaux en contact (par exemple : non corrosif).

I.3.3. Utilisation de l'eau comme MCP

L'eau est largement utilisée dans les applications industrielles énergétiques, en particulier celles du stockage du froid. Cela est dû principalement à sa chaleur latente de fusion relativement élevée, 334 kJ/kg (Akyurt M. et al. 2001). En outre, l'eau est un corps pur et possède des avantages économiques, chimiques et environnementaux :

- l'eau est un matériau qui se trouve presque partout sur terre, à l'état naturel, ce qui en fait l'un des matériaux les plus disponibles et les moins chers ;
- elle est caractérisée par ses propriétés chimiques stables ;
- elle n'a aucun effet sur l'environnement, et elle n'est pas polluante ;
- l'eau est un solvant efficace, ce qui permet de l'utiliser en tant que solution en ajoutant plusieurs solutés.

Néanmoins, l'eau et d'autres matériaux présentent un inconvénient sérieux qui est le phénomène de surfusion. En effet, ces matériaux ne solidifient pas toujours à la température d'équilibre liquide-solide, mais à une température plus basse.

Grâce à ses avantages et son potentiel industriel, l'eau est un MCP particulièrement étudié. Elle constitue donc le corps de référence parmi les substances pures prises en compte dans cette thèse. En particulier, l'eau sera le MCP utilisé lors de l'étape de validation du code numérique qui comparera les résultats expérimentaux à ceux du modèle.

La revue de la littérature sur les études expérimentales se focalisera essentiellement sur les travaux traitant l'eau. La revue de la littérature des travaux numériques sera traitée d'une façon plus générale en abordant les travaux sans se limiter au cas de l'eau.

Le chapitre suivant aborde en détails le phénomène de surfusion, les facteurs influençant ce phénomène, et les théories de la rupture de ce phénomène.

II. Surfusion et théories de la nucléation

II.1. Introduction

Dans un procédé de stockage thermique par chaleur latente, lors du refroidissement d'un liquide, celui-ci ne cristallise pas toujours à sa température d'équilibre liquide-solide T_m, mais à une température plus basse. Donc, il est possible d'observer encore l'état liquide à des températures inférieures à T_m. Ce phénomène de retard à la transformation liquide-solide est appelé la surfusion, et le liquide dit dans un état métastable ou encore surfondu.

Ce phénomène a été découvert en 1724 par Daniel Gabriel Fahrenheit (Fahrenheit, D.G., 1724). Il a fait l'objet d'anciennes études (Volmer, H. et Weber, A., 1925 ; Becker, R. et Doring, W., 1935 ; Bigg, E.K., 1953 ; Carte, A.E., 1956), et continue à faire l'objet de multiples recherches récentes (Jia, L., et al., 2014 ; Tang, X., et al., 2014).

La transition de l'état métastable de surfusion vers l'état stable solide ne se produit que si le système atteint une énergie suffisante qui s'appelle généralement énergie d'activation. Elle peut se produire spontanément suite à un refroidissement continu suffisant. Il s'agit alors d'une rupture de surfusion ou rupture de métastabilité, qui provoque la cristallisation de tout l'échantillon.

L'état de surfusion peut durer très longtemps : des heures, voire des jours (Broto, 1979). Au contraire, il est possible de déclencher la cristallisation sur demande par des chocs mécaniques, ou par l'introduction d'un germe solide dans le liquide surfondu. Il est également possible d'obtenir des cristallisations au cours du temps en restant à une température fixe T telle que $T < T_m$, la cristallisation dans ce cas est une cristallisation monotherme (Broto, 1979).

Le verglas, par exemple, peut être une manifestation commune de ce phénomène : de l'eau liquide à pression atmosphérique et à une température inférieure à 0°C (eau surfondue) percute un objet et cristallise immédiatement sous l'effet de cette perturbation.

Des études statistiques ont pu mettre en évidence le caractère stochastique ou erratique des ruptures de surfusion (Fletcher, N. H., 1987). En effet, le même refroidissement continu d'un grand nombre d'échantillons apparemment identiques, ne provoque pas la cristallisation à la même température. Il est alors nécessaire de soumettre les phénomènes à une analyse statistique. Ainsi, au cours d'un refroidissement, il est possible de définir la température moyenne de cristallisation T^*, qui correspond à la température pour laquelle le nombre des échantillons qui cristallisent est maximum.

Compte tenu de ce caractère stochastique, afin de caractériser la surfusion, on définit le degré de surfusion le plus probable $\Delta T = T_m - T^*$ qui est égal à la différence entre la température de fusion et la température moyenne de cristallisation.

Plusieurs études ont été effectuées pour déterminer les paramètres qui influent le phénomène de surfusion. Les facteurs principaux sont cités dans la section qui suit.

II.2. Facteurs influençant la surfusion

II.2.1. Influence du volume

Le volume de l'échantillon est le paramètre le plus influent sur le degré de surfusion. Un liquide surfondu dans un échantillon de volume plus faible peut atteindre des températures plus basses (degré de surfusion plus grand). Par exemple, Stan, C.A. et al. (2009) ont observé de l'eau surfondue à une température de -30 °C dans des gouttelettes de 80 µm.

D'autres travaux se sont intéressés à étudier aussi cet effet pour l'eau (Chen, S.L., et Lee, T.S., 1997 ; Lafargue, C., 1952). Ils ont montré que la diminution du volume de l'échantillon permet l'augmentation du degré de surfusion sous les mêmes conditions. Lafargue, par exemple, a constaté des cristallisations à une température de -40,5 °C pour des gouttes d'eau de quelques µm de diamètre, mais à -14°C pour des gouttes d'eau de 10 mm de diamètre.

Chen S.L. et al. (1998) ont montré également, en utilisant des capsules contenant de l'eau, que le degré de surfusion diminue avec l'augmentation de la taille de la capsule. D'autre part, Chen S.L. et Chen C.L. (1999) ont étudié la probabilité de cristallisation par échantillon, ils ont trouvé qu'avec une taille plus grande la probabilité de la cristallisation augmente.

La même influence a été déduite pour les corps organiques (Dumas, J.P., 1976) et les métaux (Perepezko, J.H. et Rasmussen, D.H., 1979 ; Lemercier, M., 1975 ; P., Monge, 1968).

II.2.2. Influence de l'histoire thermique

Il a été trouvé que la surfusion est influencée par l'histoire thermique de l'échantillon, c'est-à-dire par le nombre et les caractéristiques des cycles refroidissement-réchauffement.

Pour les corps organiques, Dumas, J.P. (1976) a montré que l'histoire thermique modifie principalement l'intervalle de température de cristallisation, mais la température la plus probable est peu modifiée.

Dans le cas d'émulsions, il a été montré que l'histoire thermique modifie les probabilités de cristallisation, autour de plusieurs températures plus probables bien identifiées selon les caractéristiques et le nombre de cycles réchauffement-refroidissement (Clausse, D., et al. 1985 ; Clausse, D., et al. 1987).

II.2.3. Influence de la vitesse de refroidissement

Selon plusieurs auteurs (Chen, S.L., et Lee, T.S., 1997 ; Okawa, S. et al., 2000 ; Debenedetti, P., 1996 ; Braga, S.L. et al., 2008), la vitesse de refroidissement (CR) peut être définie lors d'un refroidissement continu de l'échantillon par le rapport entre le degré de surfusion en K, et la période totale de la surfusion en min :

$$CR = \frac{\Delta T}{\Delta t} \qquad \text{(II-1)}$$

Braga S.L. et al. (2008) ont mené une étude de la vitesse de refroidissement dans des capsules cylindriques remplies d'eau. Ils ont trouvé que cette vitesse de refroidissement est une fonction de plusieurs paramètres : la matière de la capsule, la température du liquide de refroidissement, et le diamètre de l'échantillon. Ils ont obtenu, par exemple, des vitesses de refroidissement plus rapides avec des températures du liquide de refroidissement plus basses. Ces relations s'expliquent facilement par l'équation traduisant les transferts thermiques à travers la surface de l'échantillon. Par conséquent, toute étude d'influence de ces paramètres peut être considérée comme étude de l'influence de la vitesse de refroidissement. De nombreuses études existent dans la littérature s'intéressant à l'influence de la vitesse de refroidissement et de la température du liquide de refroidissement sur le phénomène de surfusion.

Saito, A. et al. (1989) ont conclu que le degré de surfusion augmente avec l'augmentation de la vitesse de refroidissement.

Chen et al. ont constaté que la probabilité de la cristallisation, dans des cylindres (1997) et des capsules (1998) d'eau, augmente avec la diminution de la température de refroidissement.

En 2005, Milon et Braga (Milon Guzman, J.J., et Braga, S.L.) ont montré que le degré de surfusion augmente avec la diminution de la température du liquide de refroidissement dans des capsules cylindriques d'eau.

Une étude plus poussée sur la congélation d'eau dans des cylindres horizontaux visualisée par une méthode optique (l'interférométrie) a été effectuée par Yoon et al. (Yoon, J., et al., 2000). Ils ont distingué trois types de congélation selon la vitesse de refroidissement : le premier est une couche annulaire de glace qui commence à croître de la surface interne du cylindre vers le centre pour des vitesses rapides, le deuxième est une couche asymétrique de la glace provoquée par des vitesses intermédiaires, et le dernier est une couche qui croit instantanément dans la région entière pour des vitesses lentes.

Par contre, Dumas J.P. (1976) a montré dans son étude sur la cristallisation que la vitesse de refroidissement a une influence négligeable sur la cinétique des cristallisations. De plus, Okawa, S. et al. (2000) ont montré en étudiant la congélation de

l'eau dont le refroidissement est assuré par l'intermédiaire de surfaces métalliques, que la probabilité de la cristallisation est indépendante de la vitesse de refroidissement.

Pour ce qui concerne l'effet du matériau confinant l'échantillon sur la surfusion, Saito et son équipe (1989 ; 1994) présentent, par exemple, sur la figure (II-1) ci-dessous, les résultats de l'effet du matériau au contact de l'eau sur la moyenne du degré de surfusion. Cette relation peut s'expliquer par la variation de la vitesse de refroidissement en fonction de la conductivité thermique du matériau utilisé.

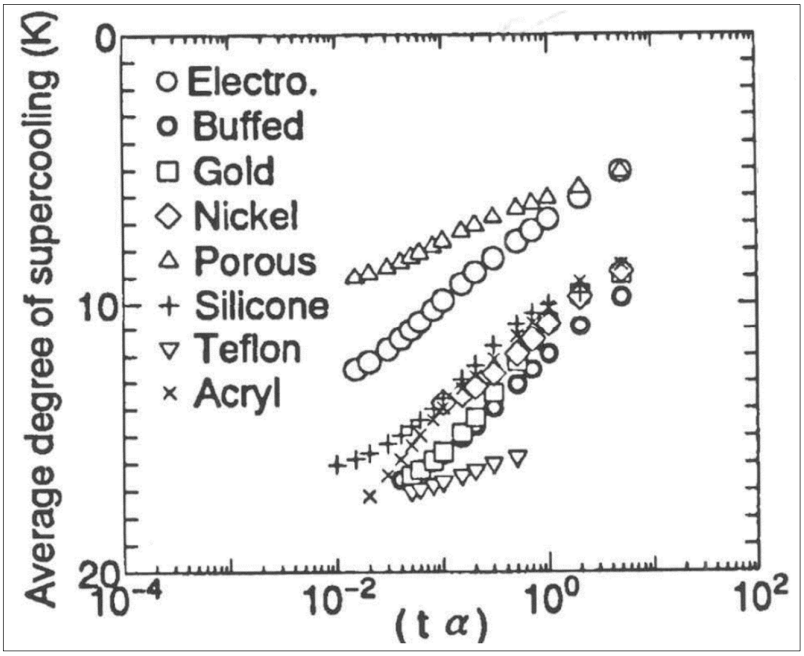

Figure II-1 : La moyenne du degré de surfusion pour différents matériaux d'échantillon (Saito, A. et Okawa, S., 1994).

II.2.4. Influence des agents nucléants

Des impuretés insolubles jouant le rôle de catalyseurs qui servent à favoriser la cristallisation et à réduire le degré de surfusion ΔT, sont appelées agents nucléants (Wall, E., 1942).

Bédécarrats J.P. (1993) a montré que le degré de surfusion des matériaux à changement de phase aqueux confinés dans des capsules sphériques peut être abaissé de 9 K à 2,5 K par l'utilisation d'un agent nucléant.

Chen S.L. et Chen C.L. (1999) ont étudié l'effet des différents agents nucléants sur la probabilité de la cristallisation de l'eau surfondue. Ils ont montré que l'utilisation des agents nucléants est la méthode la plus pratique pour réduire le degré de surfusion. De plus, ils ont trouvé que parmi les agents nucléants, l'iodure d'argent AgI est le plus efficace avec de l'eau.

Le paragraphe (II.3.2) discute plus en détails le principe d'action des agents nucléants lors des rappels de la théorie de la nucléation hétérogène.

II.2.5. Influence de la rugosité de surface interne du récipient

Plusieurs recherches ont été menées pour étudier l'effet de la rugosité de la surface interne du récipient sur le phénomène de surfusion.

Saito, A. et al. (1989) ont montré que des degrés de surfusion d'eau plus petits peuvent être obtenus avec des surfaces internes plus rugueuses.

Un résumé de ces résultats pour chaque type de surface est présenté dans la figure (II-2) ci-dessous. La glace apparait à une température négative plus élevée avec des surfaces relativement plus rugueuses.

Faucheux, M. et al. (2006) ont validé les résultats de Saito, en utilisant des tubes en aluminium de rugosité allant de 0,63 jusqu'à 13,3 μm. Ils ont montré que l'utilisation des surfaces plus rugueuses provoque la diminution du degré de surfusion d'une façon significative.

Type of surface	No. of measurements	Mean degree of supercooling (K)
(A) Electrolytically polished	285	9.5
(B) Buffed	127	13.8
(C) Gold-plated	149	13.4
(D) Nickel-plated	55	11.7
(E1) Porous	129	7.8
(E2) Porous	99	7.4

Figure II-2 : Les résultats expérimentaux de la moyenne du degré de surfusion de plusieurs types de surface interne (Saito, A. et al., 1989).

II.2.6. Influence de la pression

Certaines expériences à haute pression (≤ 2000 bars) ont démontré que plus la pression est élevée plus le degré de surfusion est important (Xans, P., et Barnaud, G., 1975 ; Xans, P., et al., 1979).

Après cette introduction aux paramètres qui influencent le phénomène de surfusion, la théorie relative à la rupture de ce phénomène est introduite à la section suivante.

II.3. Théories de la rupture de surfusion

La transformation liquide-solide peut être décomposée en deux étapes principales (Akyurt M. et al. 2001 ; Gibout, S., 2001):

1- La transition d'un état métastable (liquide surfondu) à un état stable (solide) commence par la formation d'un agrégat ou d'un germe microscopique ayant une structure cristalline très proche de la structure de l'état stable (solide) (Schulz, G., 1948). Cette première étape est appelée nucléation (Fletcher, N. H., 1987).

   Les perturbations externes et la présence des particules étrangères dans le liquide peuvent provoquer la nucléation. Dans ce cas, l'agrégat se forme sur l'interface (surface assez rugueuse, impureté, agent nucléant…), et la cristallisation est induite par des particules étrangères. La nucléation est ainsi dite hétérogène.

   En absence des perturbations externes, le refroidissement continu, ou simplement le maintien à une température inférieure à T_m, peut également provoquer la formation du germe au sein du liquide.

   Si le germe n'atteint pas une taille suffisante, il disparaît et le liquide reste dans son état métastable. Dans le cas contraire, l'agrégat est dit supercritique, et il déclenche la cristallisation de tout l'échantillon au cours de la phase de croissance cristalline (la deuxième étape de la transformation).

2- La croissance cristalline est souvent instable, et peut prendre plusieurs formes, dendritique ou cellulaire (Chikama H. et al. 1996 ; Rocha OL, et al. 2003), dépendant particulièrement du degré de surfusion. D'une façon générale, un degré de surfusion suffisamment important provoque une croissance cristalline dendritique. Cette croissance dendritique constitue le sujet de ce travail, elle sera discutée en détails au chapitre (III) ci-après.

Dans ce qui suit, les deux concepts de la nucléation, déclenchant la transition à l'état solide, sont détaillés. Ces informations sont utiles pour l'étape de la conception du banc d'essai expérimental, afin de mieux choisir entre les deux types de la nucléation selon les conditions imposées. En plus, lors des premières étapes de validation du code numérique, le concept de la nucléation homogène du rayon critique est testé (section IV.2.4.1).

II.3.1. Nucléation homogène

La nucléation homogène correspond donc à l'apparition spontanée d'un germe solide au sein même du liquide surfondu.

La théorie classique de la nucléation, extrait des travaux de Becker, R. et Doring, W. (1935), Gibbs, J.W. (1948), Volmer, M. (1939) et d'autres, est basée sur la transformation vapeur-liquide, et cette étude peut être étendue pour la transformation liquide-solide.

Considérant un système refroidi constitué d'une phase liquide surfondu, de potentiel chimique μ_l, de pression P_0, et de température T_0, avant et après la formation d'un germe sphérique de phase solide de rayon r (voir figure II-3 ci-dessous).

Le germe est supposé assez petit de sorte que le potentiel chimique, la pression et la température du système liquide restent constants.

La formation d'un germe est associée à une variation d'enthalpie libre ΔG.

À l'état initial, il n'y a que du liquide de potentiel μ_l, et de quantité supposée de Nm_0 moles des substances liquides. L'enthalpie libre dans ce cas vaut :

$$G_0 = Nm_0 . \mu_l \qquad \text{(II-2)}$$

On obtient l'expression de Nm_0 en fonction de Nm_s et Nm_l en appliquant le principe de conservation de la matière entre l'état initial et l'état après l'apparition de germe,

$$Nm_0 = Nm_l + Nm_s \qquad \text{(II-3)}$$

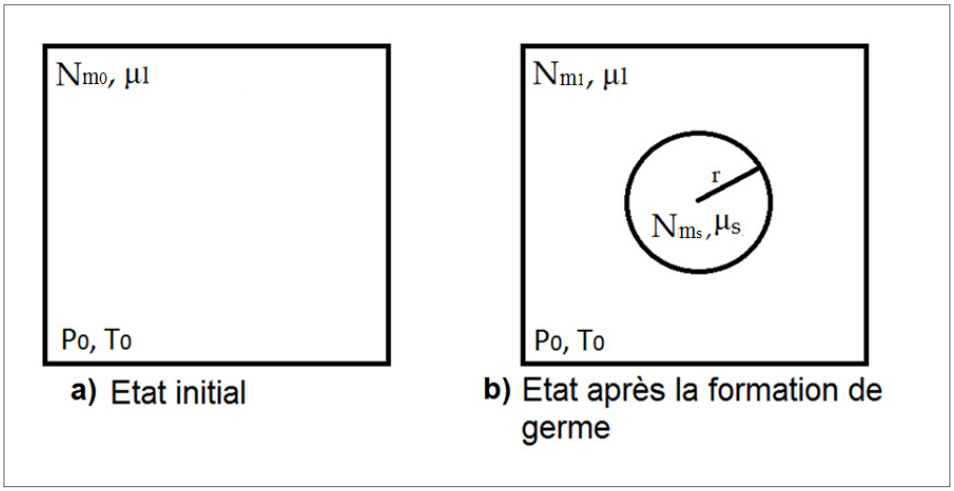

Figure II-3 : état d'un système liquide : a) avant la formation de germe et b) après la formation de germe.

Où Nm_s est le nombre de moles des substances solides dans le germe et Nm_l est le nombre de moles des substances liquides après la formation de germe.

D'où l'enthalpie libre de l'état initial (eq. (II-2)) sera :

$$G_0 = (Nm_l + Nm_s) . \mu_l \qquad \text{(II-4)}$$

À l'état final, après l'apparition du germe solide, l'enthalpie libre correspond à la somme des enthalpies de la phase liquide et de la phase solide et le potentiel énergétique dû à l'interface liquide-solide :

$$G = Nm_l . \mu_l + Nm_s . \mu_s + \gamma . A_{germe} \qquad \text{(II-5)}$$

- μ_s est le potentiel chimique du solide à P_0 et T_0 ;
- γ est la tension superficielle entre le germe solide et le liquide ;
- A_{germe} est la surface du germe (supposé sphérique) = $4\pi.r^2$.

D'où l'enthalpie de l'état final (eq. (II-5)) sera :

$$G = Nm_l.\mu_l + Nm_s.\mu_s + 4.\gamma.\pi.r^2 \quad \text{(II-6)}$$

Ainsi, la variation d'enthalpie associée à la germination est la différence entre les équations (II-6) et (II-4) qui correspondent aux enthalpies des états final et initial, après et avant l'apparition du germe solide. Elle peut être exprimée par l'expression suivante :

$$\Delta G = G - G_0 = Nm_s.(\mu_s - \mu_l) + 4.\gamma.\pi.r^2 \quad \text{(II-7)}$$

Or $Nm_s = \frac{4\pi}{3}.\frac{1}{V_m}.r^3$, où V_m est le volume molaire du solide.

Alors, la variation d'enthalpie libre (eq. (II-7)) s'exprime telle que :

$$\Delta G = \frac{4\pi}{3}.\frac{(\mu_s - \mu_l)}{V_m}.r^3 + 4.\gamma.\pi.r^2 \quad \text{(II-8)}$$

La différence des potentiels chimiques $(\mu_s - \mu_l)$ qui apparait dans l'expression (II-8) peut être exprimée en fonction de la chaleur molaire de fusion du matériau par la relation suivante (Lafargue, C., 1952 ; Dufour, L. et Defay, R., 1963):

$$\frac{\partial}{\partial T}\left[\frac{1}{T}.(\mu_s - \mu_l)\right] = \frac{l_f(T)}{T^2} \quad \text{(II-9)}$$

Où $l_f(T)$ est la chaleur molaire de fusion du matériau.

En intégrant la relation (II-9), on obtient :

$$(\mu_s - \mu_l) = T.\int_{T_m}^{T} \frac{l_f(T)}{T^2} dT \quad \text{(II-10)}$$

En supposant que $l_f(T)$ est constante par rapport à la température, la différence des potentiels est exprimée alors en fonction du degré de surfusion par la relation suivante :

$$(\mu_s - \mu_l) = -l_f.\frac{\Delta T}{T_m} \quad \text{(II-11)}$$

Enfin en remplaçant la relation (II-11) de la différence des potentiels dans (II-8), on obtient l'expression de la variation d'enthalpie en fonction du rayon du germe et du degré de surfusion,

$$\Delta G = -\frac{4\pi}{3}.\frac{l_f}{V_m}.\frac{\Delta T}{T_m}.r^3 + 4.\gamma.\pi.r^2 \quad \text{(II-12)}$$

Cette expression (II-12) montre que la variation d'enthalpie libre ΔG, associée à la formation d'un germe solide au sein du liquide surfondu, est la somme d'un terme volumique proportionnel à (r^3) et d'un terme surfacique proportionnel à (r^2).

Les deux termes dépendent du rayon du germe *r*, mais ils ont des signes opposés. En effet, le terme volumique est négatif et le terme surfacique est positif. Par conséquent, la variation d'enthalpie libre, associée à la formation d'un germe, passe par une valeur maximale. Cette valeur maximale, notée ΔG_{c-hom}, correspond à une valeur critique du rayon du germe, notée r_c (comme montré sur la figure (II-4)).

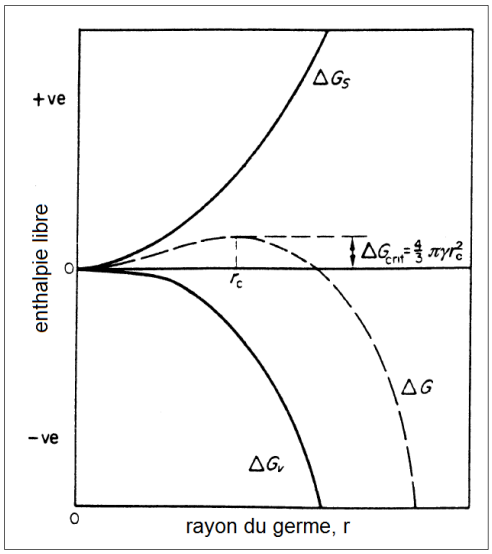

Figure II-4 : Variation de la différence d'enthalpie libre en fonction du rayon du germe (Mullin, J.W., 2001).

Afin d'obtenir la valeur critique du rayon r_c, ainsi que la valeur maximale de la variation d'enthalpie ΔG_c, on dérive l'expression (II-12) de la variation d'enthalpie libre par rapport au rayon *r*. Les résultats sont les suivants :

$$r_c = \frac{2.\gamma.V_m}{l_f}.\frac{T_m}{\Delta T} \qquad \text{(II-13)}$$

et,

$$\Delta G_{c-hom} = \frac{16.\pi.\gamma^3}{3}.\left(\frac{V_m}{l_f}\right)^2.\left(\frac{T_m}{\Delta T}\right)^2 = \frac{4}{3}.\pi.\gamma.{r_c}^2 \qquad \text{(II-14)}$$

En conclusion, pour qu'un système commence à évoluer de l'état liquide à l'état solide, la variation de l'enthalpie libre doit passer par un maximum ΔG_c qui représente une barrière d'énergie. Pour cela, le comportement d'un germe, formé spontanément au sein du liquide, dépend fortement de son rayon. En effet, il doit avoir un rayon supérieur au rayon critique r_c pour qu'il se développe. D'où le concept du rayon critique pour une nucléation homogène.

Tant que le système n'arrive pas à franchir cette barrière, autrement dit aucun germe n'est encore stable $(r < r_c)$, les germes n'entrainent pas la transformation liquide-solide.

Ce qui explique le phénomène de surfusion : il s'agit toujours de germes solides non stables au sein du liquide surfondu, qui ne déclenchent pas la transition à l'état solide.

D'autre part, le degré de surfusion intervient dans l'expression (10-a) du rayon critique. En effet, un système liquide avec un degré de surfusion plus important (température plus basse) nécessite un rayon critique plus faible, donc d'une barrière d'énergie plus faible, pour entrainer la transformation liquide-solide. La rupture de métastabilité est donc d'autant plus facile à obtenir que la température de l'échantillon est plus basse. Les deux figures (II-5 et II-6) ci-dessous, représentent un exemple de la variation de la taille critique du germe en fonction de la température de l'eau surfondue (Weickman H.K., 1951), et la variation de la variation de l'enthalpie en fonction du rayon du germe pour deux différentes valeurs de température du liquide surfondu (T_1<T_2), respectivement.

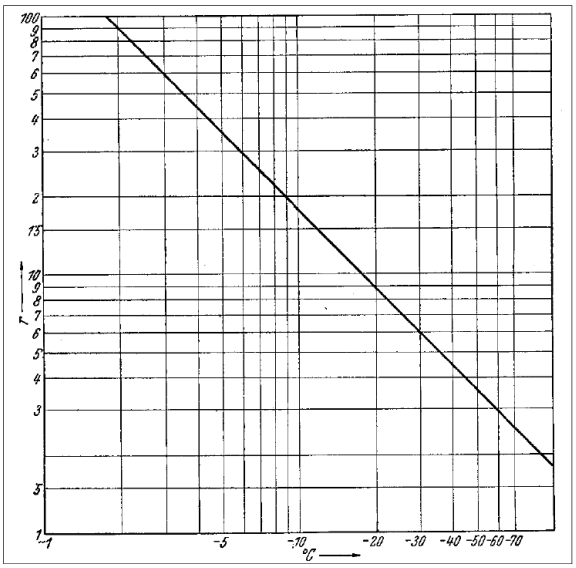

Figure II-5 : Variation de la taille critique du germe stable en fonction de la température de l'eau surfondue (Weickman H.K., 1951).

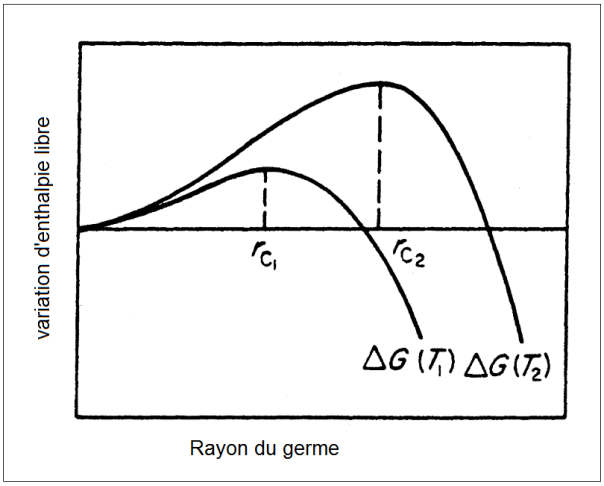

Figure II-6 : Variation d'enthalpie libre pour deux températures T1 et T2, tel que T1<T2 (Mullin, J.W., 2001).

Plusieurs auteurs se sont intéressés à étudier la nucléation homogène du liquide surfondu (Molinero, V., 2013 ; Wolk, J. et al. 2013 ; Stan, C.A. et al., 2009). Pour ce qui concerne l'eau surfondue l'équipe de Stan (2013), par exemple, a utilisé un instrument mesurant les températures de nucléation de dizaines de milliers des gouttelettes d'eau surfondue sur une durée de quelques minutes. Les résultats de mesures sur 37061 gouttelettes de 80 µm d'eau pure ont indiqué que la température de la nucléation homogène varie entre -36 et -37,8 °C.

Pruppacher a étudié l'effet des champs électriques sur la nucléation homogène de la glace. Il a montré que la présence des champs électriques améliore significativement la nucléation de la glace. Dans ce cas, la nucléation peut être appelée électro-nucléation (Pruppacher, H.R. , 1973).

II.3.2. Nucléation hétérogène

La présence d'impuretés dans le liquide surfondu peut affecter considérablement la nucléation d'un germe. En effet, le germe ne se forme plus au sein du liquide, mais sur la surface de ces impuretés. Dans ce cas, la nucléation est dite hétérogène, et les impuretés sont appelées des substrats.

Afin de résoudre les calculs de la barrière énergétique pour ce type de nucléation, plusieurs formes ont été considérées pour le germe formé sur la surface des substrats : une forme lenticulaire (Volmer, H. et Weber, A. , 1925 ; ABRAHAM, F.F. , 1968 ; Defray, R. et Prigogine, I. , 1951), sphérique (Volmer, H. et Weber, A. , 1925 ; Bigg, E.K. , 1953 ; Turnbull, D. et Vonnegut, B. , 1952) , et parallélépipédique (Binsbergen, F.L. , 1973 ; Ouchi, K. , 1954).

Le modèle considéré ici et présenté dans la suite est le modèle le plus simple qui considère une forme lenticulaire du germe formé sur la surface d'un substrat (figure II-7).

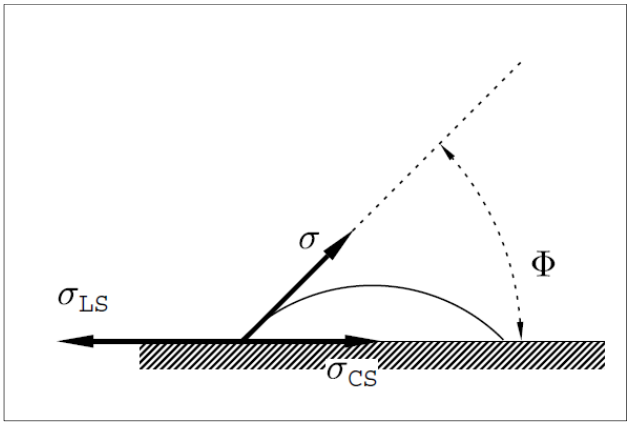

Figure II-7 : Formation d'un germe lenticulaire sur une interface (Gibout, S., 2001).

La condition d'équilibre mécanique se traduit par l'équation suivante :

$$\sigma_{LS} = \sigma_{CS} + \sigma.\cos\Phi \quad \text{(II-15)}$$

En suivant la même procédure du cas homogène, l'expression de la barrière énergétique, dans ce cas, peut être exprimée en fonction de celle obtenue pour la nucléation homogène, comme montre l'équation suivante :

$$\Delta G_{c-hét} = f(\Phi).\Delta G_{c-hom} \quad \text{(II-16)}$$

Où :

$$\Delta G_{c-hom} = \frac{4}{3}.\pi.\gamma.{r_c}^2 \quad \text{(II-17)}$$

et,

$$f(\Phi) = \frac{2 - 3.\cos(\Phi) + cos^3(\Phi)}{4} \quad \text{(II-18)}$$

La fonction $f(\Phi)$ est toujours inférieure ou égale à 1 (Defray, R. et Prigogine, I. , 1951) :

Pour $\Phi = 180°$ (un germe sphérique), la fonction $f(\Phi)$ est égale à l'unité. Ce qui signifie que la barrière énergétique à franchir dans ce cas est égale à celle du cas de la nucléation homogène dans lequel un germe sphérique est considéré.

Pour $0° < \Phi < 180°$, la fonction $0 < f(\Phi) < 1$. Cela signifie que pour d'autres formes, pour le cas d'une nucléation hétérogène, la barrière énergétique à franchir est toujours inférieure à celle trouvée pour le cas d'une nucléation homogène.

Pour $\Phi = 0°$, la fonction $f(\Phi)$ est égale à zéro. C'est le cas de la germination : l'introduction, dans le liquide surfondu, des germes de même structure cristalline que la phase solide. Cette méthode sert à briser l'état métastable, et provoquer la transition liquide-solide sur demande.

Pour conclure, la barrière de l'énergie à franchir dans un cas d'une nucléation hétérogène est inférieure ou égale à celle correspondante à une nucléation homogène. La présence des impuretés facilite donc la transformation liquide-solide. Autrement dit, pour un degré de surfusion donné, le germe, formé sur la surface d'un substrat, requis pour entrainer la cristallisation totale de l'échantillon est plus petit que celui requis dans le cas de nucléation homogène.

Les substrats sont alors considérés comme des catalyseurs de cristallisation. En effet, ils servent à favoriser la nucléation et sont appelés agents nucléants. Depuis longtemps, les auteurs se sont intéressés à étudier l'effet des divers types des agents nucléants sur la rupture de surfusion.

Des études originales sur ce sujet ont été réalisées sur l'eau par Weickman H. (1942), qui a montré que ces substrats doivent être insolubles pour avoir un effet significatif. Cela a été confirmé par Schulz en 1948 (Schulz, G., 1948) qui a montré, de

plus, que les substrats dont la structure est plus semblable à celle de la phase solide améliorent leurs efficacités.

Vonnegut (1947) a utilisé les rayons X pour étudier les structures cristallines de plusieurs types d'agents nucléants influençant la nucléation de l'eau surfondue. Il était le premier à tester l'iodure d'argent et l'iodure de plomb dans des gouttelettes d'eau surfondue. Il a trouvé que ces agents réduisent considérablement la surfusion des petites gouttelettes d'eau, grâce à leurs structures hexagonales très semblables à celle de l'eau.

Vail, G. et Stansbury, R.J. (1966) ont étudié le comportement de la nucléation des gouttelettes d'eau surfondue en gardant une vitesse de refroidissement constante. Les résultats ont montré que la nucléation est favorisé par l'addition des agents nucléants.

Plus récemment, Chen et al. ont étudié l'effet des différents types d'agents nucléants sur l'eau surfondue, dans des capsules (Chen, S.L. et Chen, C.L., 1999 ; Chen, S.L. et al., 1998) et des cylindres (Chen, S.L. et Lee, T.S., 1997). En confirmant que l'iodure d'argent est le plus efficace à favoriser la nucléation, ils ont montré en calculant la probabilité de la nucléation, que la température de la nucléation augmente avec la quantité d'agents nucléants dans le liquide jusqu'à une quantité de 1%. Au-delà de cette quantité la température de la nucléation n'augmente plus.

Okawa, S. et al. (2000) ont étudié la nucléation hétérogène de l'eau surfondue contenant des particules solides. L'effet de la taille et de la quantité de trois types de particules a été étudié. Ils ont conclu que le degré de surfusion est une fonction de la surface totale exposée à l'eau. En effet, le degré de surfusion augmente avec la diminution de cette surface totale.

De point de vue quantitatif, Heneghan, A.F. et al. (2002) ont montré en répétant 300 fois la même expérience, que l'addition d'un cristal insoluble d'iodure d'argent à l'échantillon d'eau pure surfondue diminue la température de la nucléation de 7,65 K.

De plus, Stan, C.A. et al. (2009) ont montré, en utilisant toujours leur dispositif mesurant les températures de nucléation de dizaines de milliers des gouttelettes d'eau surfondue au cours de quelques minutes, que la présence de l'iodure de l'argent diminue significativement le degré de surfusion. En effet, la température de nucléation de l'eau pure a varié entre -36 et -37,8 °C, tandis que la température de nucléation avec ces agents a varié entre -10 et -19°C.

Le chapitre suivant décrit la revue de la littérature de la deuxième étape de la transformation liquide-solide : la croissance dendritique (l'objet de ce travail).

III. Croissance dendritique

III.1. Introduction

La nucléation, i.e. l'apparition germe supercritique, qu'elle soit homogène ou hétérogène, déclenche donc brusquement la transition du liquide vers l'état solide. L'état métastable se termine alors localement, et le système tente d'atteindre l'état stable le plus proche qui est l'état solide dans ce cas. Cette formation d'une quantité de solide est accompagnée par un dégagement de chaleur latente, absorbée par le liquide surfondu. Cette phase est appelée la croissance dendritique.

Ce chapitre est consacré à l'état de l'art de la phase de la croissance dendritique qui constitue le sujet d'étude de ce projet. Deux sections viennent s'ajouter à cette introduction.

Le paragraphe III.2 présente la revue de la littérature sur l'aspect numérique du sujet, alors que le suivant propose la revue des travaux expérimentaux.

Le contenu du paragraphe III.2 est un article de revue rédigé en langue anglaise intitulé : « *A review of dendritic growth during solidification: mathematical modeling and numerical simulations* ». Cet article a été soumis à la revue « *Renewable and Sustainable Energy Reviews* ». Comme son nom l'indique, cet article présente l'état de l'art de la modélisation mathématique et des simulations numériques du problème de la croissance dendritique. Après avoir fourni les notions principales sur la croissance dendritique, il aborde les théories existantes décrivant et gouvernant cette phase. La théorie de la croissance dendritique d'une substance pure a deux composantes complémentaires. La première composante est celle de la diffusion de la chaleur décrivant la manière dont elle est redistribuée dans les deux phases liquide et solide autour de la dendrite en croissance. La deuxième composante décrit les mécanismes et les effets physiques et thermiques associés à l'interface séparant les deux phases. L'évolution de la condition de Gibbs-Thomson dans ce contexte est particulièrement discutée en introduisant les effets des différents termes inclus par cette condition. Une version complète de cette condition doit inclure les effets de la courbure, de la tension superficielle, de la mobilité cinétique, des discontinuités des propriétés thermophysiques à l'interface, et de l'anisotropie du matériau. Ensuite, le modèle mathématique de la croissance dendritique traduisant ses deux composantes théoriques est présenté. De point de vue mathématique, le problème de la croissance dendritique consiste alors à résoudre principalement : (1) les équations de diffusion de la chaleur dans les deux phases liquide et solide, (2) la condition de Stefan de la conservation de la chaleur à l'interface mobile et (3) la condition de Gibbs-Thomson avec laquelle la température de l'interface est calculée en fonction des différents effets associés à l'interface. Enfin, l'article décrit d'une façon exhaustive les différentes approches numériques développées et appliquées pour résoudre le problème dendritique. Elles sont classifiées selon la manière avec laquelle elles suivent l'interface ; explicite ou implicite.

Le paragraphe III.3 décrit la revue de la littérature des travaux expérimentaux mettant en évidence la croissance dendritique lors du processus de solidification. Cette revue se focalise particulièrement sur les travaux sur l'eau, choisie comme MCP de référence pour les essais expérimentaux prévus dans le cadre de ce projet.

III.2. A review of dendritic growth during solidification: mathematical modeling and numerical simulations: Article 1

Mohamad Ali Jaafar [1,2], Daniel Rousse [1], Stéphane Gibout [2], Jean-Pierre Bédécarrats [2]

(1) t3e Industrial Research Group, École de technologie supérieure, Montréal (Qc), Canada
(2)Univ. Pau & Pays Adour - EA1932 - LATEP - Laboratoire de Thermique Energétique et Procédés, Rue Jules Ferry, BP7511 - PAU, F-64075, France

Article soumis à la revue « *Renewable and Sustainable Energy Reviews* »

Abstract

Dendritic growth is one of the most common microstructures in metal and solution solidification. The subject of dendritic growth has received much attention from both scientific and industrial points of view. On the one hand, dendritic growth has become a deeply investigated subject in non-linear dynamics field. On the other hand, its understanding became essential for some engineering applications, mainly in metallurgy and latent thermal energy storage where phase change materials are used. Therefore, understanding and modeling the mechanisms which result the dendritic structures has been the objective of much research over the last decades. In order to understand the formation of dendrites, it is essential to understand the physical mechanisms on the interface separating the two phases. This paper reviews and discusses the available theories of dendritic growth, and then introduces the Gibbs-Thomson condition which has to be taken into account to handle all interfacial effects. Based on the Gibbs-Thomson condition, a complete mathematical model describing the dendritic growth problem for pure substances is formulated. This model includes the heat equation in both liquid and solid phases, the heat conservation equation at the interface separating these two phases, and the proposed Gibbs-Thomson equation. In order to solve this complex non-linear problem, several numerical methods have been developed. Hence, in its last section, the paper reviews these numerical methods distinguishing between two major classes involving the explicit and the implicit tracking of the moving interface.

Keywords: Dendritic growth, Gibbs-Thomson equation, Front Tracking method, Phase-field model, set-level method, enthalpy method.

Nomenclature

T	Temperature [K]	λ_c	Cutoff wavelength [m]
T_i	Initial temperature [K]	T_f	Interface temperature [K]
T_m	Equilibrium temperature [K]	γ	Surface tension [J.m^{-2}]
T_N	Nucleation temperature [K]	κ	Twice of mean curvature [m^{-1}]
T_c	Coolant temperature [K]	$\mathbb{V}_n$	Normal velocity [m.s^{-1}]
δ	Perturbation amplitude [m]	L_v	Volumetric latent heat [J.m^{-3}]
δ_D	Diffusion length [m]	υ	Kinetic mobility [m.K^{-1}.s^{-1}]
δ_c	Capillary length [m]	θ	Interface orientation [rd]
Pe	Péclet number	k	Thermal conductivity [J.m^{-1}.K^{-1}.s^{-1}]
$\mathbb{V}_t$	Tip velocity [m.s^{-1}]	t	Time [s]
r_t	Tip radius [m]	ω	Pulsation [rd.s^{-1}]
α	Diffusivity [m^2.s^{-1}]	ρ	Density [Kg.m^{-3}]
c	Heat capacity [J. Kg^{-1}.K^{-1}]	Δ	Dimensionless supercooling
L	Latent heat of fusion [J.Kg^{-1}]	ΔT_0	Initial supercooling [K]
$\vec{n}$	Normal vector at the interface	Q	Energy source [W.m^{-3}]

III.2.1. Introduction

The formation of patterns in nature is largely found everywhere [1,2], some examples are cloud formation [3], bacterial colonies [4], and grain structures in metals [5] or rocks [6]. Dendritic crystal growth is one of the most spontaneous pattern formations. For instance, snowflakes have various types of complex and fascinating shapes, although they are formed in almost uniform circumstances.

Further, dendritic structures are also commonly forms of microstructure, being present in all macroscopic castings, ingots, and welds.

During a cooling process, if care is taken and in the absence of perturbations, it is possible that the material remains in its liquid state, even below its solid-liquid equilibrium temperature. Thus supercooled liquid may appear [7]. Such a state is thermodynamically metastable [8-10]. Then the solidification can occur either homogeneously [11,12] after sufficient cooling or heterogeneously by placing for example a solid seed in the supercooled liquid [13-15]. Furthermore, once the solid is nucleated through the supercooled liquid, the subsequent growth of the solid from the seed may not to be stable and a dendritic crystal may form, depending on several factors, mainly the degree of supercooling. “Dendrites are a prototypical system evolving from homogeneous starting conditions into complex spatio-temporal patterns far from equilibrium” [16].

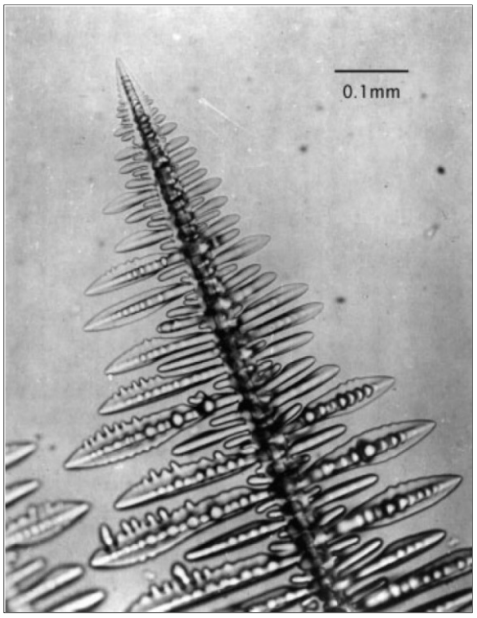

Figure III-1: Dendrite growing into a supercooled melt of pure succinonitrile [103].

The descriptive term 'dendrite' comes from the Greek word 'dendron' which means tree [17]. Like a tree, the dendrite has a highly branched, arborescent structure (see figure III-1). Due to the interface instabilities, a dendritic crystal consists of a primary stem, secondary branches, and eventually higher order branches evolving, all growing in selected crystallographic directions.

The evolution of the dendritic pattern has received much attention from both scientific and engineering points of view for its intricate pattern selection mechanisms and useful industrial applications, mainly in metallurgy and thermal energy storage fields. On the one hand, dendrites in metallurgy establish the initial microstructures of cast metals and alloys. These microstructures, in turn, strongly influence the mechanical, physical, and chemical behaviors of the material. Otherwise, they determine the qualities of the solidified raw material and often the finished product. Thus, the understanding of these dendritic microstructures formation is technologically important in order to produce better casts and pattern formation for advanced materials. On the other hand, the dendritic growth is a very important phenomenon in the process of solidification of phase change materials (PCM) which are used in thermal energy storage applications [18,19]. It relates the end of the supercooling phenomenon and the beginning of the solidification of the whole region (figure III-2).

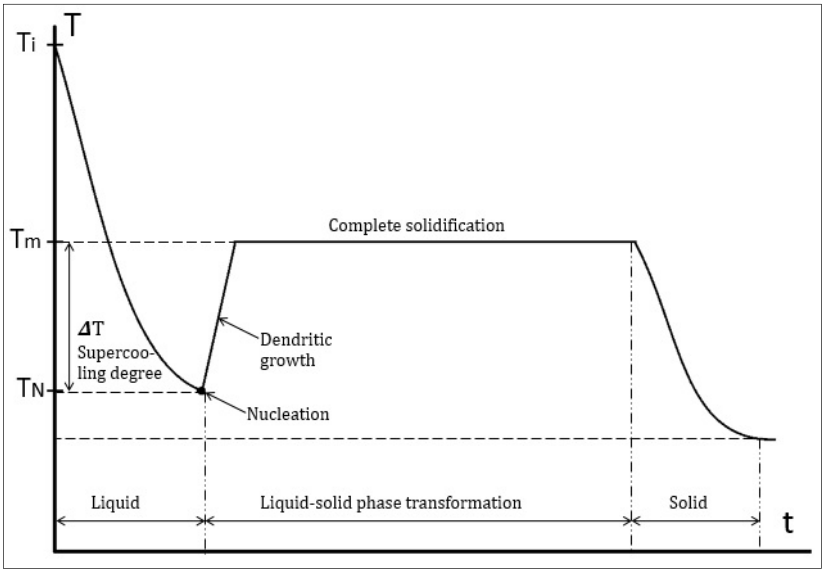

Figure III-2: Variation of the temperature (at the center of a sample) in time, during solidification process of a supercooled liquid. Phase b concerns the crystal growth.

In fact, during the propagation of dendrites through the supercooled liquid, the liquid temperature returns to its equilibrium temperature of solidification. This is due to the latent heat absorbed by the supercooled liquid, which is released from the interface during this phase. Hence, one would like to understand how the dendritic growth is driven or guided, in order to improve the solidification processes by controlling or preventing it.

Furthermore, apart these engineering applications providing its technical importance, dendritic growth also represents a pattern formation phenomenon, which in recent years has become a deeply researched subject in non-linear dynamics field.

The problem of dendritic growth has had a long and somewhat tortuous history [20,21]: In 1611 Kepler drew attention to the shapes, numbers, and geometric similarities exhibited by the six fold symmetry of snowflakes [22]. This question was posed even before the existence of atoms was recognized, but more recently, attention has focused on the question of the dynamics of crystal growth and the evolution of the liquid-solid interface during this phase. The last 50 years have seen a renaissance of interest in this problem, and it is probably fair to say that many of the basic principles have reached a good level of understanding to the satisfaction of physicists and researchers working on this subject. This understanding has emerged through a combination of experimental work, mathematical analysis, and numerical simulations.

The essential purposes in the present review paper are first, to show the available theories of dendritic growth in a simple manner to provide the reader who is interested in this problem a good and complete point of understanding and second, to present the different numerical methods used to resolve this complex problem. Thus, the paper is organized in five sections. In the second section, the dendritic growth theories starting from the Mullins-Sekerka instability as well as the history/evolution of the Gibbs-Thomson condition - which is used to calculate the interface temperature which is different than the equilibrium temperature due to the interfacial instabilities – are presented. When Gibbs-Thomson equation is appropriate, it can be coupled with the heat transport equations to give a complete understanding of the dendritic problem. The third section introduces the mathematical governing equations of the problem including the last presented Gibbs-Thomson condition at the interface. The fourth section reviews the different numerical methods which are developed and applied to track the liquid-solid interface during the dendritic crystal growth. Finally, the fifth section involves a synthesis and concluding remarks.

The rationale behind this review lies in the application to phase change materials which are used in several renewable and sustainable energy applications involving thermal energy storage.

III.2.2. Dendritic growth theories

III.2.2.1. Background

The process of freezing was present at the beginning of the Earth and continues to affect the natural and industrial worlds [23,24]. A huge majority of commercial solid materials were "born" as liquids and frozen into very useful configurations. In addition, many of the existing materials are used as phase change materials in the heat storage and stabilizing temperature systems. These materials are chosen carefully according to a list of characteristics, mainly thermal and mechanical properties. They strongly contribute in determining these systems performance.

The solidification of a liquid may involve a complex interplay of many physical effects. The solid-liquid interface is an active free boundary from which latent heat is generated and liberated away during phase transformation by thermal transport. Plus, rejection of solute occurs at the interface if the liquid is not pure but contains solute. To avoid making this paper overly lengthy, the proposed review is limited to the case of pure materials, therefore no solutal rejection is considered on the solid-liquid interface during the solidification process.

The solidification can be either a stable or unstable process. Stable solidification, traditionally known as Stefan problem [25], is characterized by conduction of heat from the solid-liquid interface through the solid and a flat growing interface. Any perturbations on the interface are indeed reduced. Stable solidification is dominated by heat diffusion while surface tension and interface kinetic effects are negligible. The existence [26] and the uniqueness [27] of a solution were proved. Analytic solutions of the Stefan problem for simple geometries and one-dimensional cases of an infinite or semi-infinite region are available [28-31]. Nevertheless, for more complex situations, numerical methods, using various methods and techniques, have been developed and used [32-33].

However, the solidification process becomes unstable when the initial liquid is metastable and cooled below its solid-liquid equilibrium temperature. In this case, heat is conducted away from the solid-liquid interface through both the liquid and the solid phases. Plus, any local perturbation on the solid-liquid interface will be enhanced. Any solid protrusion into the liquid will thus grow and produce various microstructure patterns. Two common microstructures in metals and solutions are the cellular and dendritic patterns depending on the supercooling degree. Dendritic growth is the dominant pattern when supercooling is large enough.

Understanding and modeling the mechanisms which provide the dendritic structures has been the focus of much research over the last decades. The most difficult and most important thing in understanding how the dendrites are produced is predicting the interfacial physics occurring between the phases. When these interfacial

physics are coupled with the heat transport theory, they can describe the process of dendrites formation. Otherwise, many researchers have focused on finding the appropriate boundary conditions at the moving interface which govern the interfacial physics in order to be able to predict a real growing dendrite.

III.2.2.2. Mullins-Sekerka instability

The perturbation theory of interface stability has been developed, presumably independently, by Wagner [34], Mullins and Sekerka [35-37], and Voronkov [38]. The main task of the theory is to solve the perturbed problem on simply shaped interfaces and determine if a small-amplitude perturbation will be enhanced in time and destabilize the interface, or alternatively, decay and leave the initial interface unchanged and morphologically stable. The physical origin of the instability of the solidification interface giving rise to dendritic growth was identified by Mullins and Sekerka [35]. They have analyzed the steadily advancing planar interface on which is imposed a single periodic ripple. They found a stability criterion by calculating the cutoff wavelength, which is the largest possible wavelength for a stable interface. The derivative of the amplitude of the sinusoidal perturbation with respect to time is,

$$\delta'(t) = -\Lambda(\omega)\delta(t) \qquad \text{(III-1)}$$

The perturbation will respectively grow or decay exponentially for negative and positive values of Λ. Thus, the stability limit can be found by equating Λ to zero and therefore, the cutoff wavelength is,

$$\lambda_c = 2\pi\sqrt{\delta_D \delta_C} \qquad \text{(III-2)}$$

A similar linear stability analysis was performed for growing spheres by Mullins and Sekerka [35] using a quasi-stationary assumption that has been extended to include interface kinetics [39,40].

III.2.2.3. Unstable solidification: dendritic growth

If the solidification front becomes morphologically unstable, the small perturbation at the interface will grow, on the other hand it is constrained by surface tension and interface kinetic effects. This competition between the stabilizing effect of surface tension and the destabilizing effect of supercooling is responsible for the morphologically complex dendritic structures formation.

Steady state models for dendritic growth are based on Ivantsov's solution [41] of the heat transport equation of a dendrite growing in a uniformly supercooled liquid. The principal focus of these theories was, for many years, to account for the observed values of the dendrite tip radius and velocity. The Russian mathematician G.P. Ivantsov was the first to derive a mathematical analytical solution for a 'definable shape' of a steady state dendrite growing into an infinite half-space of a supercooled liquid during diffusion-controlled phase transformation. A single needle branchless dendrite with a paraboloic

tip shape was suggested in Ivantsov's theory, based on the observations of dendritic crystals published in 1935 by Papapetrou [42]. Indeed, Ivantsov adopted a mathematical definable shape of the growing crystal tip which is demonstrated to be close to a realistic constellation [43-45].The effect of curvature on the melting point is not included in Ivantsov's model, so that the interface is assumed to be isothermal while the interface temperature equals the melting temperature T_m. The Péclet number, Pe, derived from the Ivantsov theory relates the tip velocity, $\mathbb{V}_t$, and the tip radius, r_t:

$$Pe = \frac{\mathbb{V}_t r_t}{2\alpha} \tag{III-3}$$

Ivantsov's solution relates the liquid dimensionless supercooling Δ to the Péclet number such that:

$$\Delta = Iv(Pe) = Pe.exp(Pe).E_1(Pe) \tag{III-4}$$

where the dimensionless supercooling of the liquid is defined for a pure liquid, as

$$\Delta = \frac{c.\Delta T_0}{L} \tag{III-5}$$

In equation (III-4), E_1 is an integral exponential function, defined as

$$E_1(Pe) = \int_{Pe}^{\infty} \frac{\exp(-x)}{x} dx \tag{III-6}$$

For a given initial supercooling, the solution of the Ivantsov function leads to the relationship between the dendrite's tip velocity and radius,

$$\mathbb{V}_t.r_t = 2\alpha[Iv^{-1}(\Delta)] \tag{III-7}$$

Equation (III-7) determines, for a given initial supercooling, solely the value of the product of the two dependent variables, $\mathbb{V}_t$and r_t.The Ivantsov prediction for $\mathbb{V}_t.r_t$ product is well verified experimentally; Huang and Glicksman [46,47] have shown that for a given initial supercooling, all observed needles lie on the Ivantsov curve. However, the solution describes a family of parabolas. Moreover, several others researchers [48-52], also addressed this problem but like Ivantsov's solution their results lead to an infinite number of solutions which are also given in terms of velocity-radius combinations. Hence, finding the unique solution to the needle-like dendrite problem requires an additional independent equation relating $\mathbb{V}_t$and r_t.

Consequently, to the limitation of these analytical solutions to provide a unique operating state dendrite, several ideas were proposed in order to find an additional physical principle needed to complete the mathematical model of the basic dendritic growth problem [53-61].

For a given supercooling, it was thought first that the curves should exhibit a maximum velocity in order to select the unique operating state of the dendrite. In fact, at

the maximum velocity the crystal requires that the dendrite tip radius be just twice the size of the critical radius required for homogeneous nucleation [62]. In order to check this theory, some early experiments have been done; unfortunately, the corresponding observations of the tip radius predicted do not agree well with the maximum velocity hypothesis [63].

Oldfield [55] considered that it is conditionally possible to develop an independent criterion for growth velocity as a function of tip shape. This criterion, when coupled with the relationship commonly derived from heat transport considerations, would permit a unique solution to the problem. Starting from the stability argument that the crystal adopts the shape which will grow in a stable fashion, Oldfield has proposed an independent relationship between tip radius and the adjacent gradient (a measure of growth velocity) as a replacement for the maximum velocity criterion used in prior studies to define a unique crystal. However, this theory and some others were tested by quantitative experiments performed on different well-characterized test substances. The results also showed that these theories are inappropriate to correctly predict the dendritic branching behaviour [46,47][64-67].

The following two theories are accepted nowadays: marginal stability developed in the mid-1970s [68-70], and microscopic solvability developed in 1980s [71-73]. The time dependent marginal stability theory was developed by Langer and Muller-Krumbhaar which was formulated by summarizing some experimental velocity measurements [74,75] and some extensive numerical studies of the side-branching mechanism [76]. They proposed to use marginal stability as a criterion for selection of the operating state of the dendrite tip. According to this theory, the dendrite is assumed to grow at its stability limit, which divides the two regions of stable and unstable Ivantsov solutions, when the dendrite-tip radius r_t becomes equal to the cutoff wavelength found by Mullins-Sekerka, λ_c given by the equation (III-2).

The other new dimensionless parameter in this theory is,

$$\beta = \left(\frac{\lambda_c}{2\pi r_t}\right)^2 \qquad \text{(III-8)}$$

Equation (III-8) is equal at the point of marginal stability,

$$\beta^* = \frac{1}{4\pi^2} \approx 0.0253 \qquad \text{(III-9)}$$

Equations (III-2), (III-8) and (III-9) yield the additional required equation which relates the dendrite tip radius and velocity,

$$\mathbb{V}_t . {r_t}^2 = constant \qquad \text{(III-10)}$$

This second relationship, when coupled with Ivantsov's solution (eq III-7) yields a unique operating solution. The Langer and Muller-Krumbhaar marginal stability

theory was validated experimentally for a number of simple model materials [77,78], and was called in 1978 the universal law of dendritic growth rates [71]. Nowadays, this theory seems to be the most appropriate.

III.2.2.4. Capillarity effects

Despite that Ivantsov's analysis represents a very important primitive analysis and captures several important aspects of a growing dendrite tip, it is still quite far to represent a real dendrite behavior. A real dendrite displays a branchful shape, which is different than the needle-like shape assumed by Ivantsov. Perhaps the main weakness of Ivantsov's model is the neglecting of the interface curvature effects (capillarity effects). In fact, it was found that the state variables (such as temperature) change significantly with the interfacial curvature during the crystal growth phase. Thus, to describe appropriately the morphological development during crystal growth one must take these effects into account.

Since the original treatment of the interface thermodynamics given by Gibbs [79], several studies followed [80-87] for better understanding of the interfacial effects on the state variables of the solid-liquid interface during crystal growth. The researchers have derived a number of relationships governing interfacial capillarity. With regard to the equilibrium temperature, the boundary condition of the curvature dependence is expressed by Gibbs-Thomson [88]. Hence, the temperature of a growing interface is not equal to the equilibrium temperature of solidification, but depends on the local curvature of the interface. This boundary condition should replace the original isothermal interface boundary condition assumed by Ivantsov. Such consideration is commonly found among presently available dendritic growth models.

Assuming that the variation of the total free energy associated with an arbitrary displacement of a section of the solid-liquid interface, one obtains the Gibbs-Thomson relationship [89], which relates the local interfacial temperature T_f to the mean curvature of the interface,

$$T_f = T_m - T_m \frac{\gamma \kappa}{\rho L} \qquad \text{(III-11)}$$

This condition expresses a local equilibrium between bulk and surface effects: for a protrusion of solid in liquid ($\kappa>0$) to exist, the local temperature must be colder than T_m; otherwise the protrusion would immediately melt and pull back to reduce interface energy [90].

Glicksman [62] has shown that the capillary temperature distribution along a prescribed sharp interface acts as a weak energy field. According to his paper, the Gibbs-Thomson equilibrium temperature is assumed to be much more than a boundary condition on the transport field; it acts, in fact, as an independent energy field during crystal growth and produces profound effects not recognized heretofore. Further, it has

been shown that these effects initiate rotation of the interface at specific locations determined by the surface energy and shape.

All studies dealing with capillarity effects on the interface during the crystal growth show how these effects play a very important role in providing a suitable thermal boundary condition at the solid-liquid interface, which connects the geometry and the temperature field.

III.2.2.5. Kinetics effects

It has been shown that, with an increase in the supercooling of a liquid, the diffusional growth theory admitted in several dendritic growth models should be replaced by growth determined by processes of molecular rearrangement at the interface, i.e., the surface kinetics [91].

Shibkov and al. studied the case of supercooled bidistilled water to examine kinetics effects on the crystal growth. They reported results of experimental investigations of the transition from the diffusional to kinetic ice growth at atmospheric pressure. The evolution of the shapes of growing ice crystals was video-recorded in polarized light using a microscope [43,44,92]. Using this technique, they obtained earlier [93,94] a complete morphological diagram of nonequilibrium patterns of ice growth in the range of supercoolings from 0.1 °C (small supercooling degree) to 30 °C (large supercooling degree), which covers almost the entire range of heterogeneous ice nucleation in this case [91].

They showed that data obtained before and their results are in good agreement for relatively small supercoolings. However, at larger supercoolings (>4 °C) the results show a systematic deviation from the diffusional theory.

The reason of this discrepancy is the transition from the diffusional to the kinetics-limited growth which occurs at supercoolings of 4-5 °C. In fact, the diffusional theory assumes that there is a local thermal equilibrium at the moving crystallization front, which does not hold true at high growth rates. In this case, the finite rate of penetration of H2O molecules through the interface must be taken into account. Therefore, at larger supercoolings, the growth rate is determined predominantly by the molecular attachment kinetics at the solid-liquid interface [91].

These kinetic effects are found to be an additional stabilizing term for the growing interface perturbations, especially with large supercoolings. They can be added in the Gibbs-Thomson equation. Hence, the Gibbs-Thomson condition taking the kinetic effects into account is modified such that,

$$T_f = T_m - T_m \frac{\gamma \kappa}{\rho L} - \frac{\mathbb{V}_n}{\upsilon} \qquad \text{(III-12)}$$

Finally, it is worth noting that it is not appropriate to neglect the kinetic term in equation (III-12) dealing with dendritic growth problem, especially when it is produced for relatively high initial supercooling [91].

III.2.2.6. Heat capacity discontinuity

The third term to be taken into account during dendritic crystal growth is the heat capacity discontinuity between liquid and solid phases. These effects were neglected in most crystal growth models for simplicity purposes. However, it cannot be neglected when dealing with some materials, which have an important ratio of material heat capacity discontinuity between solid and liquid phases. Such an assumption is found to affect significantly the growing dendrites shape and the growth rate. Juric and Tryggvason [95] have handled this discontinuity in their model, which includes the Gibbs-Thomson condition on a curved interface which accounts for the effect of discontinuous heat capacity. The proposed expression was derived in Alexiades and al. studies [96,97]. They showed that a small increase in the liquid to solid volumetric heat capacity ratio markedly increases the solid growth rate and interface instability. A higher liquid to solid heat capacity ratio produces a fast growing unstable solid while a low ratio produces a slow growing, more stable solid shape.

According to [95] the Gibbs-Thomson condition, including solid-liquid heat capacity discontinuity effect, can be expressed such that:

$$T_f = T_m - T_m \frac{\gamma\kappa}{\rho L} - \frac{\mathbb{V}_n}{\upsilon} - \frac{T_m(c_l - c_s)}{L}\left(T_f ln \frac{T_f}{T_m} + T_m - T_f\right) \qquad \text{(III-13)}$$

Equation (III-13) is nowadays assumed to be a sufficient boundary condition accounting for the effects of most relevant physical mechanisms present at the solid-liquid interface during unstable solidification. Thus, this boundary condition, when coupled with both liquid and solid heat diffusion problems, should provide a complete mathematical model describing dendritic growth problem. However, it is not strictly the case. Indeed, the missing ingredient is the interfacial anisotropy.

III.2.2.7. Anisotropy

The interfacial anisotropy is due to the presence of crystal lattice in the solid phase. This anisotropy does more than simply control the asymmetry of the growing crystal; it influences the dynamics in a profound way [20]. The surprisingly important role of anisotropy was first discovered [98] in a simplified model of solidification. In [98], the authors concluded, from computer simulations, that the qualitative features of dendritic growth were reproduced only when the anisotropy was taken into account. The importance of the interfacial anisotropy consideration depends strongly on the studied material. Let us make, for example, a comparison between the most thoroughly studied materials among materials which show dendritic growth: succinonitrile and water. On the one hand, succinonitrile is an ideal model material in terms of shape isotropy, and it is widely used to test the theoretical prediction of dendritic growth

[67,99]. In this case, anisotropic effects can be neglected. On the other hand, water presents a highly anisotropic behavior, showing morphological changes as it grows. One cannot neglect the effects of anisotropy while dealing with water which is one of the most common and important materials in energy storage [100,101]. Note that the origin of the high interfacial anisotropy of water is the cubic crystals of its solid phase as mentioned at the top of this paragraph.

Therefore, the anisotropic version of the Gibbs-Thomson boundary condition has to include the orientation dependence of both surface tension and kinetic mobility. Hence, Gibbs-Thomson condition becomes,

$$T_f = T_m - T_m \frac{\gamma(\theta)\kappa}{\rho L} - \frac{\mathbb{V}_n}{\upsilon(\theta)} - \frac{T_m(c_l - c_s)}{L}\left(T_f ln \frac{T_f}{T_m} + T_m - T_f\right) \qquad \text{(III-14)}$$

A special situation may occur [102]: that is when the anisotropic version of Gibbs-Thomson condition is applied to an interface with both strong shape anisotropy and crystal's energy anisotropy. The two anisotropies – shape and surface energy – interact non-linearly, and produce non-monotonic temperature distributions and anisotropic attachment mobility. These, in turn, result in a pulsatile tip motion and shape oscillations that give rise to dendritic side-branching. This has been discovered, while the characteristic dendritic form is considered in the marginal stability theory as a stochastic, noise-mediated, unstable morphology, for which side-branching is caused by selective amplification of the environmental noise spectrum imposed near the tip.

Therefore, it is well said that the qualitative features of dendritic growth are found when the considered models are supplemented by anisotropy.

Finally, this Gibbs-Thomson condition is a local equilibrium condition; otherwise, the interface continually adjusts itself to balance bulk energy and surface energy depending on different parameters controlling the dendritic growth formation. However, a slight changing of the interface temperature tends to change the latent heat amount released by this interface. The Gibbs-Thomson boundary condition when coupled with the heat transport theory, it is assumed to offer a complete theory of dendritic growth.

III.2.3. Mathematical model

Mathematically, in idealized situations which neglect natural convection due to density changes, the dendritic growth solidification problem can be classified as a special complicated case of interface heat conduction problem, which requires appropriate tracking of the moving boundary interface which separates the different phases. Furthermore, the solidification problems are generally characterized by the discontinuity of coefficients and material properties and an unidentified source term present across the interface, from which the latent heat is released through both liquid and solid phases.

Consequently, one can divide the whole system in three sub-domains: liquid region, solid region, and the moving front (heat source boundary condition). The heat equation is then solved in each phase, separately. The temperature fields are coupled through two boundary conditions at the unknown moving boundary between the solid and the liquid phases. Numerically, the resolution of such problems requires an appropriate interface tracking method and some special techniques which can handle easily the discontinuities on this interface. The first boundary condition is the velocity of the interface. It gives an idea about how fast or at which rate the latent heat of solidification is released from the interface through the liquid and the solid. It depends on the local gradients of temperature between the interface and the phases near it. The second boundary condition is the interface temperature T_f, which is in this case slightly lower than the melting temperature T_m.

These two boundary conditions can be coupled by two different equations. The first equation is the heat conservation at the moving interface. The second equation is the Gibbs-Thomson equation including the different effects introduced in the previous section, equation (III-14).

The dendritic growth problem consists then of solving: (1) the heat energy equation in both liquid and solid phases, (2) the heat conservation at the moving front, and (3) the Gibbs-Thomson equation.

First, in each phase sub-domain, the physical variables are continuous and their dynamic evolution is described by the time dependent heat conduction equation:

$$\frac{\partial(\rho_s c_s T)}{\partial t} = \vec{\nabla}.\left(k_s \vec{\nabla} T\right) + \dot{Q}_s, \quad \text{for solid region} \tag{III-15}$$

$$\frac{\partial(\rho_l c_l T)}{\partial t} = \vec{\nabla}.\left(k_l \vec{\nabla} T\right) + \dot{Q}_l, \quad \text{for liquid region} \tag{III-16}$$

where the indices l and s refer to the liquid and solid phases, respectively.

Second, the energy balance condition at the liquid-solid interface which takes into account the released latent heat and the discontinuity of heat flux between the solid and liquid can be described by the following equation:

$$\rho.L(T_f).\mathbb{V}_n = \left(k_s \vec{\nabla} T_s - k_l \vec{\nabla} T_l\right).\vec{n} \tag{III-17}$$

Finally, the temperature at the interface needs to be calculated according to the Gibbs-Thomson condition described in the previous section and repeated here for the sake of completeness of the model.

$$T_f = T_m - T_m \frac{\gamma(\theta)\kappa}{\rho L} - \frac{\mathbb{V}_n}{\upsilon(\theta)} - \frac{T_m(c_l - c_s)}{L}\left(T_f ln\frac{T_f}{T_m} + T_m - T_f\right) \tag{III-14}$$

This problem is by no mean easy to solve due first, to its non-linearity at the moving unknown interface, for which displacement rate is controlled by the latent heat

released from the interface which in turn is controlled by temperature gradients between this interface and both solid and liquid regions. A second difficulty pertains to the materials properties discontinuity at this interface which must be considered. Therefore, analytical solutions of dendritic solidification problems suffer from severe restrictions with respect to practical applicability due essentially to the use of several simplifying assumptions to treat such a complex problem. Hence, computer software has been developed to numerically simulate dendritic solidification including most, if not all, of the important factors of influence.

III.2.4. Numerical studies

Starting from the Stefan problems, simulation and modeling the solidification processes have a long history in applied mathematics and sciences [104-107] and continues to be an important topic. For instance, tracking the evolution of the moving interface of a crystal growing between phases is a computational challenge especially in unstable cases of solidification in which complex dendritic structures may appear; however, an appropriate method is required. Over the last decades, several numerical methods, mostly in two dimensions, have been developed and applied for simulating the dendritic growth problem in its full geometrical complexity under different conditions and assumptions. From a computational point of view, numerical methods, based on standard discretization techniques, can be split into two major classes according to the way in which they handle the moving boundary interface; however, the interface can be tracked either explicitly or implicitly. In the following section, the main numerical methods belonging to the two classes used to simulate the dendritic solidification problems of pure and non-pure substances are reviewed, providing also some investigated aspects of dendritic crystal growth.

III.2.4.1. Front tracking methods

The first major class consists of keeping explicitly the data of the interfacial position by satisfying suitable discrete form of the interface heat balance condition. These front tracking methods use lower dimension deforming grids that evolve with the solid-liquid interface [108]. Typically, they employ field solutions on a fixed Eulerian background mesh and continuously reconstruct a Lagrangian, lower dimension, description of the interface [109-113]. This type of methods have been developed and largely used to track the liquid-solid interface during stable and unstable solidification of pure or non-pure substance.

Roosen and Taylor [114] have introduced an explicit front tracking scheme with simplifying interface curvature measurements by assuming that the interface is a polygon. They have shown that the algorithm was relatively fast, and easy to detect and make topological changes. They indicated that the differences between their study and the Ivantsov's solutions are obviously the assumptions made by Ivantsov that no surface energy is included, and rather, that the temperature at the interface is the melting

temperature. Finally, they noted that with stronger energy the tips become much less parabolic.

Shyy et al. [115] have developed an interface motion technique which is not limited to a single-valued or isothermal interface, and produces results in close agreement with analytical solutions for the one-phase and two-phase cases. For unstable solidification problems in which they map the governing equations into curvilinear coordinates, they observed the tip-splitting and cusp formation in absence of surface tension. Addition of a small amount of surface tension completely changes the picture and a propagating finger is obtained for the duration computed which are in qualitative agreement with other previous investigations.

Juric and Tryggvason [95] have used a numerical technique based on the front tracking method to simulate the two-dimensional stable and unstable solidification. This method has been originally developed for multi-fluid flows by Unverdi [116], discussed by Unverdi and Tryggvason [117,118]. Regarding its effective handling of the front, this technique has been used widely in numerical study of solidification [119-121]. It explicitly introduces a separate interfacial grid in addition to the fixed regular one. For the dendritic solidification case reported in [95], the immersed boundary technique, introduced in [122], was coupled with the front tracking method. With this technique, the infinitely thin interface is approximated by a smooth distribution function that is used to distribute the heat sources at the interface over grid points nearest the interface, and to interpolate the temperature field from the stationary grid to the interface. Juric and Tryggvason have performed simulations for stable and unstable solidification for various ratios of properties discontinuities at the interface and types of anisotropy. The method was found to easily handle the topology changes and the interfacial anisotropies for complex cases of solidification. In fact, the numerical results reproduced the complex dendritic structures such as side-branching, and tip-splitting which are observed experimentally.

Later, a two-dimensional model for the simulation of microstructure formation during solidification in multi-component systems has been developed by Jacot and Rappaz [123]. The model is based on a new pseudo-front tracking technique for the calculation of the evolution of interfaces that are governed by solute diffusion and the Gibbs–Thomson effect. The pseudo-front tracking method is a combination of front tracking and phase-field methods (introduced later in this review). It is shown that the model is capable of reproducing the transition between globular and dendritic morphologies. This technique is then used for the description of microstructure formation during solidification in multi-component alloys [124].

In the same year, a two dimensional front tracking method is presented by Al-Rawahi and Tryggvason [125] for the simulation of dendritic growth with convection for pure substances. The results are in good qualitative agreement with published experimental results, even though only the two-dimensional aspects were examined.

Later, Zhao et al. [126] have described an interface tracking algorithm which is used for the simulations of stable and unstable solidification problems. For the case of stable solidification, this algorithm was shown to yield an additional order of accuracy in the approximation of the interface comparing with the other front-tracking algorithms. It is also shown that the method is capable to describe extremely complex morphologies and a large number of simultaneous merging/splitting events during the dendritic solidification.

Nakagawa et al. [127] have simulated a 2D dendrite growth during the solidification of binary alloys using a modified front tracking technique. The anisotropy for growth direction was reduced in the modified model and a dendrite could grow to any arbitrary preferential crystallographic orientation in the simulation of dendrite growth. It was confirmed that the modified model is capable of predicting the fraction of eutectic and the distribution of the eutectic region in alloy castings, with limited diffusion in the solid into account.

Li et al. [128] used the Lagrangian front tracking method [129,130] to study the formation of the crystal on a rock surface immersed in a saturated solute. A series of 2D and 3D simulations were performed for different conditions.

Recently, in 2014, Reuther and Rettenmayr [131] have simulated the dendritic solidification using an anisotropy-free meshless front-tracking method. The method is capable to completely remove the grid anisotropy effects common to moving interface problems. The particles track the interface directly and are embedded in the irregular grid by associating each tracking particle with a pair of grid nodes of different phases. The results demonstrate that the meshless front tracking method is able to represent anisotropic interface dynamics correctly and is also suitable for the simulation of the interaction of solidifying dendrites with varying orientations. This same approach has been taken up in another publication before by the same authors for phase transformation problems [132].

More recently, Hu et al. [133] used the front tracking data structure and functionality to track the phase transition interface accurately in both 2D and 3D domains with complex and changing interface geometry and topology. The numerical scheme used for this simulation is explicit to accurately track the dendritic growth. The results show that the tracking method gives high resolution to the dendritic structure.

Before proceeding to the second class of numerical studies (implicit tracking), the numerical study of Almgren [134] has to be mentioned. Almgren also used the principle of explicit tracking method of the interface, along with an efficient, and practical variational formulation for computing dendritic solidification. The formulation is based on minimizing energy functional made up of the bulk and surface energy contributions to track and determine the shape of the liquid-solid interface. The minimization techniques were developed earlier by Bellettini, Paolini, and Verdi [135]. Computations with isotropic and anisotropic were performed, neglecting the kinetic effect on the

interface. Almgren found that, in contrast of the isotropic case, the large scale structure which ultimately develops has absolutely no memory of the initial geometrical conditions.

These explicit front tracking methods have two main disadvantages. First, the topological changes need a special care to be handled. Second, they are usually not easy to be extended to 3D simulations. Hence, implicit tracking strategies have been formulated to overcome these drawbacks.

In implicit tracking methods, the interface is expressed implicitly using some auxiliary variables defined on every grid cell of the whole region, for which values are ranging usually between zero and unity. A zero value indicates that the cell point is completely solid; a unity value indicates that the cell point is completely liquid; and accordingly a value between zero and unity indicates that the grid cell is in the vicinity of the solid-liquid interface. In contrast to the front tracking methods, these "order parameter methods" can easily handle the complex topology since there is no need to explicitly track the interface and the calculation can be carried out on a fixed grid. However, the difficulty of these methods is in appropriately relating the parameters in the evolution equation of the order parameter to the phenomenological parameters describing the problem such as surface tension and curvature, for example. Basically the application of these methods requires some appropriate differential equations to describe both the conservation of energy at the interface and the evolution of the order parameter in terms of the other physical and geometrical parameters. Several available numerical methods, based on this second way of tracking the interface, are found in the literature: the main ones are reviewed in the following sections.

III.2.4.2. Enthalpy methods

The first and most basic order parameter method is the enthalpy method. In this approach, single energy conservation equation for the whole domain, solid and liquid, is expressed in terms of enthalpy – the sum of latent and sensible heats. Solutions can be obtained on a fixed space grid and the interface is tracked by means of the liquid fraction f, where $0 \leq f \leq 1$. The enthalpy method has received widespread use in industrial applications, where the phase change occurs over a restricted temperature range and the solid-liquid interface can be described as a mushy zone. This method has first been proposed for one dimensional cases of tracking a phase change region by Voller et al. [136]. Since then, several studies have been reported, Voller and Cross [137,138] have developed algorithms for interpreting numerical enthalpy results such that accurate tracking of a phase change in one dimension may be achieved. Voller and Shadabi [139] have investigated these enthalpy techniques for dealing with phase change problems in two dimensions. Voller and Swaminathan [140] have presented a general implicit source-based enthalpy method dealing with metallurgical solidification problems. The difference with the previous schemes is the consistent linearization of the discretized source term, which ensures its optimal convergence on all problems. A review can be

found in the work of Voller, Swaminathan, and Thomas [141]. Later, Voller and Swaminathan [142] have derived a general enthalpy method that includes both apparent heat capacity and source based methods. Date [143-145] has also reviewed some of the earlier methods and identified their shortcomings. He has presented an enthalpy formulation (strong enthalpy formulation) that eliminates the problem of prediction of unrealistic temperature histories, and allows use of an efficient line-by-line numerical integration algorithm.

Tacke et al. were the first to apply the enthalpy method to solve dendritic growth problems [146,147]. They used a three-dimensional finite difference formulation for the enthalpy equation. They concluded that dendritic structures of a supercooled pure melt are reproduced with this algorithm with some limitations. Few years later, Mackenbrock and Tacke [148] have presented a new formulation for numerical modeling of coupled phase transformation. The technique is an extension of the conventional heat diffusion enthalpy method and uses the control volume approach. The scheme is found general enough to cover an unrestricted number of species and phases in various systems and is appropriate for three-dimensional modeling. This algorithm was applied to a dendrite growth problem with metastable phase. Although many simplifications were involved, non-isothermal phase change with simultaneous diffusion of heat and species was described, which has not been previously possible.

Pal et al. [149] have then presented an enthalpy-based simulation for the evolution of equiaxial dendrites, growing in a supercooled melt of a pure substance. The enthalpy formulation is modified appropriately by combining relevant macro-scale and micro-scale features. The simulation results for dendritic growth under various conditions were presented, and compared with those employing other models found in the literature, and good qualitative agreement is observed. That shows that the model is capable to produce the dendritic growth features. Closely related work is done by Chatterjee and Charkraborty [150], that combines the enthalpy method with lattice Boltzmann methods to simulate convection-diffusion transport processes pertinent to melting/solidification problems. By comparing obtained results with other standard methods, they showed that the proposed technique is computationally more convenient to be implemented for solving complex phase boundary problems involving, for example, dendritic growth in a supercooled melt of pure materials.

A fixed grid enthalpy method has been developed for the simulation of dendritic growth in a supercooled binary alloy melt [151,152]. It is shown that the method can be readily extended to account for binary alloys and the presence of multiple grains and that this approach can predict dendrite shapes. However, a potential weakness in the method is the loss of resolution for the calculation of interface curvatures when the grid size decreases below the size of the expected tip radius. However, a real strength of the method is its low computational cost as it limits the iterative process to the narrow band of nodes in the phase change region. This feature allows the proposed method to predict physically feasible dendritic morphologies for a very modest computer time. This

method was later shown to be easily and straightforwardly modified to model, in a general solidification system, the curvature of the interface, the speed of the interface, and the redistribution of solute phases, of which the phase change temperature may depend [153].

More recently, a numerical method based on the well-established enthalpy technique, has been developed by Bhattacharya and Dutta [154] to simulate the growth of binary alloy equiaxed dendrites in presence of melt convection. It laid the foundation to develop effective multi-scale solidification. In addition, it is shown that another model using the basic structure of an enthalpy based method can be extended to include micro-structural phenomena such as growth of dendrites.

Three other methods developed for dendritic solidification simulations, which are also based on the use of an auxiliary variable defined in the whole region, are: (1) "volume of fluid", (2) "level set", and (3) "phase field". However, the main difference between these methods and the enthalpy method is that they consider the energy equation only with temperature as the dependent variable, hence, no direct relationship between enthalpy and temperature is required.

III.2.4.3. Volume of fluid method

The volume of fluid method (VOF) is the least common method for the simulation of solidification problems among the three above-mentioned methods. López et al. [155] were the first to use a numerical procedure that essentially relies on a VOF-type method to simulate dendritic growth during solidification of pure metals. To solve the energy equation, they used a diffuse interface method which avoids the need of applying thermal boundary conditions directly at the liquid-solid front. The thermal gradients on both sides of the interface, which are essentially needed to accurately obtain the front velocity, are calculated with the aid of a distance function and the interface curvature is computed using the height function technique [156-159]. The distance function is obtained at every time step by computing the exact distances from the computational cells surrounding the interface to the reconstructed interface segments (polygon in 3D). The advection equation of a discretized solid fraction function, which is equal to one in solid cells, zero in liquid cells and has a value between zero and one in interfacial cells, is solved using the unsplit VOF advection method proposed by López et al. few years earlier [160]. The numerical results obtained with the proposed model have been compared with analytical solutions and numerical results obtained by other authors for the formation of complex dendritic structures in two and three dimensions. The good degree of agreement found demonstrates that the volume of fluid method may be considered a suitable method for the simulation of dendritic solidification processes. In 2013, López et al. [161] improved the accuracy and computational efficiency of the VOF method proposed in their last work to simulate the dendritic growth of pure metals by using a two-grid approach, which involves a uniform Cartesian grid (main grid) to solve the energy equation and an adaptive Cartesian grid of higher resolution (fine grid) for

the interface representation. This approach presents a certain analogy with the front-tracking approach (described and used by Juric and Tryggvason [95]). Once again, when the results are compared to analytical solutions and numerical results obtained with other methods, a very good agreement was found.

III.2.4.4. Level set method

The second method considered herein is the level set method that generally uses a level set function in order to track the interface. The main idea behind this method is that a level set function is defined in the whole region, and that the moving interface is represented by the zero level set contour of this function. This type of methods is found to be well suited for modeling time dependent moving boundary problems. The level set method, based on Hamilton-Jacobi formulation, has been first introduced by Osher and Sethian [162]. Since then, it has been applied to numerous problems [163-165]. Sethian and Strain [166] were first to use this method to numerically compute the motion of the solid-liquid boundary in crystal growth. Their method combined a level set approach with a boundary integral formulation of the problem. Although their numerical results correctly described the evolution of complex crystalline shapes and some realistic phenomena (dendrite formation and side-branching), their method is found to be somewhat complicated and computationally expensive. Hence, Chen et al. [167] have proposed a simpler level set approach. They avoided using a boundary integral method to compute the normal velocity at the interface and reinitialized the level set function at every time step (following the work of [165]). This method represents an improvement upon the Sethian and Strain's method because it retains all the advantages of using a level set approach without any of the complications and restrictions that arise from employing a boundary integral method. For complex structures, it is shown that the method was able to handle topology changes (merging) and complicated interfacial shapes (side-branching, and dendritic fingering), and converges when appropriate amounts of surface tension and kinetic effects are included for dendritic structures. Few years later, Kim et al. [168] improved the approach described by Chen et al.: they computed the velocity with more accuracy. Their work demonstrates that, in addition, results obtained by the level set method for dendritic growth are in good agreement with those predicted by microscopic solvability theory. In both [166] and [167] the discretization of temperature near the interface produces a non-symmetric matrix that needs to be inverted for implicit time stepping. The lack of symmetry makes this approach computationally expensive. Gibou et al. [169] have exploited the second order accurate symmetric discretization of the Poisson equation. This symmetric discretization has been presented by the same authors in [170] which was originally developed in [171] inspiring by the ghost fluid method [172]. Applying this discretization technique to the temperature field near the interface allows one to use a robust and efficient Preconditioned Conjugate Gradient (PCG) [173] method to invert the constant coefficient matrix resulting from the implicit discretization in time. Gibou et al. [169] showed that this new algorithm converges to some known exact solutions, and

can be used to simulate complex interfacial shapes of dendritic solidification of a pure melt.

Fried [174] has described a new finite element algorithm for the two-dimensional Stefan problem, where the free boundary is represented as a level set. This allows easily handling topological changes of the free boundary. The accuracy of the algorithm is verified and its capability is illustrated by numerical results for the isotropic and the anisotropic mean curvature flow of level sets. One year later, Yang and Udaykumar [175] have developed a simple-to-implement formulation for phase change calculations, maintaining the global second order accuracy. This formulation is a combination of a level set method to track the sharp interface, and the finite difference solver. The simulation results showed excellent agreement with two-dimensional microscopic solvability theory for pure material solidification. For both cases pure melts and binary solutions, the method is showed to be able to produce accurate solidification simulations.

Tan's group has been interested in dendritic growth formation modeling using the level set method [176-179]. In [178], they provided a new approach combining features of front tracking and fixed-domain methods. The numerical results have demonstrated that this approach can be an accurate and computationally effective tool for modeling dendritic solidification. Extension of this work to multi-phase and multi-component alloys is presented in [179]. Further, in [177] the same method has been extended in order to study interactions between multiple dendrites during solidification in both 2D and 3D. By using markers to identify different crystals, the method was able to study the interaction between multiple dendrites with a single signed distance function. Accuracy of the proposed approach was demonstrated with some convergence studies.

Later, an efficient multi-mesh h-adaptive finite element algorithm to solve the level set method of dendritic growth in a pure supercooled melt was proposed by Di and Li [180]. In this approach, the thermal field variable and the level set function were approximated on different meshes. The level set function is resolved by an h-adaptive mesh with refinement only around the interface. The proposed method achieved the similar accuracy as the front tracking methods with about the same degrees of freedom, and is found to be efficient and able to simulate the dendritic crystallization in both two and three dimensions cases.

In 2014, the level set method, proposed earlier by Gibou's team, was extended to the simulation of the solidification of binary alloys by Theillard et al. [181]. They have produced numerical results that exhibit an excellent agreement with theoretical results. Plus, it was shown that the proposed method can reproduce a wide range of growth, from planar to cellular to dendritic growth.

III.2.4.5. Phase field method

The last considered method in the proposed classification of numerical methods is the phase field method. This method is the most popular to simulate the phase change processes, in particular, the solidification process. Hence, it is found to be one of the most powerful tools to simulate dendritic growth. The main idea behind this method is the introduction of the "phase field" variable, which defines the physical state (liquid or solid) of each grid point of the system in terms of position and time. The interface between liquid and solid phases is described by smooth but extremely localized transitions of this additional variable between values representing liquid and solid states. It is worth noting here that, phase field model is basically classified also as diffuse interface models, for which the interface is described as, in contrast to front tracking methods, a smooth region with no-zero thickness depending on computational grid spacing. The interface thickness of phase field model limits therefore its simulation scale, and quantitative simulation results need quite small grid spacing in order to be performed. Consequently, relatively large computational cost is required to obtain realistic quantitative studies basing on this approach. On the other hand, phase field model avoids explicit tracking of the interface, and can easily handle topological changes at the interface. The development of the extra field equation which is required to describe the evolution of the phase field variable borrowed ideas from earlier related physical problems [182-184]. The origin of phase field model for solidification of pure materials comes from the efforts in 80's by Langer [185] and Caginalp [186]. A significant development and analysis of a phase field model for first-order phase transitions has been done by Caginalp [187,188]. The inclusion of anisotropic effects into this model was also first done by Caginalp's group [189,190]. Since then, several studies using the phase field model have been carried out for simple geometries in 1D or 2D [190-192]. Furthermore, in 1993 dendritic crystal growth simulations employing a phase field model were performed by Kobayashi [90]. He presented a two-dimensional simple phase field model for one component melt dendritic growth including anisotropy in a certain form. He simulated the evolution of branchful dendritic structures growing into a supercooled melt. He concluded that the model used is very good for the simulation of dendritic crystal growth. Nevertheless, it still involves several problems. First, the phase field variable cannot describe a structure which is finer than or the same size as the layer thickness. Second, a computational problem is found, which comes from the fact that one of the governing equations includes small parameters. Later, he has extended his method to simulate three-dimensional dendritic structures [193]. Although the weak accuracy of phase field model behavior while dealing with some particular cases, Kobayashi's works demonstrated the potential and the capacity of the phase field model to simulate complicated, and realistic dendritic solidification structures.

Later, a phase field model described by Wang et al. [194] was used to investigate the associated important aspects for dendritic growth from a supercooled melt [195] and for the treatment of a non-isothermal binary alloy [196]. They were able to produce qualitatively realistic dendritic phenomena as the development of secondary and

tertiary dendrite arms, showing that the results were of the correct general character. Additional two-dimensional computations were performed using this model, in order to demonstrate that the phase field model can be used to simulate observed behavior in dendritic growth experiments [197]. The authors have successfully simulated for growth into a supercooled melt, the cleaving event for which an evolving solid seed splits forming two competing branches. Later, Braun and Murray [198] have carried out computations of the solidification of a pure material on adaptive meshes. Good convergence to sharp interface models (front tracking methods) is achieved for fixed small supercooling.

Karma's group has been interested in developing the phase field model for the simulation of dendritic growth due to observed limitations of other models [199-206]. Karma and Rappel [199] have developed the phase field approach, in order to perform 2D computations with a smaller capillary length, and to obtain a Gibbs-Thomson condition even without interface kinetics in the sharp-interface limit. In [202], they demonstrated that quantitative modeling of 3D dendritic growth was also possible using their proposed phase field methodology. Then, Plapp and Karma [204] have combined a multi-scale finite-difference Monte-Carlo method with the previously developed phase field formulation of the interface dynamics and demonstrated that it can accurately simulate three-dimensional dendritic growth in a previously unreachable range of low supercoolings which is of direct experimental relevance. Further, the effects of melt flow on the growth velocity, shape, and side-branching dynamics of single dendritic crystals growing into a supercooled melt were quantitatively investigated in two dimensions using the phase-field method [205-206].

Nakabeppu and Hijikata [207] studied the dendritic solidification and various pattern formations in solidification by phase field model by changing conditions such as surface tension, degree of supercooling, and anisotropy. Tonhardt and Amberg [208] have simulated the 2D dendritic growth in a shear flow using the phase field method too. The melt was assumed to be flowing due to an applied shear stress far away from the wall. It was found that the dendrite is asymmetric, due to the fluid flow which alters the local heat transfer at the solidification front. Using an adaptive grid refinement, the effect of fluid flow on 3D dendritic growth is described in [209]. Numerical simulations of isothermal dendritic growth of Fe-C alloys were performed using the phase-field model [210]. Authors obtained realistic solidification patterns at different temperatures and alloy compositions. A double grid method for efficient computation complex dendritic pattern evolving in a large scale solidifying system of pure supercooled melts was also presented by the same group [211]. Computations showed that the complex dendritic patterns with well-developed tertiary arms can be obtained even on a personal computer with a moderate memory space. Then, this approach has been extended to ternary alloys applying a dilute solution approximation for the free energy density [212]. The results showed good agreement with those of Clyne-Kurz equation. And the simulation of the microstructure evolution during rapid solidification was successfully carried out [213]. Further, the complete shape of dendrites grown in regimes of high

supercooling has been studied by means of a phase field model [214]. The results offered some new insight into the understanding of a fully developed dendrite.

Efficient adaptive phase field simulation was carried out for a free dendritic growth of a binary alloy (nickel/copper) by Lan et al. [215]. This scheme allowed large domain simulation of thermal boundary layer, while keeping fine mesh near the diffuse interface. The smallest cell size near the interface was smaller than their previous ones, while the domain size was several orders larger. They obtained a truly free growth simulation for the first time for a non-isothermal dendrite. George and Warren [216] have described an implementation of a parallel finite-difference phase field algorithm for 2D and 3D simulations of alloy solidification. The ability to explore 3D dendritic growth with high-resolution is demonstrated using this algorithm. Later, a new finite-element formulation was proposed by a slight modification of the phase field algorithm used for dendritic growth modeling where both the phase field and the temperature were discretized [217]. The 2D simulations illustrated the performance and the accuracy of the proposed method. A finite-element phase field method was then developed by Slavov et al. to model the 2D free dendritic growth into supercooled melt [218]. A second order modification of the Runge-Kutta method with automatic choice of the time step was used here to solve the resulting differential equations in time. The results for the dimensionless dendritic tip velocity, of a spherical seed for isotropic and different kinds of anisotropy cases, were compared with results from the microscopic solvability theory and with numerical results [206], in order to demonstrate reliability of the proposed method. In this same year, some computations for free dendritic growth in alloys [219] were performed to test standard theorical models: Lipton, Glicksman, and Kurz (for details see [220, 221]) or Lipton, Kurz and Trivedi (see [222]). The phase field model, which was used here, was derived earlier by the same authors and co-workers in [223]. It was found that the obtained results for the dendrite tip growth Péclet number were in good agreement with both of two theories predictions if the tip radius is based on a parabolic fit to the actual dendrite shape and the capillary supercooling is neglected.

Further, the effect of the fluid flow on 3D free dendritic growth of a pure material into a supercooled melt was investigated using the phase field model [224]. By comparing the results with some other results, with and without fluid flow, the predicted growth Péclet numbers as a function of the flow Péclet number were found to be in good agreement with the theoretical predictions in some cases. Shih et al. have presented [225] a simple approach in order to help quantitative phase field simulation for dilute-alloy solidification dendritic growth. In order to test the feasibility of this model, they have simulated a free dendritic growth from a small nucleus, and a good agreement with Karma's model [205] was obtained. Additional quantitative results in multi-component alloys using phase field model can be found in [226]. For several technical alloys, Bottger et al. have been interested in using phase field model coupled to thermodynamic databases to simulate the equiaxed solidification [227]. It has been shown that the proposed method can be a valuable tool for that purpose. In this same

year, the effect of the ratio of solid to liquid conductivity on the side-branching characteristics of dendrites in a pure supercooled melt within a phase field model of solidification was examined by Mullis [228]. He found that high thermal conductivity in the solid favors extensive side-branching while low thermal conductivity appears to strongly suppress side-branching. One year later, Hu and Chen [229] employed the phase field method to simulate the growth of dendrite in supercooled pure metal in order to obtain the optimized values of some parameters. Results showed that with the increase of supercooling rate and the coupled coefficient, the equiaxed dendrite exhibits a morphology involving more developed side-branching. Moreover, the modified dendrite can be observed with high anisotropy level.

Most previous studies revealed the knowledge that the phase field method requires high mesh resolution at the interface thus making the use of adaptivity essential, especially for fast evolving interfaces in order to correctly capture the physics of the phase transformation. Consequently, several algorithms, using an adaptive mesh near the interface for example, have been proposed. Do-Quang et al. [230] have proposed a parallel adaptive finite element scheme, in which the exchange of information was minimized and less memory was used. This parallel adaptive algorithm was successfully implemented in the numerical simulation of dendritic growth. Based on such ideas, Narski and Picasso have presented numerical results for the solidification of binary alloys in two [231] and three [232] dimensions. The numerical results showed that the method is effective and allows performing complicated simulations with relatively few computer resources needed. Do-Quang and Amberg [233] have later used a semi-sharp phase field model to simulate the two-dimensional evolution of free dendritic crystal growth in a gravity environment. This model was introduced by Amberg [234]. The main idea behind the model is the use of two different meshes: one is a fixed background mesh, which covers the whole domain; the other is an adaptive mesh, where the node points are modified as the solid particle evolves. It was found that the shape and the symmetry of the dendritic solidification depend on the growth orientation of the dendrite and the Prandtl numbers. In this same year, Wang et al. [235] have presented an efficient r-adaptive mesh algorithm for the phase field model of dendritic growth of pure substance in both two and three dimensions. The novel aspect of the proposed method was the choice of a regularized monitor function; which was found to be an important factor for enhancing the efficiency and quality of the moving mesh simulations. The moving grid method enabled them to obtain accurate numerical solutions with much less degree of freedoms and smaller costs than the previous studies. The produced results of 2D and 3D dendritic structures demonstrated that the method has the potential to simulate more realistic physical problems with less computing resources. The selection of spacing in directional dendritic solidification was investigated numerically by Steinbach [236] using the phase field method in two and three dimensions. The results demonstrated that a sharp minimum or critical spacing of a dendritic array exists depending on the anisotropy of the solid-liquid interface energy. At this critical spacing, both competing mechanisms cancel each other out and a stable

growth solution is not possible. Steinbach [237] has shown also later that in the presence of melt convection driven by solutal buoyancy using the phase field model, there was a significant effect of solutal buoyancy on the spacing of dendritic arrays and that the phase field method can be successfully applied to perform virtual solidification experiments under combined diffusive-convective conditions.

Furthermore, the qualitative effects of the surface tension anisotropy on dendritic growth, during isothermal alloy solidification, were investigated by Wang et al. [238] using the phase field approach. The simulation results indicated that the side-branching is strongly affected by the surface tension anisotropy. Indeed, with large surface tension anisotropy a branchless needle crystal was obtained, while with small anisotropy side-branches appeared clearly behind the dendrite tip. Later, Chen and Lan [239] have presented an efficient adaptive 3D phase field simulation for dendrite crystal growth from a supercooled melt. At a wide range of supercoolings, the simulated results were found to be in good agreement with the Ivantsov solution and the obtained shapes were with experimental observations. Same authors examined one year later in another study [240] the effect of natural convection for various supercoolings on free dendritic growth. They found that at lower supercoolings, the dendrite growth is more sensitive to the gravity level, which is consistent with the thermal convection theory for dendritic growth proposed by Ananth and Gill [241]. Furthermore, a multi-mesh adaptive finite element approximation of phase field model for simulating the dendritic growth in two and three dimensions was proposed by Hu et al. [242]. The authors have shown that this technique was useful in solving phase field models and can save significantly the computation time. The effect of density change between solid and liquid phases on free dendritic growth of a pure material into a supercooled melt was investigated by Sun and Beckermann [243] using phase field simulations. They noted that the density change should generally be taken into account when analyzing dendritic growth. Further, based on the adaptive finite element method, the free dendritic growth including capillary anisotropy was simulated using the phase field model by Zhao and Li [244]. It was shown that the dendritic growth depends sensitively on the degree of the capillary anisotropy of the solid-liquid interface; as the anisotropies were enhanced, the dendrite tip growth velocity increased, but the dendrite tip radius decreased. Quantitative numerical simulation of 3D dendritic growth in pure supercooled melt was carried out based on phase field approach by Zhu et al. [245]. Incorporating interfacial energy anisotropy, they have faithfully described the dendritic growth, and proved that it was feasible and effective to simulate three-dimensional dendritic growth using phase field method. In addition, Tóth and al. [246] have used the phase field model to address polymorphism, crystal nucleation and crystal growth in the diffusion-controlled limit. The growth rate was found to be time dependent and anisotropic; this anisotropy depended on the driving force. Further, large-scale simulations starting with seeds lead to the formation of dendritic structures. In addition, Zhu and Wang [247] have carried out some quantitative numerical simulation of 3D dendritic growth in pure supercooled melt based on phase field model of thin interface limit and incorporating interfacial

energy anisotropy which was solved by an accelerated arithmetic algorithm of the dynamic computing regions (AADCR). The dendritic growth was successfully implemented and truly described. They found also that the use of AADCR could decrease significantly the computational time (70% for a 3D domain of size 300×300×300 grids, for example).

Recently, Lin et al. [248] have developed an adaptive 3D phase field model to treat dendritic crystal growth of highly anisotropic materials. They concluded that the development of facets with the anisotropy was quantified and explained by the increase of the fraction in the {1 1 1} faces in consuming the {1 0 0} and {1 1 0} faces, and from the other hand that at high anisotropy the dendritic growth was preferred at low supercooling. Wang et al. [249] have investigated, the effect of supercooled melt forced laminar flow on dendritic growth, using the phase field method by incorporating melt convection. The considered flow is perpendicular to dendritic growth direction. They concluded that, when melt flow is considered, the secondary dendritic arm in upstream looked like shred and the spacing of them becomes small, and that the growth velocity of the dendritic tip perpendicular to the flow was higher. Yamanaka et al. [250] have presented a solution of the phase field simulation for dendritic solidification of a binary alloy on graphic processing unit (GPU). The performance test clearly demonstrated the feasibility of accelerating the phase field simulation using GPU; this performance is 100 times faster than that by a singly CPU core. Consequently, the proposed GPU-accelerated phase field simulation makes it possible to enable performing a real-time, quantitative and three-dimensional microstructure simulation on an inexpensive personal computer. In the same year, Li and al. [251] have proposed an operator splitting technique for phase field simulations of dendritic growth solidification of a pure substance in both two and three dimensions. This technique allowed the use of a sufficiently large time step without the technical limitations. They have split the governing phase field equation into three parts; the first equation is calculated by using an explicit Euler's method. The second is a heat equation with a source term and is solved by a fast solver such as a multi-grid method, and the third is a nonlinear equation and is evaluated using a closed form solution. The obtained results were in good agreement with previous numerical experiments, and have shown that the proposed technique is fast, robust, and accurate. Pan and Zhu have developed a quantitative phase field model with an anti-trapping current to simulate the dendritic growth [252]. The convergence test with respect to the interface width exhibited an excellent behavior for the proposed model. The performance of the model was then compared with predictions of the Gibbs-Thomson relation, and of the linearized solvability theory, demonstrating that the proposed model can quantitavely describe dendritic growth with various solid diffusivities. A phase field approach to simulate Al-Si binary alloy solidification was proposed [253] in order to investigate the effect of force flow on the dendrite growth. It was found that the dendritic growth symmetry was broken; indeed the growth velocity of the upstream tip was faster than the downstream tip.

More recently, a phase field modeling of multi-crystalline crystal growth involving an anisotropic surface free energy was implemented [254]. The anisotropic interfacial free energy was proposed as a new anisotropic function having a simple parameter m in the phase field model. Both 2D and 3D Comparisons between this anisotropic function with the original fourfold symmetry function from Kobayashi [90] have been performed; they were found to be consistent, although some discrepancy existed due to the second derivative term of the interfacial free energy. Du et al. [255] have proposed a phase field model with forced liquid metal flow to study the effect of boundary heat flux on the dendritic structure forming of a Ni-40.8%Cu alloy with liquid flow. They found that the forced liquid flow could significantly affect the dendrite morphology: first, the primary arm growing in horizontal direction was lopsided due to the forced liquid flow introduced at the initialization; second, they have found that there was a transition of development patterns of the secondary arms with increasing the heat extraction at the boundary, and with increasing initial liquid flow. Xie et al. [256] studied the evolution of secondary dendrite arms of Fe-0.3 wt% C alloy during transient directional solidification by means of phase field method [256]. They found that the secondary arms undergo a ripening process in which other secondary arms remelt by shrinking from their tips, rather than by detachment from the primary stalk. The surviving arms were finer than those found under steady-state growth conditions, and their size decreased with decreasing growth velocity. Once again the phase field method based on GPU showed its highly computational efficiency in the study of dendritic growth done by Zhu et al. [257]. In this study, the calculated values of the dendritic tip velocities and the tip radius on the GPU were identical with the values of the microscopic solvability theory and the references simulation results. Further, the quantitative effect of supercooling degree on the microstructural dendritic growth pattern in directional solidification process was studied for an Mg-Al binary alloy using phase field model [258]. The obtained results indicated that as the supercooling degree increases, the dendrite tip radius and second dendrite arms became smaller, and the crystal structure was found to be more uniform and dense. The morphological transition of the crystal growth of equilibrium crystal shape, dendrite, and spherical crystal shape were simulated by using the phase field crystal model [259]. The pattern selection of dendritic growth in the diffusion controlled regime under low-crystal-growth velocities was found to be given rise by the competition between interface energy anisotropy and interface kinetic anisotropy. They also constructed a morphological phase diagram of crystal growth as a function of the phase field crystal model parameters. Plus, the microstructural evolution during the solidification with lateral constraints was investigated using a phase field model [260]. It was found in [260] that the lateral constraints have a significant effect on the microstructure formation during solidification that is a cellular dendrite transition could be achieved with lateral constraints, and that the solute segregation was also influenced due to the confinement effect of lateral constraints.

Very recently, there is already fair number of articles that appeared in SCOPUS using phase field model to study some dendritic growth features [261-264]. This demonstrates the major interest of the method in improving crystal growth modelling. Zhu et al. [262] have studied the dendrite growth under the condition of forced flow using a phase field model of pure material combined with the projection algorithm. Plus an efficient adaptive finite element method was applied to reduce the computational cost. They found mainly that the symmetry of dendrite shape was collapsed with the increase of the flow velocity; while with a low velocity, the effect of the forced flow on the dendrite morphology was slight. That proves that the dendritic crystal growth during solidification is a very active domain, and there is still many features and various aspects need to be explored or explained.

III.2.5. Conclusion

In this review paper, the available theories of dendritic growth are first reviewed. The formation of dendritic crystals can be provided by two different processes occurring simultaneously: (1) the steady-state propagation of the dendrite tip, accounting for the formation of the main primary stem, resolved first by Ivantsov for parabolic shape, and (2) the time-dependent formation of the secondary and tertiary side branches. The dendritic growth involves therefore wide range of time and length scales.

An appropriate mathematical modeling for the dendritic growth must handle the different difficulties involving the interfacial physics between the two phases in the boundary conditions. For pure substances, these difficulties include the understanding of the heat transfer from the interface through the two phases, the curvature effect of a non-plane interface, the kinetics effects when large supercoolings are considered, the anisotropy of both surface tension and kinetic mobility especially for highly anisotropic materials, and, finally, the discontinuity of properties between the phases. When the appropriate boundary conditions are coupled with the energy equations in both liquid and solid phases, they are assumed to offer a complete mathematical model of complex dendritic solidification.

The complete mathematical model is non-linear and complex and thus calls for numerical solutions involving more or less sophisticated mathematical techniques. Otherwise, analytical solutions are limited to the cases embedding limiting simplifying assumptions. For this reason, several numerical methods were proposed, and continue to be developed to find satisfying numerical solutions for various conditions real growth conditions.

These methods can be classified into two major classes according to the way they track the liquid-solid interface: Front Tracking and Order Parameter methods.

The front tracking methods track explicitly the interface using a lower dimension deforming grids that evolve with the interface on a fixed global mesh. They classically classified also as sharp interface methods; the described interface has no thickness while

using these methods. These methods have various advantages. They are characterized by their relatively small computational loads and they can be easily used in order to provide quantitative studies of dendritic growth features. However, they need special care for topological changes, and are not easy to be extended for three dimensional cases.

On the other hand, there are some implicit representations which represent the front as a special value of an order parameter. Consequently, the topological changes are easily handled in a straightforward fashion. These methods can be easily implemented in both two and three spatial dimensions. However, basing on these numerical methods, an additional appropriate equation, which describes the additional variable evolution, is generally needed to provide a complete mathematical formulation. They require also a large computational capacity, especially in order to provide quantitative studies, unless they are coupled with some efficient adaptive techniques.

A compromise has to be done when choosing the relevant numerical method for a specific application. This compromise mainly includes the following considerations: the available computational capacity, the purpose of the study, the geometry (2D or 3D), the required level of accuracy, the substance or substances involved, and finally the magnitude of property discontinuities at the front of solidification.

It is worth noting finally that despite the large volume of literature dealing with dendritic growth, the problem is still not completely understood. Numerical investigations have had only limited success when assessed against experiments. That is due mainly to the difference between length scales, and the complex interaction between the physical effects of many parameters involving the solid-liquid interface evolution during the dendritic growth.

References

[1] Fleury V., Gouyet J. F., and Léonetti M. *Branching in Nature*. Springer: ISBN 10: 3540418881. Berlin. (2001).
[2] Langer, J. *Chance and Matter: Les Houches*. Elsevier Science. Amsterdam. (1987).
[3] Feder J. *Fractals*. Plenum. New York. (1988).
[4] Matsuyama T., and Matsushita M. Critical Reviews in Microbiology. Vol. 19: 117-135. (1993).
[5] Stefanenscu D. M. *Science and Engineering Casting Solidification*. Springer. New York. (2009).
[6] Augustithis S. S. *Atlas of the Textural Patterns of One Minerals and Metallogenetic Processes*. De Gruyter. Berlin. (1995).
[7] Akyurt M., Zaki G., Habeebullah B. Energy Conversion and Management. Vol. 43: 1773-1789. (2002).
[8] Callen, H. B. *Thermodynamics. J*. Wiley. New York. (1960)
[9] Turnbull D. Phase Changes in *Solid State Physics*. Academic Press. vol 3: 225-306. New York. (1956).
[10] Turnbull D. *The undercooling of liquids*. Scientific American. (1965).
[11] Claudiu A. S., Gregory F. S., Sergey S. S., Michinao H.,a Mihai I., Benjamin J. W. and George M. W. RSC Publishing. Vol. 9: 2253-2408. (2009).
[12] Molinero V. AIP Conference Proceedings. AIP Publishing. 1527: 82-88. (2013).
[13] Pruppacher H. R. pure and applied geophysics. Vol. 104, no 1: 623-634. (1973).
[14] Okawa S., Saito A., Minami R. International Journal of Refrigeration. Vol. 24: 108-117. (2001).
[15] Heneghan A. F., Wilson P. W., and Haymet A. D. J. Proceedings of the National Academy of Sciences. Vol. 99, no 15: 9631-9634. (2002).
[16] Singer H. M. Physical Review E. Vol. 73, no 5: 051606. (2006).
[17] Karma A. *Dendritic growth*. In *Branching in Nature*: 365-402. Springer Berlin Heidelberg. . (2001).
[18] Farid M.M., Khudhair A.M., Razack S.A.K., Al-Hallaj S. Energy Convers Manage. Vol. 45:1597–1615. (2004).
[19] Sharma, A., Tyagi, V. V., Chen, C. R., Buddhi, D. Renewable and Sustainable energy reviews. Vol. 13: 318-345. (2009).
[20] Goldenfeld N. Journal of Power Sources. Vol. 26: 121-128. (1989).
[21] Bejan A. *Shape and structure, from engineering to nature*. Cambridge university press. (2000).
[22] Kepler J. *De Nive Sexangula*. Godfrey Tampach, Frankfurt am Main. (1611).
[23] Kreith F. Principles of heat transfer. 2nd ed. Scranton, PA: International Textbook: 471–477. (1968).
[24] Cheng, K. C., and Seki N. *Freezing and melting heat transfer in engineering: selected topics on ice-water systems and welding and casting processes*. CRC Press. New York. (1991).
[25] Stefan J. Sber Akad Wiss Wien. Vol. 98 :473–84. (1889).
[26] Evans G.W. Quarterly of Applied Mathematics. Vol. 9:185–93. (1951).
[27] Douglas J. Proceedings American Mathematical Society. Vol. 8:402–408. (1957).
[28] Crank J. *Free and moving boundary problems*. Clarendon Press. Oxford. (1984).
[29] Hill J.M. *One-dimensional Stefan problems: an introduction*. Longman Scientific Technical. Harlow. (1987).
[30] Carslaw H.S., Jaeger J.C. *Conduction of heat in solids*. Clarendon Press. Oxford. (1959).
[31] Lunardini V.J. *Heat transfer in cold climates*. Van Nostrand Reinhold. New York. (1981).
[32] Landau H.G. Quarterly of Applied Mathematics. Vol. 8: 81-94. (1950).
[33] Rose M. E. Mathematics of Computation. Vol. 14: 249-256. (1960).
[34] Wagner C. Jounrnal of Electrochemical Society. Vol. 103: 571 . (1956).
[35] Mullins W.W., Sekerka R.F. Journal of Applied Physics. Vol. 34: 323-329. (1963).
[36] Mullins W.W., Sekerka R.F. Journal of Applied Physics. Vol. 35: 444-451. (1964).
[37] Sekerka R. F. Journal of Applied Physics. Vol. 36: 264 (1965).
[38] Voronkov V. V. Soviet Physics, Solid State. Vol. 6: 2378. (1965).
[39] Chan J.W. In *Crystal Growth*. Edited by Peiser H.S.: p. 703. Pregamon, Oxford. (1967).
[40] Coriell S.R. and Parker R.L. In *Crystal Growth*. Edited by Peiser H.S.: p. 703. Pregamon, Oxford. (1967).
[41] Ivantsov G. Doklady Akademii Nauk. SSSR 558: 567-569. (1947).
[42] Papapetrou A. Zeitschrift für Kristallographie. Vol. 92: 89. (1935).
[43] Shibkov A.A., Golovin Y.I., Zheltov M.A., Korolev A.A., Vlasov A.A. Crystallography Reports. Vol. 46: 496-502. (2001).
[44] Shibkov A.A., Golovin Y.I., Zheltov M.A., Korolev A.A., Leonov A.A. Physica A. Vol. 319: 65-79. (2003).

[45] Shibkov A.A., Zheltov M.A., Korolev A.A., Kazakov A.A., Leonov A.A. Journal of Crystal Growth. Vol. 286: 215-227. (2005).
[46] Huang S.-C., Glicksman M.E. Acta Metallurgica et Materialia. Vol. 29: 701-716. (1981).
[47] Huang S.-C., Glicksman M.E. Acta Metallurgica et Materialia. Vol. 29: 717-731. (1981).
[48] Temkin D.E. Doklady Akademii Nauk. SSSR 132: 1307. (1960).
[49] Bolling G.F., Tiller W.A. Journal of Applied Physics. Vol. 32: 2587. (1961).
[50] Triveldi R. Acta Metallurgica. Vol. 18: 287. (1970).
[51] Glicksman G.E., Schaefer R.J. Crystal Growth. Vol. 1: 297. (1967).
[52] Glicksman G.E., Schaefer R.J. Crystal Growth. Vol. 2: 239. (1968).
[53] Holtzmann E.G. Journal of Applied Physics. Vol. 41: 1460. (1970).
[54] Holtzmann E.G. Journal of Applied Physics. Vol. 41: 1469. (1970).
[55] Oldfield W. Journal of Materials Science and Engineering. Vol. 11: 211-218. (1973).
[56] Nash G.E., Glicksman M.E. Acta Metallurgica. Vol. 22: 1283. (1974).
[57] Barbieri A., Langer J.S. Physical Reviews A. Vol. 39: 5314. (1987).
[58] Xu J.J. *Advances in Mechanics and Mathematics*. Springer. Vol. 1: 213. New York. (2002).
[59] Xu J.J. *Introduction of Dynamical Theory of Solidification Interfacial Instability*. Chinese Academy Press. Beijing, China. (2007).
[60] Chen X.J., Chen Y.Q., Xu J.P., Xu J.J. Frontiers of Physics in China. Vol. 3: 1. (2008).
[61] Chen Y.Q., Tang X.X., Xu J.J. Chinese Physics B. Vol. 18: 686. (2009).
[62] Glicksman M.E. Metallurgical and Materials Transactions B. Vol. 43B: 207-220. (2011).
[63] Glicksman M.E. Marsh S.P. In *handbook of Crystal Growth*. Vol. 1B: p.1075. Edited by Hurle D.T.J. North-Holland, Amsterdam. (1993).
[64] Glicksman G.E., Schaefer R.J., Ayers J.D. Metallurgical Transactions A. Vol. 7A: 1747. (1976).
[65] Esaka H., Kurz W. Z. Metall. Vol. 76:127. (1985).
[66] Muschol M., Liu D., Cummins H.Z. Physical Review A. Vol. 46: 1038. (1992).
[67] Losert W., Shi B.Q. Cummins H.Z. Proceedings of the National Academy of Sciences U.S.A. Vol. 95: 431. (1998).
[68] Langer J.S., Sekerka R.F., Fujioka T. Journal of Crystal Growth. Vol. 44: 414-418. (1978).
[69] Langer J.S., Muller-Krümbhaar H. Acta Metallurgica. Vol. 26: 1681. (1978).
[70] Langer J.S. Reviews of Modern Physics. Vol. 52: 1. (1980).
[71] Kessler D., Levine H. Physical Review Letters. Vol. 57: 3069. (1986).
[72] Kessler D., Levine H. Physical Review A. Vol. 36: 2693. (1987).
[73] Kessler D., Levine H. Acta Metallurgica. Vol. 36: 2693. (1987).
[74] Fujioka T. Ph. D. Thesis. Carnegie-Mellon University. (1978).
[75] Sekerka R.F. In *Physical Chemistry in Metallurgy*. Proceedings Darken Conference. US Steel Research Laboratory: p. 311. (1976).
[76] Langer J.S., Muller-Krümbhaar H. Journal of Crystal Growth. Vol. 42: 11. (1977).
[77] Rubinstein E.R., Glicksman M.E. Journal of Crystal Growth. Vol. 112: 84. (1991).
[78] Rubinstein E.R., Glicksman M.E. Journal of Crystal Growth. Vol. 112: 97. (1991).
[79] Gibbs J.W. *On the equilibrium of Heterogeneous Substances*. Collected Works. Vol. 1: 219. Longmans, Green & Co. London. (1928).
[80] Hilton H. *Mathematical Crystallography*. Ch. XI: p. 105. Dover. New York. (1963).
[81] Wulff G. *Mathematical Crystallography*. Ch. XI: p. 109. Dover. New York. (1963).
[82] Tolman R.C. Journal of Chemical physics. Vol. 16: 758. (1948).
[83] Tolman R.C. Journal of Chemical Physics. Vol. 17: 333. (1949).
[84] Shuttleworth R. Proceedings of Physical society. Vol. A63: 444. London. (1950).
[85] Buff F.P. Journal of Chemical Physics. Vol. 19: 1591. (1951).
[86] Herring C. In *Physics of Powder Metallurgy*: p.143. Edited by Kingston R.E. McGraw-Hill. New York. (1971).
[87] Herring C. In *Structure and Properties of Solid Surfaces*. Edited by Gomer R., Smith C.S. University of Chicago Press. Chicago. (1952).
[88] Adam N.K. *Physics and Chemistry of Surfaces*. Oxford University Press. Oxford. (1930).
[89] Glicksman M.E. Journal of Crystal Growth. Vol. 42: 347-356. (1977).
[90] Kobayashi R. Physica D. Vol. 63: 410-423. (1993).
[91] Shibkov A.A., Zheltov M.A., Korolev A.A., Kazakov A.A., Leonov A.A. Crystallography Reports. Vol. 49: 1056-1063. (2003).
[92] Shibkov A.A., Golovin Yu.I., Zheltov M.A. Crystal Growth. Vol. 236: 434. (2002).

[93] Shibkov A.A., Zheltov M.A., Korolev A.A., Leonov A.A. Doklady Akademii Nauk. Vol. 389: 94. (2003).
[94] Shibkov A.A., Golovin Yu. I., Zheltov M.A. Materialovedenie. No. 11: 15. (2002).
[95] Juric D., Tryggvason G. Journal of Computational Physics. Vol. 123: 127-148. (1996).
[96] Alexiades V., Solomon A.D. *Mathematical Modeling of Melting and Freezing Processes*. p. 92. Hemisphere. Washington. (1993).
[97] Alexiades V., Solomon A.D., Wilson D.G. Journal of Non-equilibrium Thermodynamics. Vol. 13: 281. (1988).
[98] Ben-Jacob E., Goldenfeld N.D., Langer J.S., Schön G. Physical Review Letters. Vol. 51: 1930. (1983).
[99] Glicksman M.E., Koss M. B., Bushnell L.T., Lacombe J.C., Winsa E.A. ISIJ International. Vol. 35: 604-610. (1995).
[100] Singer H.M. Physical Review E. Vol. 73. 051606: 1-4. (2006).
[101] Furukawa Y., Shimada W. Journal of Crystal Growth. Vol. 128: 234-239. (1993).
[102] Glicksman M.E. *Principles of Solidification*. Springer. Springer. New York. (2011).
[103] Jackson K.A. *Kinetic Processes; Crystal growth, Diffusion, and Phase Transitions in Materials*. Wiley-VCH. Weinheim. (2004).
[104] Franke H., Lacmann R. Physica status solidi (a). Vol. 55: 415-425. (1979).
[105] Saito, Y., Goldbeck-Wood G., and Müller-Krumbhaar H. Physical Review A. Vol. 38:. 2148- 2157. (1988).
[106] Sullivan J.M., John M., and Daniel R. Lynch. International journal for numerical methods in engineering. Vol. 25.2: 415-444. (1988):
[107] Brush, L. N., and R. F. Sekerka. Journal of Crystal Growth. Vol. 96.2: 419-441. (1989):
[108] Sullivan Jr. J.M., Lynch D.R. Journal of Computational Physics. Vol. 69: 81–111. (1987).
[109] Plapp M., Karma A. Jounral of Computational Physics. Vol. 165: 592–619. (2000).
[110] Udaykumar H.S., Marella S., Krishnan S. International Journal of Heat and Mass Transfer. Vol. 46: 2615–2627. (2003).
[111] Pal D., Bhattacharya J., Dutta P., Chakraborty S. Numerical Heat Transfer B. Vol. 50: 59-78. (2006).
[112] Ramirez J.C., Beckermann C., Karma A., Diepers H.-J. Physical Review E. Vol. 69. (2004).
[113] Zhao P., Ve´nere M., Heinrich J.C., Poirier D.R., Journal of Computational Physics. Vol. 188: 434-461. (2003).
[114] Roosen A. R. and Taylor J. E. Journal of Computational Physics. Vol. 114**:** 113 (1994).
[115] Shyy W., Udaykumar H. S., and Liang S.-J. International Journal of Heat and Mass Transfer. Vol. 36: 1833 (1993).
[116] Unverdi S. O. Ph.D. thesis, The University of Michigan, (1990).
[117] Unverdi S. O. and Tryggvason G. Physica D. Vol. 60**:** 70. (1992).
[118] Unverdi S. O. and Tryggvason G. Journal of Computational Physics. Vol. 100 (1): 25. (1992).
[119] Jan Y.-J. and Tryggvason G. Phys. Fluids, submitted.
[120] Nobari M. R., Jan Y.-J., and Tryggvason G. Phys. Fluids A, submitted.
[121] Nas S. and Tryggvason G. in *AMD 174/FED 175 Fluid Mechanics Phenomena in Microgravity, ASME Winter Annual Meeting,* edited by D. A. Siginer, R. L. Thompson, and L. M. Trefethen, p. 71. (1993).
[122] Peskin C. S. Journal of Computational Physics Vol. 25: 220. (1977).
[123] Jacot A., and Rappaz M. Acta Materialia. Vol. 50: 1909-1926. (2002).
[124] Du, Q., and Jacot A. Acta Materialia. Vol. 53: 3479-3493. (2005).
[125] Al-Rawahi, N., and Tryggvason G. Journal of Computational Physics. Vol. 180: 471-496. (2002).
[126] Zhao, P., Heinrich J. C., and Poirier D. R. International journal for numerical methods in engineering. Vol. 61: 928-948. (2004).
[127] Nakagawa, M., Yukinobu N., and Kenichi O. ISIJ international. Vol. 46: 909-913. (2006).
[128] Li, X. Glimm, J., Jiao, X., Peyser, C., and Zhao, Y. Acta Mathematica Scientia Vol. 30: 377-390. (2010).
[129] Chern I -L, Glimm J, McBryan O, Plohr B, Yaniv S. Journal of Computational Physics. Vol. 62: 83–110. (1986).
[130] Glimm J, Grove J W, Li X -L, Shyue K -M, Zhang Q, Zeng Y. SIAM Journal on Scientific Computing. Vol. 19: 703–727. (1998).
[131] Reuther, K., and M. Rettenmayr. Journal of Computational Physics. Vol. 279: 63-66. (2014).
[132] Reuther, K., and M. Rettenmayr. Acta Materialia. Vol. 60: 2128-2134. (2012).
[133] Hu, Y., Shi, Q., De Almeida, V. F., and Li, X. Chemical Engineering Science. (2014).
[134] Almgren, R. Journal of computational physics. Vol. 106: 337-354. (1993).

[135] Bellettini G., Paolini M., and Verdi C., Convergence of discrete approximations to sets of prescribed mean curvature, preprint.
[136] Voller V. R., Cross M., and Walton P. in *Numerical Methods in Thermal Problems,* edited by R.W. Lewis and K. Morgan. Pineridge Press, Swansea. p. 172. (1979).
[137] Voller V. R. and Cross M. International Journal of Heat and Mass Transfer. Vol. 24: 545. (1981).
[138] Voller V. R. and Cross M. International Journal of Heat and Mass Transfer. Vol. 26: 147 (1983).
[139] Voller, V. R., and Shadabi, L. International communications in heat and mass transfer. Vol. 11: 239-249. (1984).
[140] Swaminathan, C. R., and Voller, V. R.. Metallurgical transactions B. Vol. 23: 651-664. (1992).
[141] Voller, V. R., Swaminathan, C. R., and Thomas, B. G. International Journal for Numerical Methods in Engineering. Vol. 30: 875-898. (1990).
[142] Swaminathan, C. R. and Voller, V. R. International Journal of Numerical. Methods. Heat Fluid Flow. Vol. 3**:** 233. (1993).
[143] Date, A. W. Sadhana. Vol. 19: 833-850. (1994).
[144] Date A W. International Journal of Heat and Mass Transfer. Vol. 34: 2231-2235. (1991).
[145] Date A W. Numerical Heat Transfer. B21:231-235. (1992).
[146] Tacke K.-H., in: *Application of finite difference enthalpy methods to dendritic growth, free boundary problems: theory and applications*, edited by K.-H. Hofmann, J. Sprekels. Longman Sci. Tech., Essex. (1990).
[147] Tacke, K.-H., Harnisch, A. Proceedings of the International Conference on Computational Modeling of Free and Moving Boundary Problems, WIT press, Southampton. (1991).
[148] Mackenbrock, A., and Tacke, K-H. Metallurgical and Materials Transactions B. Vol. 27: 871-881. (1996).
[149] Pal D., Bhattacharya J., Dutta P., Chakraborty S. Numerical Heat Transfer. B 50: 59–78. (2006).
[150] Chatterjee D., Chakraborty S. Physics Letters. A 351: 359–367. (2006).
[151] Voller V.R. An enthalpy based scheme for simulating dendritic growth, in: *Modeling of Casting, Welding and Advanced Solidification Processes-XI*, edited by Gandin C.A., Bellet M. TMS, Warrendale, PA, pp. 465–472. (2006).
[152] Voller V. R. International Journal of Heat and Mass Transfer. Vol. 51: 823-834. (2008).
[153] Voller V.R. TMS Annual Meeting: 113-122. (2010).
[154] Bhattacharya, A., and Dutta P. International Journal of Numerical Methods for Heat and Fluid Flow. Vol. 23: 1121-1135. (2013).
[155] López, J., Gómez P., and Hernández J. Journal of Computational Physics. Vol. 229: 6663-6672. (2010).
[156] Cummins SJ, Francois MM, Kothe DB. Journal of Computers and Structures. Vol. 83:425–234. (2005).
[157] Francois MM, Cummins SJ, Dendy ED, Kothe DB, Sicilian JM, Williams MW. Journal of Computational Physics. Vol. 213:141–173. (2006).
[158] Malik M, Fan ES-C, Bussmann M. International Journal of Numerical Methods in Fluids. Vol. 55:693–712. (2007).
[159] Hernández J, López J, Gómez P, Zanzi C, Faura F. International Journal of Numerical Methods in Fluids. Vol. 58: 897–921. (2008).
[160] López J., Hernández J., Gómez P., Faura F. Journal of Computational Physics. Vol. 195:718–742. (2004).
[161] López, J., Gómez, P., Hernández, J., and Faura, F. Computers and Fluids. Vol. 86: 326-342. (2013).
[162] Osher S., Sethian J.A. Journal of Computational Physics. Vol. 79:12. (1988).
[163] Merriman B., Bence J.K., Osher S.J. Journal of Computational Physics. Vol. 112: 334. (1994).
[164] Sethian J., Strain J. Journal of Computational Physics. Vol. 98: 231. (1992).
[165] Sussman M., Smereka P., Osher S. Journal of Computational Physics. Vol. 114: 146. (1994).
[166] Sethian J.A. Journal of Computational Physics. Vol. 98: 231-253. (1992).
[167] Chen S., Merriman B., Osher S., Smereka P. Journal of Computational Physics. Vol. 135: 8-29. (1997).
[168] Kim Y.-T., Goldenfeld N. Dantzig J. Physical Review E. Vol. 62: 2471. (2000)
[169]
[170] Gibou F., Fedkiw R., Cheng L.-T., Kang M. Journal of Computational Physics. Vol. 176: 205. (2002).
[171] Fedkiw R. *A symmetric Spatial Discretization for Implicit Time Discretization of Stefan Type Problems.* Unpiblished. June 1998.
[172] Fedkiw R., Aslam T., Merriman B., Osher S. Journal of Computational Physics. Vol. 152: 457. (1999).
[173] Gloub G. Loan Van C. *Matrix Computations.* The Johns Hopkins University Press. Baltimore. (1989).
[174] Fried M. Computing and Visualization in Science. Vol. 7: 97-110. (2004).
[175] Yang Y., Udaykumar H.S. Journal of Computational Physics. Vol. 210: 55-74. (2005).

[176] Zabaras N., Ganapathysubramanian B., Tan L. Journal of Computational Physics. Vol. 218 : 200-227. (2006).
[177] Tan L., Zabaras N. Journal of Computational Physics. Vol. 226 : 131-155. (2007).
[178] Tan. L., Zabaras N. Journal of Computational Physics. Vol. 211: 36-63. (2006).
[179] Tan. L, Zabaras N. Journal of Computational Physics. Vol. 221: 9-40. (2007).
[180] Di Y., Li R. Journal of Scientific Computing. Vol. 39: 441-453. (2009).
[181] Theillard M., Gibou F., Pollock T. Journal of Scientific Computing: 1-25. (2014).
[182] Cahn J.W., Hilliard J.E. Journal of Chemical Physics. Vol. 28: 258. (1958).
[183] Halperin B.I., Hohenburg P.C., Ma S.-K. Physical Review B. Vol. 10:139. (1974).
[184] Allen S.M. Cahn J.W. Acta Materialia. Vol. 27: 1085. (1979).
[185] Langer J.S. In *Directions in Condensed Matter Physics.* Edited by Grinstein G. and Mazenko G. p. 580. World Scientific. Philadelphia. (1986).
[186] Caginalp G. In *Applications of Field Theory to Statistical Mechanics*. Edited by Garrido L. p. 216. Springer. Berlin. (1985).
[187] Caginalp G. Archive for Rational Mechanics and Analysis. Vol. 92: 205. (1986).
[188] Caginalp G. Fife P. Physical Review B. Vol. 33: 7792. (1986).
[189] Caginalp G. Annals of Physics. Vol. 172: 136. (1986).
[190] Caginalp G., Lin J.-T. IMA Journal of Applied Mathematics. Vol. 39: 51. (1987).
[191] Lin J.-T. SIAM Journal on Numerical Analysis. Vol. 25: 1015. (1988).
[192] Caginalp G., Socolovsky E.A. Journal of Computational Physics: 85. (1991).
[193] Kobayashi R. Experimental Mathematics. Vol. 3: 59. (1994).
[194] Wang S.-L., Sekerka R.F., Wheeler A.A., Murray B.T., Coriell S.R., Braun R.J., McFadden. Physica D. Vol. 69: 189. (1993).
[195] Wheeler A.A., Murray B.T., Schaefer R.J. Physica D. Vol. 66: 243. (1993).
[196] Warren J.A., Boettinger W.J. Acta Metallurgica et Materialia. Vol. 43 (2): 689. (1995).
[197] Murray B.T., Wheeler A.A., Glicksman M.E. Journal of Crystal Growth. Vol. 154: 386. (1995).
[198] Braun R.J., Murray B.T. Journal of Crystal Growth. Vol. 174: 41. (1997).
[199] Karma A., Rappel W.-J. Physical Review E. Vol. 53 (4): R3017. (1996).
[200] Karma A., Rappel W.-J. Physical Review Letters. Vol. 77 (19) : 4050. (1996).
[201] Karma A., Rappel. W.-J. Journal of Crystal Growth. Vol. 174: 54. (1997).
[202] Karma A., Rappel W.-J. Physical Review E. Vol. 57 (4) : 4323. (1998).
[203] Karma A., Rappel W.-J. Physical Review E. Vol. 60 (4) : 3614. (1999).
[204] Plapp M., Karma A. Journal of Computational Physics. Vol. 165: 592. (2000).
[205] Karma A. Physical Review Letters. Vol. 87 (11): 115701. (2001).
[206] Tong X., Beckermann C., Karma A., Li Q. Physical Review E. Vol. 63: 061601. (2001).
[207] Nakabeppu O., Hijikata K. 日本機械学会論文集 B 編 64.618: 463-470. (1998).
[208] Tönhardt R., Amberg G. Journal of Crystal Growth. Vol. 194:406. (1998).
[209] Jeong J.-H., Goldenfeld N., Dantzig J.A. Physical Review E. Vol. 64: 041602. (2001).
[210] Lee J.S., Suzuki T. ISIJ International. Vol. 39: 246. (1999).
[211] Kim S.G., Kim W.T., Lee J.S., Ode M., Suzuki T. ISIJ International. Vol. 39 (4): 335. (1999).
[212] Ode M., Lee J.S., Kim S.G., Kim W.T., Suzuki T. ISIJ International. Vol. 40 (9): 870. (2000).
[213] Suzuki T., Ode M., Kim S.G., Kim W.T. Journal of Crystal Growth. Vol. 237-239: 125. (2002).
[214] Golzález-Cinca. Physica A. Vol. 314: 284. (2002).
[215] Lan C.W., Chang Y.C., Shih C.J. Acta Materialia. Vol. 51: 1857. (2003).
[216] George W.L., Warren J.A. Journal of Computational Physics. Vol. 177: 264. (2002).
[217] Belhamadia Y., Fortin A., Chamberland É. Journal of Computational Physics. Vol. 194: 233. (2004).
[218] Slavov V., Stefka D., Oleg I. Phase-field method for 2D dendritic growth. In *Large-Scale Scientific Computing*. p. 404.Springer Berlin Heidelberg. (2004).
[219] Ramirez J.C., Beckermann C. Acta Materialia. Vol. 53: 1721. (2005).
[220] Lipton J., Glicksman M.E., Kurz W. Materials Science and Engineering. Vol. 65:57. (1984).
[221] Lipton J., Glicksman M.E., Kurz W. Metallurgical and Materials Transactions A. Vol. 18: 341. (1987).
[222] Lipton J., Kurz W., Trivedi R. Acta Materialia. Vol. 35: 957. (1987).
[223] Ramirez J.C., Beckermann C., Karma A, Diepers H.-J. Physical Review E. Vol. 69: 051607. (2004).
[224] Lu Y., Beckermann C., Ramirez J.C. Journal of Crystal Growth. Vol. 280: 320. (2005).
[225] Shih C.J., Lee M.H., Lan C.W. Journal of Crystal Growth. Vol. 282: 515. (2005).
[226] Zhang R., Jing T., Jie W., Liu B. Acta Materialia. Vol. 54: 2235. (2006).
[227] Böttger B., Eiken J., Steinbach I. Acta Materialia. Vol. 54: 2697. (2006).
[228] Mullis A.M. Computational Materials Science. Vol. 38: 426. (2006).

[229] Weiying H., Chen C. Special Casting and Nonferrous Alloys. Vol. 3: 008. (2007).
[230] Do-Quang M., Villanueva W., Singer-Loginova I., Amberg G. Technical Sciences. Vol. 55: 2. (2007.
[231] Jacek N., Picasso M. Computer methods in applied mechanics and engineering. Vol. 196 (37): 3562. (2007).
[232] Jacek N., Picasso M. Fluid Dynamics and Materials Processing. Vol. 3 (1): 49. (2007).
[233] Do-Quang M., Amberg G. Journal of Computational Physics. Vol. 227: 1772. (2008).
[234] Amberg G. Physical Review Letters. Vol. 91 (26): 265505. (2003).
[235] Wang H., Li R., Tang T. Journal of Computational Physics. Vol. 227: 5984. (2008).
[236] Steinbach I. Acta Materialia. Vol. 56: 4965. (2008).
[237] Steinbach I. Acta Materialia. Vol. 57: 2640. (2009).
[238] Wang Z., Wang J., Yang G. Physical Review E. Vol. 78: 042601. (2008).
[239] Chen C.C., Lan C.W. Journal of Crystal Growth. Vol. 311: 702. (2009).
[240] Chen C.C., Lan C.W. Journal of Crystal Growth. Vol. 312: 1437. (2010).
[241] Ananth R., Gill W.N. Journal of Crystal Growth. Vol. 179: 263. (1997).
[242] Xianliang H., Li R., Tang T. Communications in Computational Physics. Vol. 5 (5): 1012. (2009).
[243] Sun Y., Beckermann C. Journal of Crystal Growth. Vol. 311: 4447. (2009).
[244] Da-Wen Z., Li J.-F. "Phase-field modeling of the effect of liquid-solid interface anisotropies on free dendritic growth." (2009).
[245] Chang-Sheng Z., Li F. E. N. G., Zhi-Ping W., Rong-Zhen, X. "Numerical simulation of three-dimensional dendritic growth using phase-field method." (2009).
[246] Tòth G.I., Tegze G., Pusztai T., Gránásy. Journal of Physics: Condensed Matter. Vol. 22 (36): 364101. (2010).
[247] Zhu C., Wang J.W. Advanced Materials Research. Vol. 97-101: 3769. (2010).
[248] Lin H.K., Chen C.C., Lan C.W. Journal of Crystal Growth. Vol. 318: 51. (2011).
[249] Wang Z.-p., Wang J.-w., Zhu C.-s., Feng L., XIAO R.-z. Transactions of Nonferrous Metals Society of China. Vol. 21: 612. (2011).
[250] Yamanaka A., Aoki T., Ogawa S., Takaki T. Journal of Crystal Growth. Vol. 318: 40. (2011).
[251] Li Y., Lee H. G., Kim J. Journal of Crystal Growth. Vol. 321: 176. (2011).
[252] Pan S.Y., Zhu M.F. IOP Conf. Series: Materials Science and Engineering. Vol. 33: 012096. (2012).
[253] Long W., Wang W., Yao J. Applied Mechanics and Materials. Vol. 217-219: 1516. (2012).
[254] Lin H.K., Chen C.C., Lan C.W. Journal of Crystal Growth. Vol. 362: 62. (2013).
[255] Du L., Zhang R., Zhang L. Science China : Technological Sciences. Vol. 56 (10) : 2586. (2013).
[256] Xie Y., Dong H., Dantzig J. ISIJ International. Vol. 54 (2) : 430. (2014).
[257] Zhu C., Jia J., Feng L., Xiao R., Dong R. Computational Materials Science. Vol. 91: 146. (2014).
[258] Dong Y., Chen M., Wang X. Advanced Materials Research. Vol. 842: 57. (2014).
[259] Tang S., Yu Y.-M., Wang J., Li J., Wang Z., Guo Y., Zhou Y. Physical Review E. Vol. 89: 012405. (2014).
[260] Du L., Zhang R. Progress in Natural Science: Materials International. Vol. 24: 291. (2014).
[261] Tourret D., Karma A. Acta Materialia. Vol. 82 (1): 64. (2015).
[262] Zhu C.-s., Lei P., Xiao R.-z., Feng L. Transactions of Nonferrous Metals Society of China. Vol. 25: 241. (2015).
[263] Choi J., Park S.-K., Hwang H.-Y., Huh J.-Y. Acta Materialia. Vol. 84: 55. (2015).
[264] Mullis A.M. Journal of Applied Physics. Vol. 117: 114305. (2015).

Suite à cette revue des travaux numériques modélisant la croissance dendritique, la section suivante décrit une sélection des travaux expérimentaux, les plus pertinents, de visualisation mettant en évidence la croissance dendritique à la rupture de surfusion de l'eau.

III.3. Revue de littérature des travaux expérimentaux

La croissance dendritique est une phase où les phénomènes physiques associés sont relativement rapides. Le développement de méthodes de visualisation et d'acquisition de données permet actuellement d'observer avec plus de précision ce qui se passe pendant cette phase relativement courte de la rupture de surfusion.

Les premiers travaux proviennent de R.R. Gilpin qui s'est intéressé à la croissance dendritique dans une canalisation d'eau immobile de diamètre assez grand (150 mm) (Gilpin, R.R., 1976). Il a pu visualiser la croissance dendritique durant le processus de cristallisation. La figure (III-3) montre les clichés représentant la section de la canalisation durant toutes les étapes de la cristallisation. La figure (III-3 - a) montre la section de la canalisation contenant de l'eau surfondue à une température de -3 °C juste avant l'instant de la nucléation de la glace. Les figures (III-3 - b, c et d) montrent la croissance des dendrites de la glace partant du site de la nucléation, sur la paroi interne de la partie supérieure de la canalisation jusqu'au remplissage quasiment total de la section de la canalisation. La durée totale de cette croissance dendritique est d'environ 30 secondes.

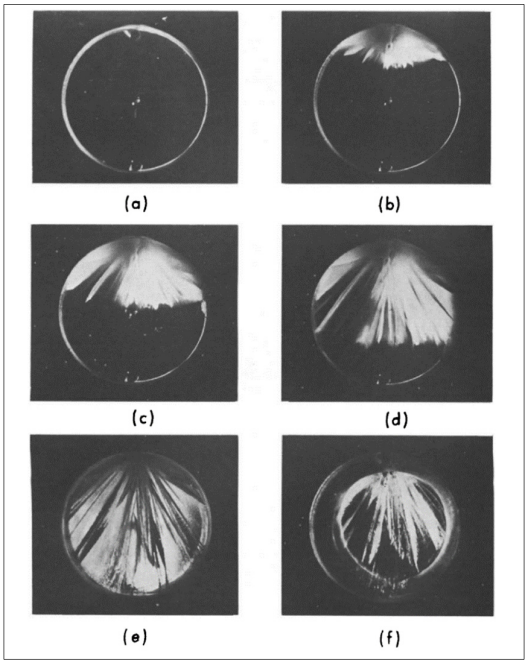

Figure III-3 : Photos qui montrent l'évolution de la croissance dendritique dans une conduite d'eau (Gilpin, R.R., 1976).

À la fin de cette phase, la température de l'eau liquide est retournée à 0 °C (température d'équilibre liquide-solide). La croissance dendritique est alors terminée, et un front annulaire de cristallisation vient transformer lentement le liquide restant en glace. Les figures (III-3 – e et f) ont été prises au bout de 3 et 18 heures après l'instant de nucléation, respectivement.

Dans un autre article, R.R. Gilpin (Gilpin, R.R., 1977) a étudié l'effet de la vitesse de refroidissement et du degré de surfusion sur la formation de la glace dendritique dans une conduite d'eau de diamètre de 137 mm. Il a trouvé que si le degré de surfusion est supérieur à 2 °C au centre du cylindre, alors un blocage complet de la section du cylindre est obtenu. Les figures (III-4 – a, b et c) montrent la croissance dendritique pour plusieurs degrés de surfusion. De plus, il a observé un blocage total de section pour des vitesses de refroidissement lentes. Les figures (III-4 – d, e et f) montrent les sections de la conduite pour plusieurs vitesses de refroidissement.

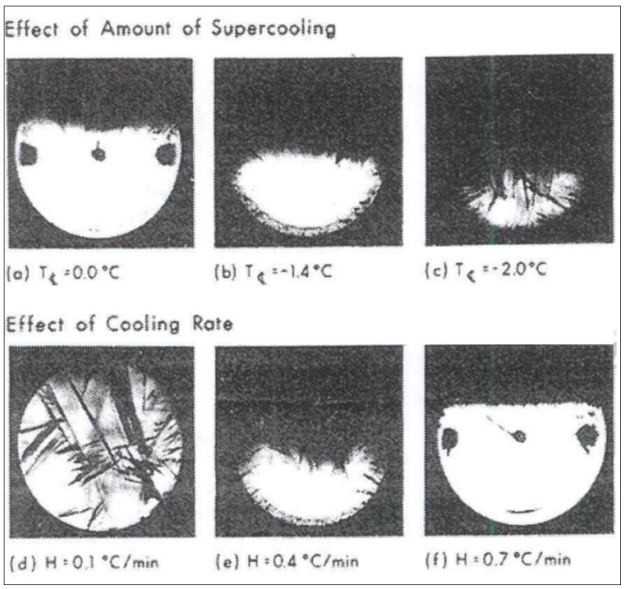

Figure III-4 : Blocage de la canalisation pour plusieurs degrés de surfusion et vitesses de refroidissement (Gilpin, R.R., 1977).

Tirmizi et Gill ont visualisé la croissance dendritique (Tirmizi, S.H. et Gill, W.N., 1987), en utilisant un tube capillaire dans une goutte sphérique d'eau pure surfondue où la dendrite peut se propager librement. Ils ont observé que les dendrites commençaient à se propager en prenant la forme de disques. Ensuite, elles ont changé séquentiellement de forme en passant par des disques perturbés, des disque-dendrites, puis des dendrites partiellement développées, pour obtenir enfin des dendrites complétement développées. Ce développement structurel est représenté sur la figure (III-5). Tirmizi et Gill ont remarqué que le développement des dendrites dépend du degré de surfusion. En effet, pour un degré de surfusion faible, le développement est lent et les transformations géométriques au cours du temps sont faciles à observer. Mais pour un degré de surfusion plus important, le développement observé a été beaucoup plus rapide.

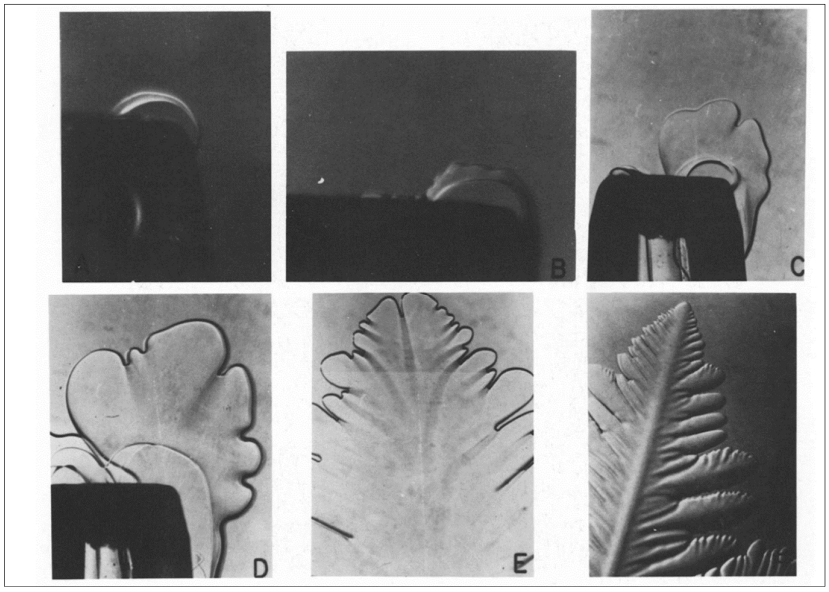

Figure III-5 : Photos montrant l'évolution structurale d'une dendrite en échelle microscopique (Tirmizi, S.H. et Gill, W.N., 1987).

Plus tard, sont venues les études plus fines réalisées en 1991 par Koo et al. (Koo, K-K., et al., 1991). Les auteurs ont observé la croissance d'une dendrite, émergée également d'un tube capillaire, en utilisant une caméra microscopique. Ils ont étudié particulièrement le phénomène de la scission de la dendrite (dendrite splitting) pour différents degrés de surfusion. Ils ont conclu que ce phénomène n'apparait que pour des degrés de surfusion inférieurs à 0,35 K. Mais pour des degrés de surfusion plus importants la dendrite croît avec une forme invariante. La figure (III-6) présente, par exemple, le phénomène de la scission de la dendrite pour un degré de surfusion de 0,09 K.

Gonda et Nakahara (1995) ont également visualisé au niveau microscopique le mécanisme de formation des branches secondaires sur la branche principale de la dendrite de la glace croissant de la vapeur d'eau dans l'air sursaturé avec une pression de $1x10^5$ Pa et une température d'environ -15 °C. La sursaturation est l'état d'un gaz lorsque la concentration d'un constituant est supérieure à celle à laquelle apparait la saturation. Ils ont pu montrer que ces branches ne se forment pas sauf si la sursaturation totale de l'air en vapeur est variable. La figure (III-7) présente les photographies d'un cristal dendritique de glace lors de sa croissance dans l'air avec une sursaturation variable. Les figures (III-7 – c, d et e) présentent la dendrite quand la sursaturation vaut 15%. Les figures (III-7 – f, g et h) présentent la dendrite quand la sursaturation vaut 20%. La figure (III-7 - i) présente la dendrite quand la sursaturation vaut 40%. On voit bien que lorsque la sursaturation augmente (figures (III-7 – f et i)), les branches secondaires sont formées sur la branche primaire par les instabilités morphologiques. Bien que cette étude traite les transformations gaz-solide, mais elle présente le phénomène de formation des branches secondaires qui est communément observé durant la phase de la croissance dendritique.

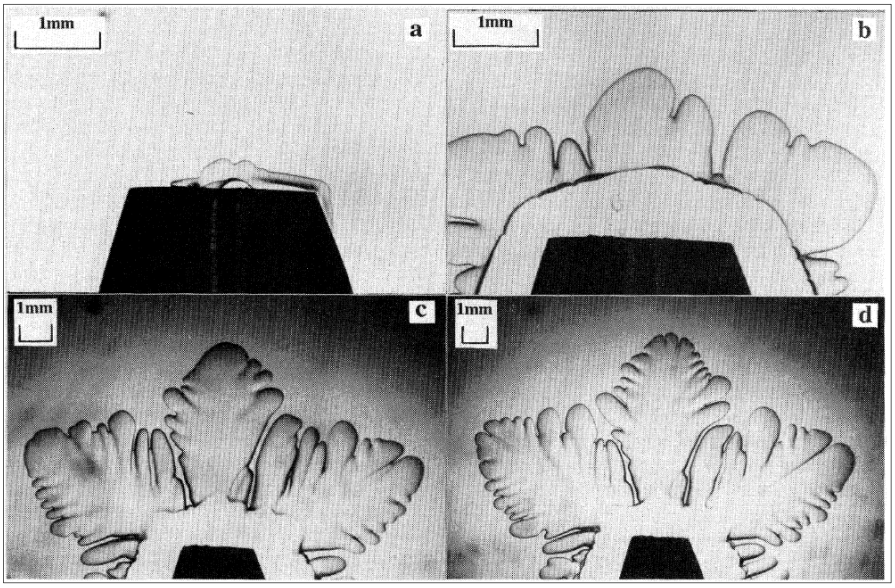

Figure III-6 : Photos montrant le phénomène de la scission d'une dendrite en croissance (Koo, K-K., et al., 1991).

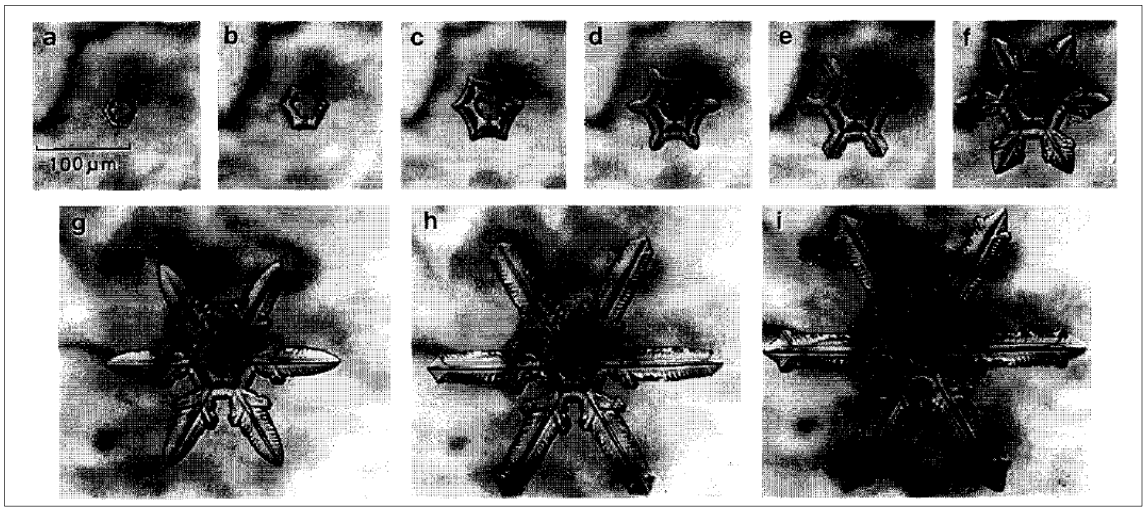

Figure III-7 : Formation des branches-coté sur la branche primaire de la dendrite (Gonda, T., et Nakahara, H., 1995).

En 1997, Chen et Lee ont présenté, pour différentes vitesses de refroidissement, des schémas de la phase de la croissance dendritique dans des cylindres horizontaux contenant de l'eau (Chen, S.L., et Lee, T.S., 1997). Les photos de la figure (III-8) ci-dessous montrent que pour une vitesse de refroidissement lente, il y a plus de formation de dendrites. C'est parce que il y a plus du liquide surfondu, et les dendrites se forment dans les endroits où la température du liquide est inférieure à celle de fusion.

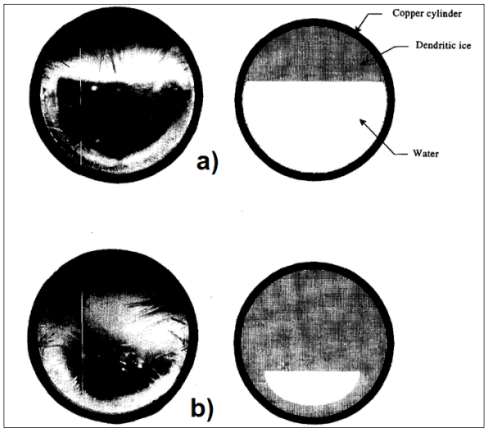

Figure III-8 : Croissance dendritique de glace dans un cylindre horizontal avec une vitesse de refroidissement de a) 1,7°C/min et b) 1,5°C/min (Chen, S.L., et Lee, T.S., 1997).

Plus récemment, en 2012, une équipe brésilienne s'est intéressée à la visualisation de la croissance dendritique de la glace dans des capsules cylindriques (Braga S.L., Milon, J.J., 2012). Ils ont développé un dispositif expérimental pour étudier cette croissance, en mesurant les températures en plusieurs points de la section du cylindre en fonction du temps à l'aide des thermocouples. Les résultats indiquent que la croissance dendritique n'apparaît que dans les régions où l'eau est surfondue à l'instant de la nucléation (régions de températures négatives). La figure (III-9) ci-dessous montre les résultats d'une expérience réalisée avec une température de refroidissement de -16 °C. Les photographies originales, les schémas associés, le temps correspondant, et les valeurs des températures mesurées sur l'axe vertical sont présentés. L'instant initial (0 sec) correspond à l'instant de la nucléation, on remarque que la température de la partie supérieure est négative ($T<T_m$), et celle de la partie inférieure est positive ($T>T_m$). Par conséquent, juste après l'instant de la nucléation les dendrites commencent à propager de la partie supérieure où la température est la plus basse, jusqu'à que la température de toute la section soit plus grande ou égale à zéro, à l'instant 2,5 s.

La section inférieure du cylindre gardait une température positive (environ 5° C) pendant toute la durée de l'expérience, parce que la nucléation a commencé rapidement après le démarrage du système de refroidissement.

La présence d'une température positive (supérieure à la température d'équilibre liquide-solide) dans la section du cylindre à l'instant de la nucléation permet de distinguer le blocage partiel et total de la conduite provoqué par la croissance dendritique. En répétant l'expérience plusieurs fois et en mesurant la durée de la phase dendritique, Braga et Milon ont pu montrer aussi que dans les cas où cette croissance dendritique avait lieu, sa durée dépendait de la température du liquide de refroidissement. Cette durée augmente d'ailleurs avec la diminution de la température du liquide de refroidissement. Le blocage total a également plus de chance d'être observé avec des températures du liquide de refroidissement plus élevées. Un résumé de ces résultats est présenté sur la figure (III-10).

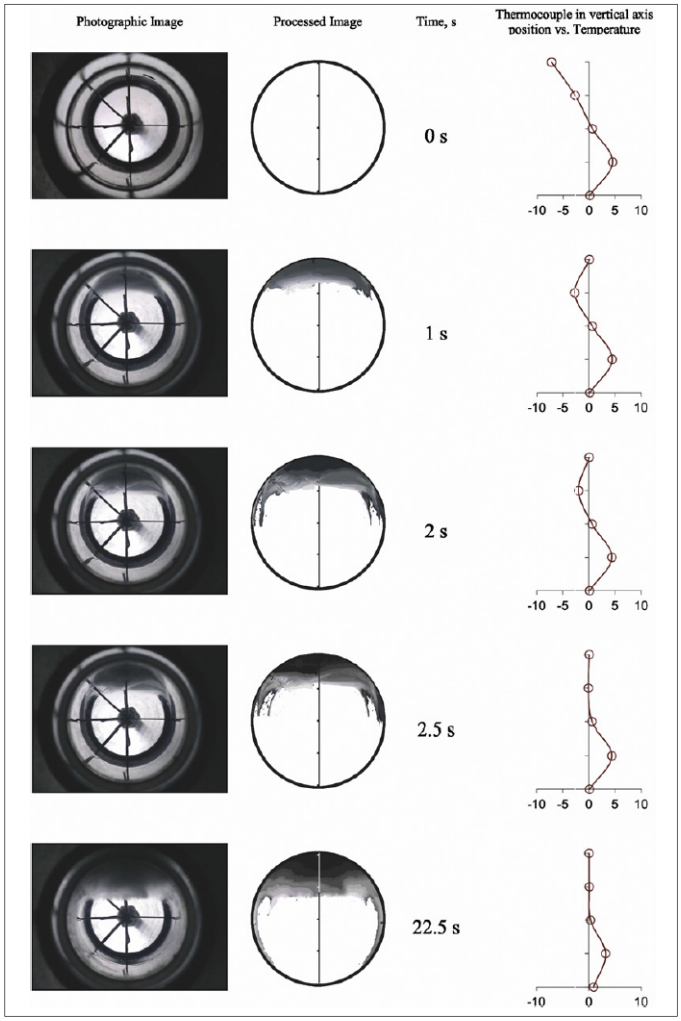

Figure III-9 : Photographies et schémas associés de l'évolution dendritique dans une capsule cylindrique et valeurs des températures sur l'axe vertical de la capsule. (Braga S.L., Milon, J.J., 2012).

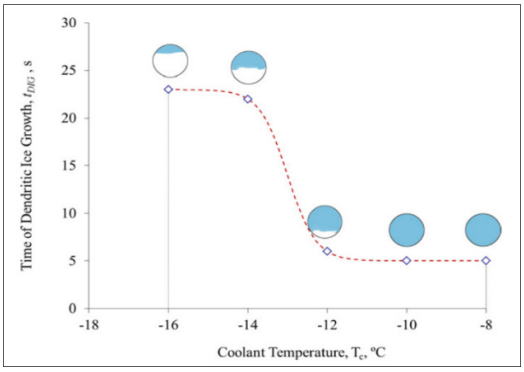

Figure III-10 : Différents états du blocage provoqué par la croissance dendritique en fonction du temps t et de la température du liquide de refroidissement Tc °C (Braga S.L., Milon, J.J., 2012).

Dans le chapitre suivant, la méthode numérique est décrite et les résultats numériques sont discutés.

IV. Étude numérique

IV.1. Introduction

L'étude numérique proposée consiste à modéliser l'évolution dynamique de l'interface liquide-solide durant la phase dendritique lors du processus de solidification des corps purs. Elle s'appuie sur un code, développé dans le langage C++ (programmation orientée objet), modélisant la croissance dendritique bidimensionnelle, en tenant compte de tous les effets associés à l'interface et aux transferts thermiques. La méthode numérique est basée sur une approche de suivi explicite d'interface (*Front-Tracking Method*). Bien que cette méthode est relativement difficile à implémenter, elle possède l'avantage principal d'utiliser deux maillages indépendants, un premier cartésien fixe employé pour la résolution des équations de transfert dans les parties liquide et solide, et un deuxième mobile (ensemble discret de points), complètement découplé du maillage cartésien, employé pour suivre l'interface. Cela permet d'obtenir une localisation précise d'une *sharp-interface*, indépendamment de la finesse du maillage cartésien global.

De plus, cette méthode résout séparément les composants du problème mathématique. Cela rend le problème divisible en deux sous-problèmes exécutables simultanément par différents processus (ou machines), en permettant la parallélisation. Elle résout également les équations de la chaleur non modifiées (aucun paramètre supplémentaire n'est requis) dans les deux phases, et applique directement sur le front de solidification les conditions de Gibbs-Thomson et de bilan de l'énergie. Cela permet des études paramétriques des grandeurs physiques réelles.

L'algorithme numérique comporte principalement deux étapes itératives au cours du temps. La première est l'estimation du mouvement élémentaire de tous les points d'interface en déduisant à la fois la nouvelle géométrie de l'interface et les chaleurs latentes libérées. En négligeant la convection naturelle dans la phase liquide, la seconde étape consiste à la mise à jour des champs de température des cellules, décomposant les deux phases liquide et solide, tenant compte des flux conductifs échangés avec les cellules entourant, ainsi que des flux latents provenant du changement de phase suite à la progression de l'interface.

La première étape préliminaire du développement du code numérique consistait à modéliser les transferts thermiques dans un milieu à propriétés thermophysiques déterminées sans et avec une source chaleur (immobile), a été réalisée. Les résultats sont présentés dans l'annexe B.

Deux sections viennent de s'ajouter à cette introduction et sont présentées sous formes d'articles scientifiques rédigés en langue anglaise.

La section (IV.2) détaille la méthode numérique ainsi que son implémentation sur laquelle s'appuie l'étude de la croissance dendritique. Ensuite, elle présente des résultats validant la méthode numérique proposée et montrant la capacité du code numérique à traiter des cas instables de solidification comprenant une croissance cristalline. Enfin,

elle fournit quelques études paramétriques pertinentes et décrit l'évolution d'une interface suffisamment non-stable montrant des phénomènes dendritiques réalistes.

La section (IV.3) examine des cas particuliers de la croissance dendritique dans des conditions thermiques différentes imposées par les conditions aux limites du système. Elle étudie qualitativement et quantitativement l'effet de ces conditions sur le comportement et la symétrie de la propagation dendritique.

IV.2. Numerical study of dendritic growth using a double-mesh sharp-interface front tracking method: Article 2

Mohamad Ali Jaafar [1,2], Stéphane Gibout [1], Daniel Rousse [2], Jean-Pierre Bédécarrats [1]

(1)Univ. Pau & Pays Adour - EA1932 - LATEP - Laboratoire de Thermique Energétique et Procédés, Rue Jules Ferry, BP7511 - PAU, F-64075, France

(2) t3e Industrial Research Group, École de technologie supérieure, Montréal (Qc), Canada

Article soumis à la revue « *International Journal of Thermal Sciences* »

Abstract

An explicit two-dimensional front tracking method is developed in order to model dendritic growth during solidification processes of pure substances. The main idea behind this method is the use of two independent meshes. The first is fixed, which describes the whole medium. The second is a sequential set of moving marker points to describe and track the sharp liquid-solid interface which evolves over the fixed background mesh. The front tracking technique is combined, from one hand, with a finite volume method to discretize the partial differential equations describing heat transfer in both phases, and from the other hand, with an explicit first-order forward Euler method for the time integration. The primary behavior of the numerical code is first tested to provide the critical radius concept of homogeneous nucleation correctly. Then, the numerical technique is checked by an isotropic circular stable case of solidification to provide homogeneous velocities along interface marker points. Unstable cases of solidification, considering different modes of anisotropy are performed next, and an orientation test is provided for a four-fold symmetry case. Effects of both initial temperature of liquid and surface tension on a four-fold symmetry case are investigated. Finally, interface evolution, providing realistic dendritic features as tip-splitting and secondary branches, is described, showing the ability of the code to deal with complicated dendritic growth and to study its characteristics.

Keywords: Solidification process, Dendritic growth, Front tracking method.

IV.2.1. Introduction

Solidification processes are involved in many industrial applications, mainly in metallurgy and thermal latent heat storage fields. In several circumstances, some materials may remain in their liquid states far below the solid-liquid equilibrium temperature. The liquid is then supercooled and metastable. Hence, nucleation may be either homogeneous [1] after sufficient cooling or heterogeneous [2] by placing for example a solid seed in the supercooled liquid. Once nucleation has occurred through the supercooled liquid, the solidification is unstable and may involve a complex interplay of many physical effects. Many microstructures patterns may be produced

depending mainly on the degree of supercooling i.e. the difference between the equilibrium temperature and liquid temperature at solid nucleation instant ($\Delta T = T_m - T_\infty$). When supercooling degree is large enough, dendritic microstructure is commonly observed. It is worth noting here, that dendritic crystal growth pattern is one of the most spontaneous pattern formations. For instance, snowflakes have various types of complex and fascinating shapes. Dendritic growth pattern is due, by definition, to the competition between the stabilizing effects of surface tension and the supercooling at the interface. The rationale behind the appellation 'dendrite' is the Greek word 'dendron' which means tree [3]. Like a tree, the dendrite has a highly branched, arborescent structure, consisting of primary stem, as well as secondary and higher order branches.

The evolution of dendritic pattern has received much attention from both scientific and engineering points of view for its intricate pattern selection mechanisms and useful industrial applications, mainly in metallurgy and thermal energy storage fields. On the one hand, dendrites in metallurgy establish the initial microstructures of cast metals and alloys. These microstructures, in turn, strongly influence mechanical, physical, and chemical behaviors of the material. In other words, they determine qualities of the solidified raw material and often the finished product. Thus, understanding of these dendritic microstructures formation is technologically important in order to produce better casts and pattern formation for advanced materials. On the other hand, dendritic growth is a very important phenomenon in process of solidification of phase change materials (PCM) which are used in thermal energy storage applications [4]. Indeed, during the propagation of dendrites through supercooled liquid, liquid temperature returns locally to its equilibrium temperature of solidification. This is due to the latent heat absorbed by the supercooled liquid, which is released from the interface during this phase. Hence, one would like to understand how dendritic growth is driven or guided, in order to improve solidification processes by controlling or preventing it.

In this context, the history of dendritic growth involves both experimental studies and numerical investigations. On the one hand, many in-situ visualizations were carried out in order to understand the physical mechanisms which result dendritic structures, as well as their consequences on supercooled liquid. As the present paper focuses on the numerical aspect of dendritic problem, only selected experimental studies are reviewed. R.R. Gilpin, for example, has studied dendritic growth in supercooled water in pipes [5]. Water temperature at the nucleation instant was -3°C. He observed ice dendritic growth that evolved quickly from the nucleation center until the cross-section has been blocked. At the end of this phase, the temperature of the remaining water in the pipe has returned to the equilibrium temperature i.e. 0°C. After that, no more dendritic ice growth has occurred, but an annulus of solid ice then began to grow slowly from the inside wall of the pipe toward the center. Later, Tirmizi and Gill [6] have made a microscopic study of ice crystals growth in pure water. The structures which were photographed, changed sequentially from disks to perturbed disks, to disk-dendrites, to partially developed dendrites, and finally to fully developed dendrites. Recently, Braga

and Milon [4] have developed an experimental device to study cylindrical capsules blockage due to dendritic ice growth. They have showed, first, that dendritic growth appears only in supercooled liquid regions at the nucleation instant, and second, that blockage by dendritic ice growth depends on capsule material and coolant temperature.

On the other hand, from numerical point of view, dendritic growth represents a pattern formation phenomenon, which in recent years has become a deeply investigated subject in non-linear dynamics field. Plus to dendritic problem non-linearity at the moving interface, the principal difficulty while dealing with this problem lies in the fact that the interface constitutes at the same time one of problem unknowns and one of boundary conditions separating two phases. Such problem is called a "moving boundary problem". Therefore, without simplifying assumptions, dendritic solidification problems cannot be described by analytical solutions. However, specific numerical methods are required to simulate this complex case of solidification. The most computational numerical challenge is tracking of the moving interface which evolves due to competition between several thermal and geometrical effects. Over the last decades, several numerical methods have been developed and applied for simulating dendritic crystal growth in its full geometrical complexity under different conditions and assumptions. These numerical methods can be split into two major classes according to the way in which they handle the moving boundary interface; however, the interface can be tracked either explicitly or implicitly (details and main numerical methods are reviewed in [7]).

The first class of numerical methods consists of keeping explicitly the data of interfacial position by satisfying suitable discrete own forms of the interface. These Front Tracking methods (FT) use lower dimension deforming grids that evolve with solid-liquid interface. Typically, they employ field solutions on a fixed Eulerian background mesh and continuously reconstruct a second Lagrangian, lower dimension, description of the interface. Roosen and Taylor [8], for example, have introduced an explicit front tracking scheme with simplifying interface curvature measurements by assuming a polygon interface. They have shown that the algorithm was relatively fast, and easy to detect and make morphological changes. Shyy et al. [9] have developed an interface motion technique which is not limited to a single valued or isothermal interface, and produces results in close agreement with analytical solutions for the one-phase and two-phase cases. For unstable solidification problems, they observed tip-splitting and cusp formation in absence of surface tension, and a propagating finger when small amount of surface tension is added. Juric and Tryggvason [10] have used a numerical method based on front tracking approach to simulate dendritic solidification. It explicitly introduces a separate interfacial grid in addition to the fixed regular one. Front tracking method is coupled with immersed boundary technique in order to distribute heat sources at the interface over the nearest grid points to the interface, and to interpolate the temperature field from the stationary grid to the interface. The method was found to easily handle topological changes and interfacial anisotropies for complex cases of solidification. Complex dendritic structures, such as side branching and

tip-splitting, were reproduced. Later, this method has been extended by Al-Rawahi and Tryggvason in order to include convection effects [11]. Results obtained are in good qualitative agreement with published experimental results. Zhao et al. have described a direct front tracking method using an Eulerian-Lagrangian formulation for simulating interface problems with different conditions [12]. They have shown that the method is capable to describe extremely complex morphologies and a large number of simultaneous merging/splitting events during the dendritic solidification.

On the other hand, implicit tracking methods have been developed in order to model solidification with dendritic growth. These Order Parameters methods (OP) use some auxiliary variables defined on every grid cell of the whole region, for which values are ranging usually between zero and unity in function of the local physical state. The value of the variable provides the information whereas the grid cell is liquid, solid, or in the vicinity of solid-liquid interface. Then, a modified energy equation is solved for the whole domain. Several available numerical methods, which are part of the second major class, can be found in the literature.

The first and most basic one is the enthalpy method. In this approach, single energy conservation equation for the whole domain, solid and liquid, is expressed in terms of enthalpy – the sum of latent and sensible heats. The enthalpy method was widely used for phase change problems in one and two-dimensional space [13,14]. Tacke et al. were the first to apply it to solve dendritic growth problems [15]. They concluded that dendritic structures of a supercooled pure melt are more or less adequately reproduced with this algorithm. Pal et al. [16] have then presented an enthalpy-based simulation for the evolution of equiaxial dendrites, growing in a supercooled melt of a pure substance. By combining relevant macro-scale and micro-scale features, it was shown that the model is capable to produce dendritic growth features. Later, Voller [17] has extended the enthalpy method to account for dendritic growth in both pure and binary alloy melts.

Two other popular approaches were also developed to deal with dendritic solidification growth: level-set method and phase-field model. In contrast to enthalpy method, they express the energy equation only with temperature as the dependent variable. Level-set method generally uses a level-set function in order to track the interface; the function is defined in the whole domain, and the front is always represented by the zero level set value. A Hamilton-Jacobi level-set formulation was first used by Sethian and Straint [18] to simulate solid-liquid interface in crystal growth. They combined a level-set approach with a boundary integral formulation of the problem. The method has provided correct description of the evolution of complex crystalline shapes, but was found to be somewhat complicated and computationally expensive. Hence, Chen et al. [19] have improved this method by avoiding using a boundary integral method to compute the normal velocity at the interface. It was shown that this modified method was able to handle topology changes and complicated interfacial shapes such as side branching and dendritic fingering. Further, Kim et al. [20]

improved the approach proposed by Chen et al. by computing the velocity with more accuracy. They demonstrated that results obtained by their improved method for dendritic growth are in good agreement with those predicted by microscopic solvability theory. Later, Gibou et al. [21] showed that a new level-set algorithm, using in addition the second order accurate symmetric discretization of the Poisson equation, converges to some known exact solutions, and can be used to simulate complex interfacial shapes of dendritic solidification of a pure melt. Fried [22] has also described a finite element algorithm for the 2D Stefan problem, where the free boundary is represented as a level set. This allows easily handling topological changes of the free boundary. One year later, the simple-to-implement formulation proposed by Yang and Udaykumar [23] showed an excellent agreement with 2D microscopic solvability theory for pure material solidification. Later, an efficient multi-mesh h-adaptive finite element algorithm to solve the level set method of dendritic growth in a pure supercooled melt was proposed by Di and Li [24]. The proposed method achieved similar accuracy as the front tracking methods with about same degrees of freedom. Recently, an extension of level set method is proposed to simulate solidification of binary alloys is proposed by Theillard et al. [25].

On the other hand, phase field model introduces the phase field variable, which defines the physical state (liquid or solid) of each grid point in the calculation domain. The interface between liquid and solid is then described by smooth transitions of this additional variable between values representing liquid and solid states. First simulations demonstrating the ability of phase field model to simulate complicated dendritic solidification structures were done by Kobayashi [26]. He presented a two-dimensional simple phase field model for one component melt dendritic growth including anisotropy in a certain form. He provided the evolution of branchful dendritic structures growing into a supercooled melt. A phase field model was then described by Wang et al. [27] to investigate the associated important aspects for dendritic growth from a supercooled melt [28] and for treatment of a non-isothermal binary alloy [29]. The proposed model was able to produce qualitatively realistic dendritic structures such as secondary and tertiary dendrite arms. Using the same model, additional two-dimensional computations were performed [30] to demonstrate that phase field model can be used to simulate observed behavior in dendritic growth experiments. Phase field model was then found to require high mesh resolution at the interface to provide quantitative computations and correctly capture the physics of the phase transformation. Consequently, several algorithms, using an adaptive mesh near the interface have been developed and used for dendritic growth. Later, Do-Quang et al. [31] have proposed a parallel adaptive finite element scheme, which was successfully implemented in the numerical simulation of dendritic growth. It was found that exchange of information was minimized and less memory was used. Wang et al. [32] have then presented an efficient r-adaptive mesh algorithm for phase field model of dendritic growth of pure substance in both 2D and 3D. Results indicated that the method has the potential to produce more realistic dendritic structures with less computing resources. Further, an efficient adaptive 3D phase field method was presented to simulate dendritic crystal growth by Chen and Lan

[33]. The simulated results for various supercooling levels were found to be in good agreement with Ivantsov solution. A multi-mesh adaptive finite element approximation of phase field model for dendritic growth was also proposed by Hu et al. [34]. They showed that the proposed technique was useful in solving phase field models and can save storage and the CPU time significantly. Furthermore, quantitative numerical investigations of dendritic growth which were done by Chang-Sheng et al. can be found in [35].

Although these OP methods are found to be easier to handle topological changes during dendritic growth solidification, they need an extra equation to describe the additional variable evolution, and they require large computational capacity to be used for quantitative studies for which the moving interface has to be thickness-less. For these reasons mainly, a front tracking method is chosen for the present study. Based on this numerical approach, the evolution of a sharp interface is tracked explicitly using a moving independent second mesh, solving the unmodified energy equation on both phases of the medium with no need for an additional non-physical variable. Plus, front tracking method resolves thermal fields of two phases individually, which makes code parallelization easier. In this context, the present paper has three main purposes: (1) to describe a general numerical method based on front tracking approach and show its robustness and correctness to be used for modeling dendritic growth solidification in pure material of supercooled melt without being restricted to limiting conditions or materials, (2) to provide investigations of some involved parameters effects on the evolution of liquid-solid interface, and (3) to describe dynamically the evolution of an advanced growing interface showing realistic dendritic features. The paper is then divided into four sections. The following section briefly overviews the theoretical background behind the subject, providing the complete mathematical formulation of dendritic solidification problem. Then, the third section describes the proposed numerical method. Finally, the fourth section presents and discusses simulation results validating the proposed method and showing its ability to deal with realistic dendritic growth.

IV.2.2. Theoretical background

History of freezing processes mathematical formulation starts with the simplest freezing (or melting) model: the Classical Stefan Problem. This problem is the most basic one, for which a planar and stable liquid-solid front is assumed, and many simplifying assumptions are considered: heat transfer occurs by conduction only (convection and radiation are neglected), phase-change temperature is a fixed known temperature (liquid-solid equilibrium temperature), latent heat is constant, and there is no anisotropy effects. Stefan problem is nonlinear, and its principal difficulty lies in the fact that, in addition to the temperature field, the location of the interface is unknown and has to be solved (moving boundary problem). Analytical solutions are available for Stefan problem in plane geometries [36,37] and spherical geometries [38].

The physical origin of the solidification front instability, giving rise to dendritic growth, was identified by Mullins and Sekerka [39]. They have analyzed the steadily advancing planar interface on which is imposed a single periodic ripple, and asked how fast it would grow. During solidification process, when liquid is supercooled below its equilibrium temperature, the interface becomes unstable due to the destabilizing effect of supercooling. In such a case, any perturbation on the interface will be enhanced, and constrained by surface tension effects on the interface. Dendritic structures are then produced due to the competition between the various effects on the interface, forming the most complex case of unstable freezing process. However, dendritic growth problem still referred as a Stefan-type problem, but for which, the morphology of the interface itself plays a role, and surface tension as well as kinetic mobility at the interface cannot be neglected. Indeed, local freezing temperature at a curved interface becomes slightly lower than the equilibrium temperature depending mainly on these factors. This is so-called Gibbs-Thomson effect, which is introduced subsequently in eq. IV-5. Ivantsov was the first to derive a mathematical analytical solution for a paraboloic tip shape of a steady state dendrite growing into an infinite half-space of a supercooled liquid [40]. He adopted the definable shape basing on the realistic observations of dendritic crystals. The second main assumption in Ivantsov's model is that curvature effect is neglected, so that the interface is assumed to be isothermal (T_m). For a given initial supercooling degree, Ivantsov's solution determines the value of the product of growth velocity and tip radius of a growing dendrite, and then describes only a family of parabolas. Despite that Ivantsov's model seeks an additional independent equation, and is far to represent a real branchful dendrite, the needle-like Ivantsov's solution captures several important aspects of a growing dendrite, and constitutes a base from which more sophisticated dendritic growth models are built.

Furthermore, the physical domain is generally sub-divided into three regions, solid phase, liquid phase, and the separating moving interface (figure IV-1). For pure substances, only heat transfer is involved during solidification processes, and the solidification front is able to move if latent heat is released from it. Several mechanisms may be involved to transfer heat between interface and phases, as well as between each phase molecules, as convection and conduction. The present study deals with the idealized situation of dendritic solidification of pure substances, for which the dependence of density on temperature in both phases is neglected, so that convection in liquid is neglected. That is due to the small involved thickness in order to produce results that could be compared to experimental visualizations obtained with the bench which is dedicated to this project. This device (still under construction) is designed in order to ensure enough small thickness along the ground-gravity axis to prevent natural movement in liquid in the third dimension. Therefore, a horizontal two-dimensional model is considered, and mass densities of liquid and solid phases are assumed to be equal. However, discontinuities in other thermophysical properties, such as heat conductivity and heat capacity, between solid and liquid phases are taken into account.

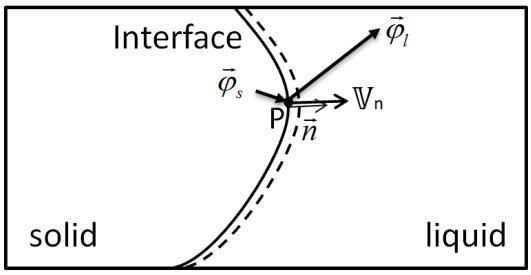

Figure IV-1: Interface separating solid and liquid regions.

Consequently, temperature field in each phase is described by the time dependent heat conduction equation:

$$\rho.c_s.\frac{\partial T_s}{\partial t} = \vec{\nabla}\cdot\left(k_s\vec{\nabla}T_s\right) + \dot{Q}_s \qquad \text{solid phase region} \tag{IV-1}$$

$$\rho.c_l.\frac{\partial T_l}{\partial t} = \vec{\nabla}\cdot\left(k_l\vec{\nabla}T_l\right) + \dot{Q}_l \qquad \text{liquid phase region} \tag{IV-2}$$

where ρ is both liquid and solid density, c is the specific heat, and k is the thermal conductivity. Subscripts s and l refer to solid and liquid phases, respectively. $\dot{Q}$ is an energy source term due to liquid-solid interface movement.

Temperature fields $T_s(x,y)$ and $T_l(x,y)$ are coupled through two boundary conditions at the moving interface between phases. The first is the Stefan condition (energy balance equation) in a more complicated form, which takes into account the released latent heat at the interface temperature and discontinuity of local gradients of temperature between interface and phases near it (figure IV-1):

$$\rho.L\left(T_f\right).\mathbb{V}_n = \left(-\overrightarrow{\varphi_s} + \overrightarrow{\varphi_l}\right)_P\cdot\vec{n} = \left(k_s\vec{\nabla}T_s - k_l\vec{\nabla}T_l\right)_P\cdot\vec{n} \tag{IV-3}$$

where $\mathbb{V}_n$ is the normal velocity of the interface, $\vec{n}$ the normal vector at the interface, and $L\left(T_f\right)$ the latent heat at the interface temperature T_f:

$$L\left(T_f\right) = L + (c_l - c_s)(T_f - T_m) \tag{IV-4}$$

with L the latent heat at T_m.

Interface temperature has to be calculated satisfying a particular local equilibrium. Indeed, the growing interface continually adjusts its temperature to balance bulk energy and surface energy depending on several effects controlling solid growth. This leads to the second boundary condition at the interface which is the Gibbs-Thomson condition:

$$T_f = T_m - T_m.\frac{\gamma(\theta).\kappa}{\rho.L} - \frac{\mathbb{V}_n}{\upsilon(\theta)} - T_m.\frac{(c_l - c_s)}{L}.\left(T_f.ln\left(\frac{T_f}{T_m}\right) + Tm - T_f\right) \tag{IV-5}$$

where κ is twice of the interface mean local curvature, $\gamma(\theta)$ is the anisotropic surface tension, and $\upsilon(\theta)$ represents the anisotropic kinetic mobility. θ is the angle between normal vector at the interface and an arbitrary reference axis depending on the crystal germ.

It is worth noting here that a mathematical model with a standard version of Gibbs-Thomson condition, for which only isotropic capillarity effects are included, was supposed to be sufficient to describe dendritic growth solidification. This assumption was questioned subsequently due to the fact that the needle-like model provided by Ivantsov is transformed to a branchful dendrite when supplementing his model by the capillarity effects. This standard model has been used widely [41], even recently [42], to deal with dendritic growth, mainly, for simplicity purposes. However, the present study deals with the complete version of the Gibbs-Thomson condition (eq. IV-5) [7], without neglecting any physical phenomenon described in the equation. Indeed, on the one hand, kinetic mobility effects limit the degree of supercooling. It has been shown [43,7] that, with an increase in the supercooling of a liquid, the diffusional growth theory admitted in several dendritic growth models should be replaced by growth determined by processes of molecular rearrangement at the interface, i.e. the surface kinetics. On the other hand, specific heat discontinuity at the interface limits the choice of the studied material. However, only when dealing with materials for which the ratio of material heat capacity discontinuity tends to unity, this term can be neglected. Moreover, it has been shown that this ratio affects significantly dendrites growing shape and growth rate [10]; a higher liquid to solid ratio produces a fast growing unstable solid while a low ratio produces a slow growing, more stable solid shape.

IV.2.3. Numerical method

A two-dimensional front tracking method has been developed to simulate dynamical interface evolution during dendritic solidification in pure material of supercooled melt. The main idea behind this method is that it tracks explicitly the interface and applies directly the Gibbs-Thomson equilibrium equation and the Stefan condition at the interface. It solves individually the heat equation in both phases in a fixed background mesh, and reconstructs at each step the representation of a sharp moving interface which separates these phases. The front tracking method is coupled with a finite volume method which is implemented to discretize the spatial variables in the energy partial differential equations in both liquid and solid phases, eqs. IV-1 and IV-2. Herein, as shown in figure IV-2, a regular mesh is used for dividing solid and liquid regions in elementary square volumes of unit thickness. Moreover, an explicit first-order forward Euler time integration method is used. The numerical resolution can be divided into two major parts: interface treatment and temperature fields resolution. These two parts are independent so that it does not matter in what order they are performed.

IV.2.3.1. Interface treatment

The interface is described and tracked using a set of moving separate marker points which are connected by a sequential order using linear interpolation to form a one dimensional mesh evolving over the two dimensional fixed mesh defining the whole physical domain. The proposed method is a sharp interface method in which the interface has no thickness and no additional parameter or indicator is used. The numerical method is able to involve not only one, but several interfaces. These interfaces can be either closed or open (figure IV-2). Interfaces are usually given by an initial list of points or by a functional defined form relating Cartesian variables. For closed interface, the last point of the representing set is at the same time the first point. However, for an open interface the last and initial points are different and are usually at one of the domain boundaries. Interface treatment can be summarized by four steps: updating the interface discretization (step I-1), evaluating the required parameters at each interface point (step I-2), solving the interface problem (step I-3), and moving the interface (step I-4).

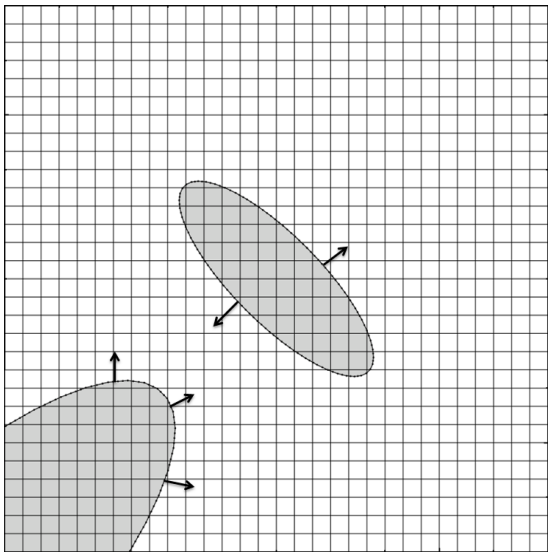

Figure IV-2: Closed and open interfaces over the medium regular grid.

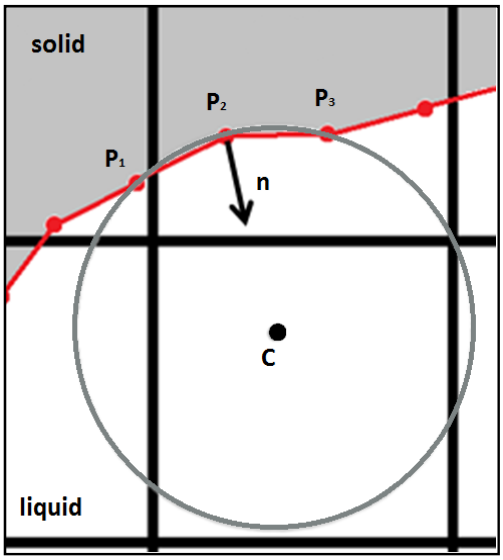

Figure IV-3: Three non-aligned interface marker points, with the unique circle connecting them.

For the interface discretization, a characteristic distance (Δl) is defined, which is generally chosen according to the fixed grid cells dimensions so that one grid cell can contain several marker points. Initially, interface marker points are calculated to be uniformly distributed along the interface with respect to Δl. However, during dendritic growth, interface usually deforms greatly, so stretching and contracting of some parts are quickly produced. In order to maintain a good resolution for the interface, addition and suppression of marker points are continuously required. That can be done by defining a tolerated range for each two adjacent marker points distance based upon the characteristic distance Δl; minimum (d_{min}) and maximum (d_{max}) limits. Spacing

between each adjacent points is then checked: if the distance between two adjacent marker points is detected to be larger than d_{max}, then a suitable number of marker points are uniformly added in between; if the distance is detected to be smaller than d_{min}, then the second point is deleted. When a marker point is deleted, a distance larger than d_{max} between the new neighbors is often generated, so a check test is required. In the present work, the maximum limit is chosen to be equal to the characteristic distance ($d_{max} = \Delta l$), however, the minimum limit is chosen to be equal to its half ($d_{min} = \frac{\Delta l}{2}$).

Once the set of marker points is updated, all the required parameters must be evaluated at each point. For the evaluation of curvature and normal vector orientation, alignment of each three consecutive marker points has to be checked. If a linear interface is taking place along these three points, then a null curvature for the mid-point is deduced. If one point and its two neighbors are not aligned (curved), local curvature as well as normal vector orientation at the point have to be appropriately evaluated. For that purpose, the unique circle, connecting the marker point and its two neighbors, is constructed. Figure IV-3 represents, for example, three non-aligned marker points (P_1, P_2 and P_3) of an interface portion separating two phases: solid (grey) and liquid (white). The unique circle, which connects the three points, is shown in order to get the curvature κ and the normal vector components ($a_{\vec{n}}, b_{\vec{n}}$) of the mid-point (P_2). As observed in this figure, normal vector is always considered to be oriented towards the liquid phase side. Coordinates of the circle center (black dot) are calculated as follow:

$$x_C = \frac{c_1 . b_1 - c_1 . b_3}{a_1 . b_3 - a_3 . b_1} \tag{IV-6}$$

$$y_C = \frac{-c_1 - a_1 . x_C}{b_1} \tag{IV-7}$$

where,

$$a_i = x_{Pi} - x_{P1} \tag{IV-8}$$

$$b_i = y_{Pi} - y_{P1} \tag{IV-9}$$

$$c_i = \frac{1}{2} . [(x_{P2}^2 - x_{Pi}^2) + (y_{P2}^2 - y_{Pi}^2)] \tag{IV-10}$$

Then, normal vector components and curvature can be directly deduced:

$$\vec{n} = \begin{pmatrix} a_{\vec{n}} \\ b_{\vec{n}} \end{pmatrix} = \begin{pmatrix} x_{P2} - x_C \\ y_{P2} - y_C \end{pmatrix} \; ; \quad \theta = tan^{-1}\left(\frac{b_{\vec{n}}}{a_{\vec{n}}}\right) \tag{IV-11}$$

$$\kappa = 2. curvature = \frac{2}{Radius} = \sqrt{(x_{P2} - x_C)^2 + (y_{P2} - y_C)^2} \tag{IV-12}$$

The orientation angle θ is calculated with respect to the horizontal x-axis.

Surface tension and kinetic mobility in this study are chosen to be anisotropic. The reasons behind this choice are, first, the important role of anisotropy, which has been discovered by [44], does more than simply control the asymmetry of the growing crystal, but also influences the dynamics in a profound way (an excellent overview can be found in [45]). Second, some selected materials which present a crystalline lattice in their solid phase are the focus of this study. The functional expressions are respectively given by (similar to [10] and [41]):

$$\gamma(\theta) = \gamma.\left\{1 + A_\gamma\left[\frac{8}{3}.sin^4\left(\frac{1}{2}.m_\gamma.\left(\theta - \theta_\gamma\right)\right) - 1\right]\right\} \quad \text{(IV-13)}$$

$$\frac{1}{\upsilon(\theta)} = \left(\frac{1}{\upsilon}\right).\left\{1 + A_\upsilon\left[\frac{8}{3}.sin^4\left(\frac{1}{2}.m_\upsilon.(\theta - \theta_\upsilon)\right) - 1\right]\right\} \quad \text{(IV-14)}$$

where γ is the isotropic surface tension, υ is the isotropic kinetic mobility, A_γ and A_υ determine the magnitude of anisotropy of surface tension and kinetic mobility, respectively. m_γ and m_υ determine the mode of symmetry of the crystal. θ_γ and θ_υ determine the angle of the symmetry axis with respect to the x-axis. Figures IV-4 and IV-5 represent in polar coordinates system, the functional form of anisotropy expressions (same in eqs. IV-13 and IV-14) for a four-fold material ($m_\gamma = m_\upsilon = 4$, $\theta_\gamma = \theta_\upsilon = 0$) and for a six-fold material ($m_\gamma = m_\upsilon = 6$, $\theta_\gamma = \theta_\upsilon = {}^{\pi}/_{6}$), respectively.

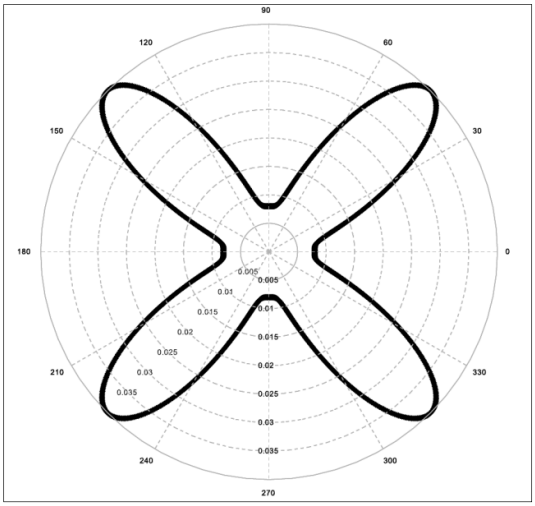

Figure IV-4: Anisotropy form for a four-fold material.

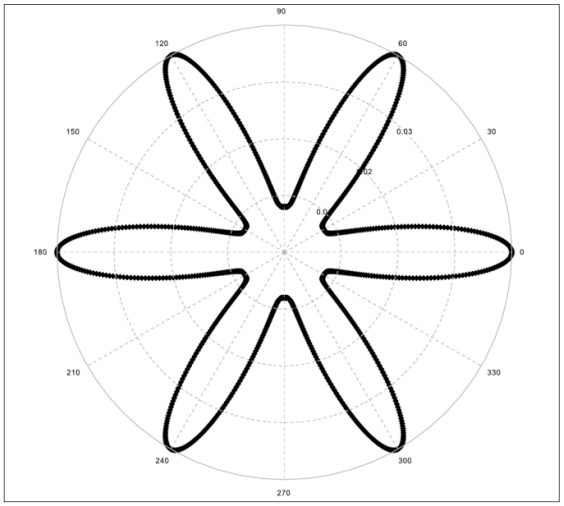

Figure IV-5: Anisotropy form for a six-fold material.

Local thermal gradients vectors between the interface and phases near it (eq. IV-3) are explicitly evaluated at the current time step. This feature is the most critical aspect of the method because, first, it determines the velocity which then gives movement of the interface, and second due to the temperature discontinuity at the interface between phases. The approach in the present study consists, for each phase, of

estimating a thermal linear plan taking into account the temperature value at the interface and the local temperature distribution around it. This approach has been tested with different meshes considering a fixed temperature at the interface, and homogeneous temperature fields in liquid and solid phases. For an initial circular interface, the approach is found to be correct because it provides homogeneous thermal gradients over all the marker points of the interface, and a growing circular interface is obtained over the whole time of the simulation (numerical results are showed later in section IV.2.4.2).

The third step of interface treatment consists of resolving the interface problem (eqs. IV-3, IV-4, and IV-5) in order to find each marker point temperature and velocity values. In functions of the obtained velocities, the fourth and last step is done by calculating the elementary displacement of marker points in their normal directions and then get a new geometry of the interface.

IV.2.3.2. Medium treatment

Spatial and temporal discretization techniques have to be coupled with the front-tracking approach in order to solve heat transfer equations in the liquid and solid regions (eqs. IV-1 and IV-2). As mentioned in the top of this section, a finite volume method is implemented in order to discretize the computational domain within phases, and an explicit first-order forward Euler scheme is used for the time integration. Herein, the whole medium is sub-divided into $M \times N$ elementary square volumes of unit thickness forming a stationary background mesh. Where M and N are, respectively, the number of grid cells by length and width. Each mesh cell is characterized by both geometrical and thermo-physical properties. Geometrical properties are centroid location, volume, as well as side exchange surfaces, while thermo-physical properties are density, thermal conductivity, and specific heat. In the proposed method, although both phases density are supposed to be equal, the other properties are not constant and change due to the evolution of the interface dividing medium into liquid and solid phases. Indeed, on the one hand, the thermo-physical properties which have to be applied depend on the physical phase of the mesh cell, and on the other hand, geometrical properties depend on the interface position; a mesh cell is regular if it does not contain an interface, and is considered irregular if it does. Consequently, at each time step, information must be transmitted between the moving representation of the interface and the stationary grid in order to update grid cells properties. In such a way, two virtual grids for phases are constructed over the stationary grid according to the actual position of the interface (step M-1).

For this critical computational aspect, the numerical code must be able to distinguish between grid cells which involve an interface and both phases coexist, and calculate each phase's geometrical properties, and grid cells which do not contain an interface and define the involved single phase (solid or liquid). Figure IV-6 presents for

instance three adjacent grid cells; the interface passes through the middle one, and does not through the two others (right and left).

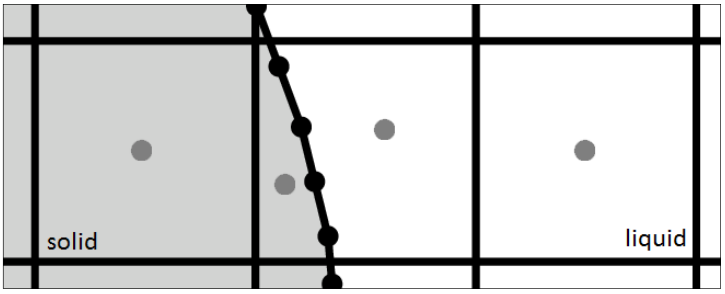

Figure IV-6: Three adjacent grid cells: the interface passes through the middle one, and does not through the two others (right and left).

For a regular single-phase grid cell (without interface) the phase's geometrical properties are deduced directly from the stationary grid dimensions, while the second phase (which does not exist) is considered as null. In figure IV-6, right and left cells are regular cell examples with different phases; the right cell is fully filled by liquid phase, while the left is fully filled by solid phase. On the other hand, when dealing with an irregular grid cell in which an interface occurs and both phases coexist (middle grid cell in figure IV-6), all intersection points between interface segments and its boundaries must be calculated and appropriately added to its points list. Interface segments and points list are defined, respectively, as the linear interpolation between two adjacent marker points on the interface, and the set of interface marker points involving the grid cell.

Figure IV-7 summarizes all the possible ways in which an interface segment can cross cell boundaries. Generally, there are either one or two intersection points between an interface segment and grid cells boundaries. If the grid cells handling interface points have one common side, then there is one intersection point (figure IV-7 (a) and (b)). Whereas, if involving grid cells do not have any common side, then there are two intersection points (figure IV-7 (c)). A particular case may take place when grid cells do not have any common side, and there is only one intersection point (figure IV-7 (d)). One has to be careful to identify this case because, in contrast to case (c), the calculated intersection point in case (d) has not to be added to the grid cell which is adjacent to both grid cells containing the interface points (the grey cell in figure IV-7).

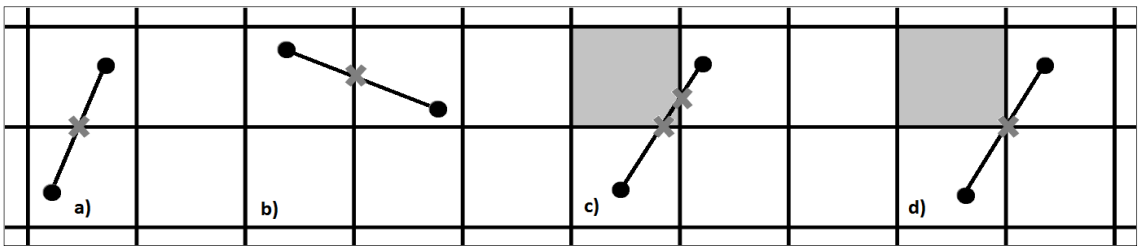

Figure IV-7: Possible ways in which an interface segment can cross a grid cell boundaries.

After the intersection points calculation procedure, geometrical properties of solid phase portions can be calculated from the final points list of each grid cell. We define here the index of grid cells as m, n, where $0 \leq m \leq M-1$, and $0 \leq n \leq N-1$. For an arbitrary grid cell of index (m, n), involving K closed paths of interface, and each path contains I_k marker points, the volume V of the involving solid phase can be calculated as follow:

$$V = 1 * S = 1 * \sum_{k=0}^{K-1} S_k = 1 * \sum_{k=0}^{K-1} \left\{ \frac{1}{2} . \sum_{i=0}^{I_k-1} \left[\left(x_{P_i} . y_{P_{i+1}} \right) - \left(y_{P_i} . x_{P_{i+1}} \right) \right] \right\} \quad \text{(IV-15)}$$

where S is the total area of solid portions, and the thickness is unity. Then, the centroid coordinates (x_c, y_c) of the solid portions are calculated as follow:

$$x_c = \frac{1}{S} \sum_{k=0}^{K-1} S_k . x_k = \frac{1}{S} \sum_{k=0}^{K-1} \left\{ \frac{1}{6} . \sum_{i=0}^{I_k-1} \left[\left(x_{P_i} + x_{P_{i+1}} \right) . \left(x_{P_i} . y_{P_{i+1}} - y_{P_i} . x_{P_{i+1}} \right) \right] \right\} \quad \text{(IV-16)}$$

$$y_c = \frac{1}{S} \sum_{k=0}^{K-1} S_k . y_k = \frac{1}{S} \sum_{k=0}^{K-1} \left\{ \frac{1}{6} . \sum_{i=0}^{I_k-1} \left[\left(y_{P_i} + y_{P_{i+1}} \right) . \left(x_{P_i} . y_{P_{i+1}} - y_{P_i} . x_{P_{i+1}} \right) \right] \right\} \quad \text{(IV-17)}$$

Afterwards, geometrical properties of liquid phase portions can be deduced as the complement of the solid phase portions.

IV.2.3.3. Heat release and temperature fields evolution

The heat release step consists in computing and taking away the latent heat produced during solidification process due to the interface progress. Indeed, the latent heat is released from the interface through both liquid and solid phases according to local thermal gradients between phases and the interface. Then, each phase temperature field is updated (step M-2). Based on the explicit finite volume scheme, the temperature of each elementary volume of each phase virtual grid is updated taking into account the different entering conductive heat flows which are exchanged with surrounding volumes as well as the latent heat which is released from the interface at the previous time iteration (eqs IV-1 and IV-2):

$$T_{m,n}^{i+1} = T_{m,n}^{i} + \frac{\sum_s \emptyset_s^i + \sum_k \emptyset_{f_k}^i}{\rho . c . V_{m,n}^i . \Delta t} \quad \text{(IV-18)}$$

This equation is applied at each time step i for each phase grid cell (m, n) in order to update its temperature in terms of conductive heat flows with adjacent same-phase grid cells $\sum_s \emptyset_s^i$ and latent heat released by all involving interface marker points $\sum_k \emptyset_{f_k}^i$. s refers to the cell side; $s = t, b, l$ and r for top, bottom, left, and right, respectively. Figure IV-8 presents, for instance, three typical medium grid cells: the interface passes through the middle one, and does not through the two others.

The grid cells (a) and (c) in figure IV-8 do not contain any interface, so they are two regular grid cells, but with different phases ((a) solid, and (c) liquid). Consequently, equation IV-18 is easily applied in terms of dimensions of regular grid with no additional latent heat from the interface, with different thermo-physical properties of the involving phase of each cell. However, the middle grid cell (b) is crossed by the interface through its top and bottom sides. The grid cell is then non-regular. In that case, geometrical properties of each phase portion must be passed according to the interface geometry (step described in the previous section), and then the involving latent heat released from it must be evaluated. Afterwards, equation IV-18 is applied for each phase volume basing on these data as well as the thermo-physical properties of the involving phase. It is worth noting that some conductive heat flows are prevented according to the interface geometry separating two phases within the grid cell. For instance, in this irregular grid cell (figure IV-8 (b)), there is no conductive heat flow neither through the right side of solid volume nor through the left side of liquid volume.

Finally, the time step is considered constant over the whole iterative procedure. In addition to the classic convergence criterion which has to be respected in order to avoid the divergence of temperature fields in both phases due to conductive heat flows from the surroundings, in such a moving boundary problem due to latent heat released from the interface and for numerical computational purposes, the time step must be selected so that several time steps are needed for an interface marker point to pass through a grid cell.

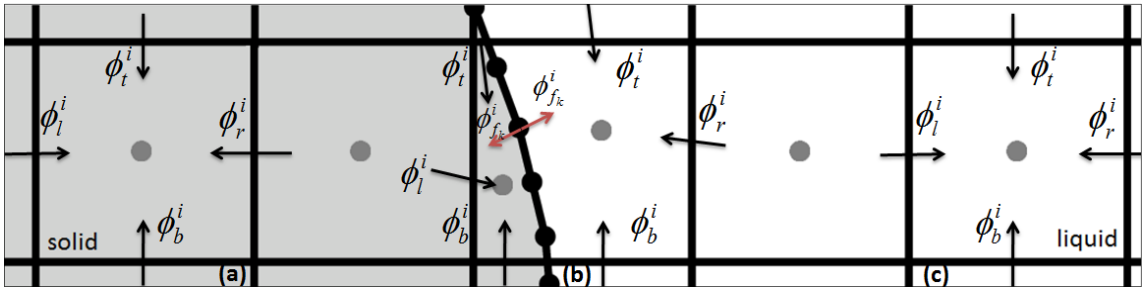

Figure IV-8: Three typical medium grid cells: the interface passes through the cell (b), and does not through (a) and (c).

IV.2.3.4. Numerical algorithm

At the initialization, a homogeneous set of marker points forming an interface, as well as temperature fields in liquid and solid phases are given. This initial interface representation does not necessarily respect the spacing range defining the interface resolution. Therefore, the first step must be done is to update the interface representation by adding and deleting marker points. Then according to this representation, physical state (liquid or solid) and all geometrical properties of each grid cell are deduced. Afterwards, from the updated interface shape and the given temperature fields in liquid and solid phases, the numerical algorithm tracks the

dynamical evolution of the interface proceeding iteratively through the main steps showed in figure IV-9.

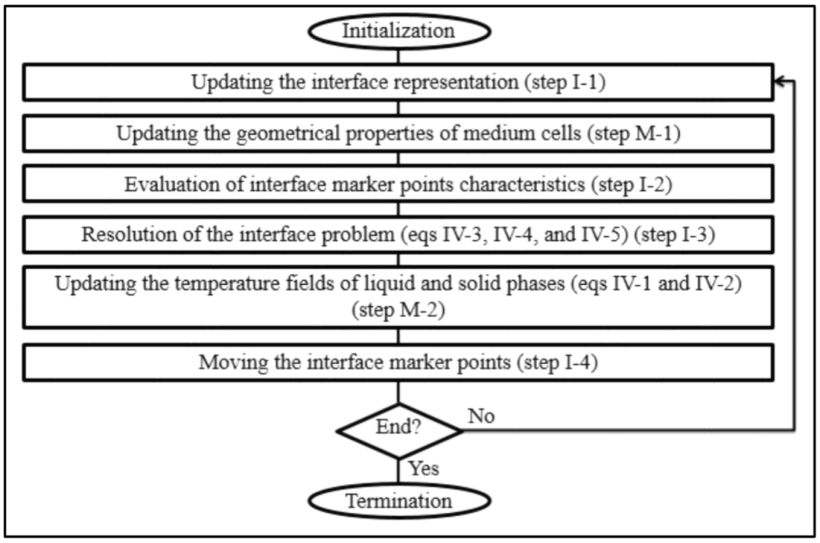

Figure IV-9: General numerical algorithm.

In order to solve the interface problem (eqs. IV-3, IV-4, and IV-5), all marker points characteristics must be appropriately evaluated. Then, temperature and velocity values of each marker point are obtained. According to these quantities, latent heat released by each marker point in the involved grid cell can be calculated. In terms of these calculated latent heat and surrounding conductive heat flows, temperature value of each cell of both phases is explicitly updated through the given time step. Finally the elementary displacement of each marker point is calculated, and a new interface geometry is completely determined. After the interface-moving step, a termination condition must be validated. The iterative procedure is stopped if the interface reaches one of the domain boundaries.

The whole numerical code is written in C++ language using an object-oriented programming approach. This approach allows defining for each physical structure a separate independent class with its own variables as well as functions which are used to manipulate these variables. Once all essential classes are defined, they may be easily combined and information may be safely passed between them.

IV.2.4. Results

In this section, numerical results, which are obtained by the numerical code described in the previous section in two dimensional space domain, are presented and discussed. The evolution of the liquid-solid interface during the solidification process of a supercooled pure substance is described. The solidification is initiated by introducing a small solid seed of radius r within the domain, which contains a supercooled liquid. Initially, the solid temperature is assumed to be equal to the equilibrium fusion temperature T_m, and the supercooled liquid temperature is considered homogeneous

and equal to $T_\infty < T_m$. Results are presented in seven sub-sections. In first two sub-sections, numerical tests of simple cases are discussed in order to demonstrate the validation of the proposed numerical method. Sub-sections IV.2.4.3 and IV.2.4.4 provide four- and six-fold interfaces as well as an orientation test, in order to check the robustness and the correctness of the numerical method implementation. Then, sub-sections IV.2.4.5 and IV.2.4.6 discuss, respectively, effects of surface tension and initial liquid temperature on the evolution of the interface. Finally, in sub-section IV.2.4.7 the dynamical evolution of an advanced interface showing realistic dendritic growth features is described. In each sub-section, the physical parameters are presented, numerical details follow, and the results are then described and discussed. The model name of the used processor is Intel® Xeon® CPU E5-2665 0 @ 2.40 Ghz, with total memory of 64 Gb.

IV.2.4.1. Critical radius

The solid germ formation through a supercooling liquid is involved by a free energy variation ΔG. For a spherical germ, this energy variation can be expressed in function of germ radius through surface and volume terms, as follows:

$$\Delta G = -\frac{4\pi\rho L}{3}.\frac{\Delta T}{T_m}.r^3 + 4.\gamma.\pi.r^2 \qquad \text{(IV-19)}$$

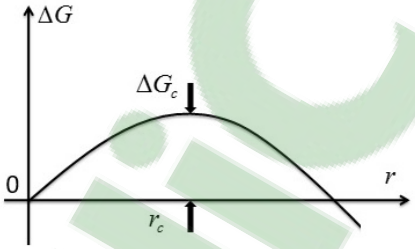

Figure IV-10: Variation of free energy in function of radius.

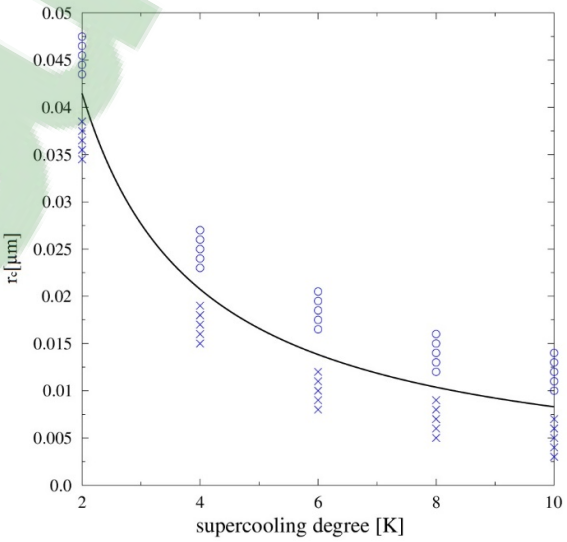

Figure IV-11: Variation of critical radius in function of supercooling degree. Circle and cross markers show first five numerical radii for which the imposed germ has grown or disappeared, respectively.

The spherical germ tends to minimize the free energy, so its behavior depends on the associated free energy variation. The derivation of the free energy expression in function of r leads to a critical radius concept for the homogeneous nucleation of solid. Indeed, it grows if the radius is larger than the critical radius r_c, and disappears if the initial radius is smaller than the critical one (see figure IV-10). Consequently, a solid

germ in a supercooled liquid can be responsible on the solid nucleation, which implies the complete phase change of the sample if, and only if, its radius is larger than the critical one r_c. The theoretical critical radius can be given by the following expression (this same expression can be deduced from the Gibbs-Thomson condition at the interface given by equation IV-5):

$$r_c = \frac{2.\gamma}{\rho L}.\frac{T_m}{\Delta T} \qquad \text{(IV-20)}$$

A numerical model of solidification processes must be examined to provide, from one hand, a growing interface in case with initial germ with a sufficient radius (larger enough than the critical one) and, on the other hand, a collapsing interface in the opposite case (smaller than the critical radius). For this purpose, for a reasonable range of different supercooling degrees, spherical seeds with different radii are imposed through the liquid to examine their tendencies. For each supercooling degree, as predicted, instead of the exact theoretical critical radius, an acceptable range around it, for which the seed neither grows nor collapses, has been obtained (see figure IV-11). If the radius of the imposed seed is below this range, the seed disappears, and if it is beyond this range, the seed grows.

In figure IV-11, variation of the theoretical critical radius in terms of degree of supercooling is plotted. In addition, for the different supercooling degrees ($\Delta T = \{2,4,6,8,10\}$), first five radii below the calculated critical radius for which the imposed seed disappeared, as well as first five radii beyond the critical one for which the imposed seed grew are shown with cross and triangular markers, respectively. The applied thermophysical properties are those of water/ice system at 0 °C, and the difference between examined radii is about 0.5 nm. As observed in this figure, the proposed numerical code reflects correctly the physical concept behind the homogeneous nucleation. Indeed, figure IV-11 shows that the numerical code is able to distinguish, according to both supercooling degree of liquid and seed radius, whether the seed has to grow or disappear. This primary step, dealing with the physical origin of solidification processes in a supercooled medium, is essential to give a primary trust to the proposed numerical code.

IV.2.4.2. Stable isotropic solidification: circular symmetry test

The numerical method must also be able to simulate the circular symmetry test of stable case of solidification, for which anisotropies effects are neglected. In such case, velocity must be homogeneous along the marker points of the interface and the developing structure must retain its circular initial shape. The main purpose behind this test is to check if the interpolation, used to calculate the local temperature gradients at the interface as well as the interface velocity, is not mesh dependent. In other words, regardless of the direction of the normal vector and of the manner in which the marker point crosses grid cells, the code must predict a constant velocity over all interface marker points to keep the interface morphologically stable. Therefore a circular stable

solidification case, with radius larger than the critical one, is examined in order to check the code behavior. An initial solid circular seed ($r = 1\ \mu m$) is introduced at the center of a supercooled liquid with $\Delta T = 10\ K$. Adiabatic conditions are assumed on all domain boundaries. The interface evolution is shown in figure IV-12. A domain of 100*100 μm^2 is considered.

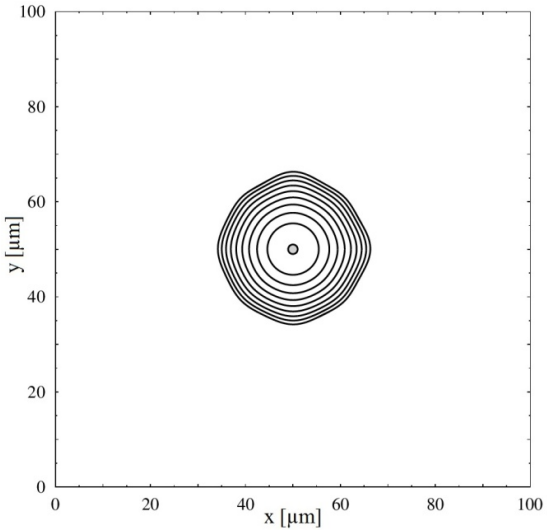

Figure IV-12: Interface evolution in a stable solidification case. $\boldsymbol{r = 1\ \mu m}$. $\boldsymbol{\Delta T = 10\ K}$. Anisotropic effects are neglected. Adiabatic boundary conditions. Interval time between interfaces 1 ms.

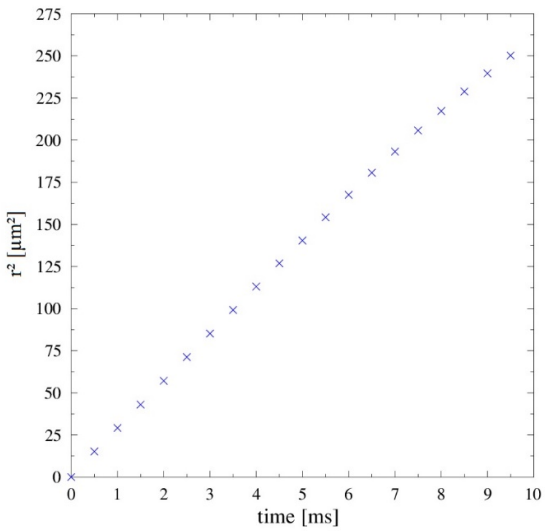

Figure IV-13: Numerical results of variation of the average of interface marker points radius in function of time. Linear variation is found.

As observed in figure IV-12, at early stages the interface evolves homogeneously retaining its initial circular shape. Indeed, at each time step, marker points have the same radius forming a circle for which radius increases with time. This result demonstrates that the numerical interpolation calculating the velocity of marker points, which is a critical aspect in the proposed method, is correct and accurate. It has to be noted that as the interface advances, difference between interface marker points radius increases but within an acceptable range around the radius average. These unstable deviations can be explained by cumulated numerical errors, and can be neglected while the average evolves correctly. Carslaw and Jaeger have developed analytical solutions for spherical solidification interfaces for similar conditions [38], and shown that the interface radius is proportional to square root of time. In order to show the correctness and robustness of the proposed numerical method, at each time interval, the average of interface marker points radius is calculated, then the square of this average is plotted as a function of time in figure IV-13. It has found that the average radius varies linearly with time, which is in agreement with the exact solution found in [38].

IV.2.4.3. Unstable solidification: four-fold and six-fold

After the previous two validation steps, the numerical code can be tested to determine its ability to solve for unstable cases of solidification, in which dendritic

structures may appear due to the complex interaction between destabilizing effects of liquid supercooling and the stabilizing effects of surface tension and kinetic mobility at the interface. These cases may be produced assuming anisotropic surface tension and kinetic mobility, given by eqs. IV-13 and IV-14, respectively. Two different modes of anisotropy are investigated. Under the same geometrical and thermal conditions, figures IV-14 and IV-15 represent unstable liquid-solid interface evolution with four-fold ($m_\gamma = m_\upsilon = 4$) and six-fold ($m_\gamma = m_\upsilon = 6$) anisotropies, respectively. An initial circular seed of solid ($r = 1\ \mu m$) is introduced at the center of a supercooled liquid ($\Delta T = 10\ K$). The isotropic surface tension is arbitrary chosen in order to provide a clear and branchless dendritic structure, $\gamma = 0.05$. The effect of isotropic surface tension is discussed later. To ensure a continuous evolution of the interface, a slightly smaller temperature is imposed on all the domain boundaries ($T_\infty - 1K$). Same conditions have been performed with adiabatic boundaries in order to see how an imposed temperature on boundaries affects the interface evolution. It is found that it has no effect on the global shape, but it just amplifies the evolution of the obtained branches at advanced stages of computations toward the domain boundaries. A domain of 100*100 μm^2 is considered for both cases.

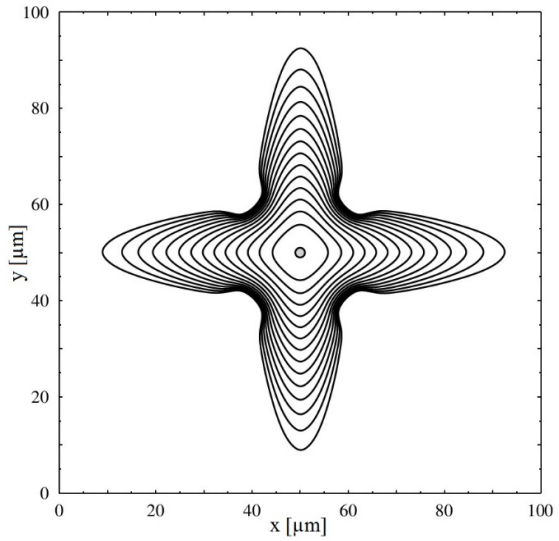

Figure IV-14: Interface evolution of four-fold symmetry. $\boldsymbol{r = 1\ \mu m}$. $\boldsymbol{\Delta T = 10\ K}$. $\boldsymbol{m_\gamma = m_\upsilon = 4}$. $\boldsymbol{\gamma = 0.05}$. $\boldsymbol{\theta_\gamma = \theta_\upsilon = 0}$. Boundary temperature $\boldsymbol{T_\infty - 1K}$. Interval time between interfaces 1 ms.

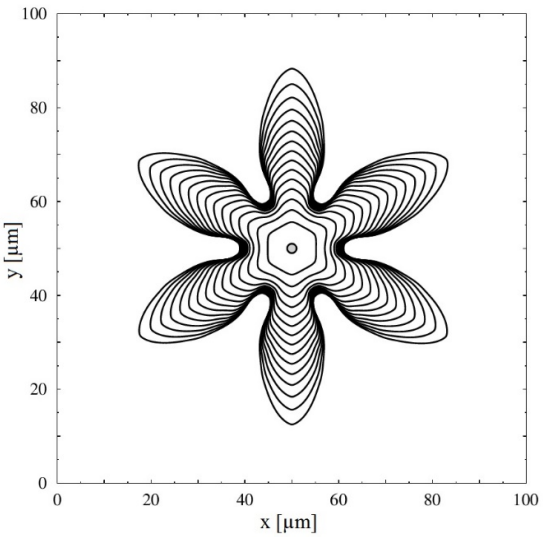

Figure IV-15: Interface evolution of six-fold symmetry. $\boldsymbol{r = 1\ \mu m}$. $\boldsymbol{\Delta T = 10\ K}$. $\boldsymbol{m_\gamma = m_\upsilon = 6}$. $\boldsymbol{\gamma = 0.05}$. $\boldsymbol{\theta_\gamma = \theta_\upsilon = \frac{\pi}{6}}$. Boundary temperature $\boldsymbol{T_\infty - 1K}$. Interval time between interfaces 1 ms.

In contrast to the isotropic case (figure IV-12), these results represent non-homogeneous interface evolution. The growing interface does not have the memory of its initial circular shape, and, according to the imposed anisotropy mode, privileged growth directions appear breaking the global stable form. In figure IV-14, in which four-fold anisotropy is considered, the interface has grown in four particular directions starting from the x-axis which is considered as the reference axis ($\theta_\gamma = \theta_\upsilon = 0$). However, in figure IV-15, which considers ice-flake's anisotropy mode (six-fold), six privileged growth directions have appeared starting here from the axis with angle π/6,

providing a reasonable shape of ice crystal ($\theta_\gamma = \theta_\upsilon = \pi/6$). The obtained primary branches and particular growth directions demonstrate the correctness of the numerical method implementation in which the involved effects at the interface appropriately interact to deal with unstable cases of solidification and to provide the suitable crystal symmetry according to the imposed parameters. In the next sub-section, an orientation test is provided for a four-fold symmetry case.

IV.2.4.4. Test of orientation

From a numerical point of view, it is important to test different orientations of the mesh. For that purpose, several different reference rotation angles for four-fold symmetry were simulated ($\theta_\gamma = \theta_\upsilon = \pi/2$ and $\theta_\gamma = \theta_\upsilon = \pi/4$). Figures IV-16 and IV-17 present two of these series of tests. All parameters and conditions are identical as in the case of four-fold symmetry presented in the previous section in figure IV-14, which is considered as reference case to compare.

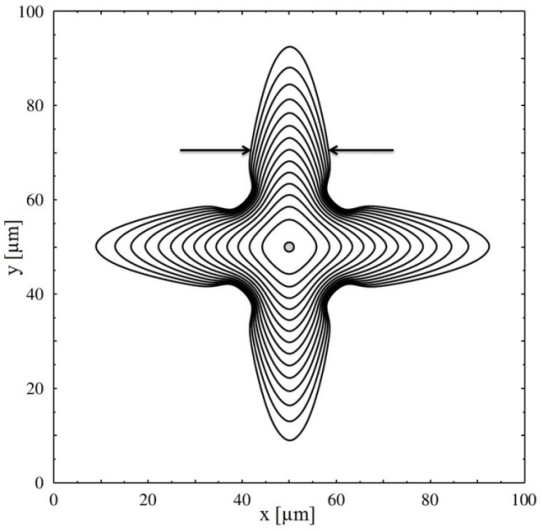

Figure IV-16: Interface evolution of four-fold symmetry. $\boldsymbol{r} = \mathbf{1}\ \mu\boldsymbol{m}.\ \Delta\boldsymbol{T} = \mathbf{10}\ \boldsymbol{K}.\ \boldsymbol{m_\gamma} = \boldsymbol{m_\upsilon} = \mathbf{4}.\ \boldsymbol{\gamma} = \mathbf{0.05}.\ \boldsymbol{\theta_\gamma} = \boldsymbol{\theta_\upsilon} = \frac{\boldsymbol{\pi}}{\mathbf{2}}$. Boundary temperature $\boldsymbol{T_\infty} - \mathbf{1}\boldsymbol{K}$. Interval time between interfaces 1 ms.

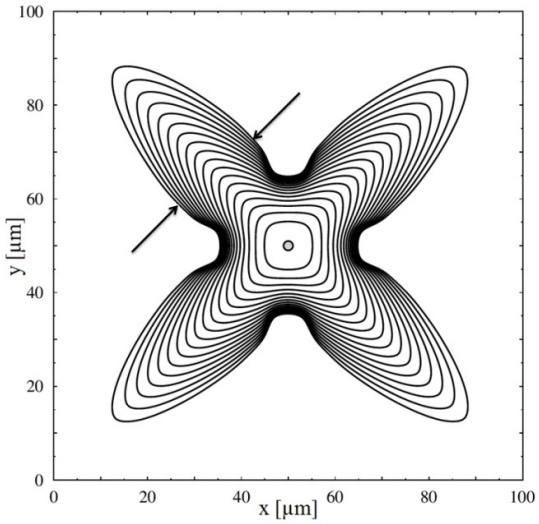

Figure IV-17: Interface evolution of four-fold symmetry. $\boldsymbol{r} = \mathbf{1}\ \mu\boldsymbol{m}.\ \Delta\boldsymbol{T} = \mathbf{10}\ \boldsymbol{K}.\ \boldsymbol{m_\gamma} = \boldsymbol{m_\upsilon} = \mathbf{4}.\ \boldsymbol{\gamma} = \mathbf{0.05}.\ \boldsymbol{\theta_\gamma} = \boldsymbol{\theta_\upsilon} = \frac{\boldsymbol{\pi}}{\mathbf{4}}$. Boundary temperature $\boldsymbol{T_\infty} - \mathbf{1}\boldsymbol{K}$. Interval time between interfaces 1 ms.

For the first case presented in figure IV-16, in which $\theta_\gamma = \theta_\upsilon = \pi/2$, there is no difference comparing with the reference case (figure IV-14), in which $\theta_\gamma = \theta_\upsilon = 0$. This is just normal and predictable for successive $\pi/2$ rotations. However, in figure IV-17, four growth directions are privileged starting with the positive diagonal axis according to the imposed reference angle in anisotropies expressions instead of x-axis in figure IV-16. It has to be noted that, in advanced stages of computations, the primary branches in figure IV-17 are somewhat thicker (determined by arrows) and shorter than those in the reference case (figure IV-16). This is due to the lower imposed temperature on the domain boundaries which tends in both cases to extend the crystal toward the

boundaries. However, although this difference, this simulation shows that the growing interface is mesh-independent in whatever the direction in which it passes through grid cells.

The next two sub-sections discuss the effect of liquid initial temperature and surface tension on the interface evolution. The purposes behind these two sections are to: (1) show that the numerical code produces appropriate results with different parameters and (2) see in a clear manner how these parameters - which are the main responsible on the dynamical evolution of the interface - affect the global shape.

IV.2.4.5. Effect of liquid initial temperature

The origin of morphological instabilities at the solid-liquid interface is supercooling. The more important the supercooling degree is, the more unstable the involved solid-liquid interface is and the more branchfull the produced structure is. In order to observe the effect of liquid temperature on dendritic growth, a four-fold symmetry is performed with smaller supercooling degree. The result is shown in figure IV-18, and is compared with figure IV-14. All imposed parameters are similar, but the supercooling $\Delta T = 5\ K$, and the imposed temperature on domain boundaries is updated to be also $T_\infty - 1K$ in this case.

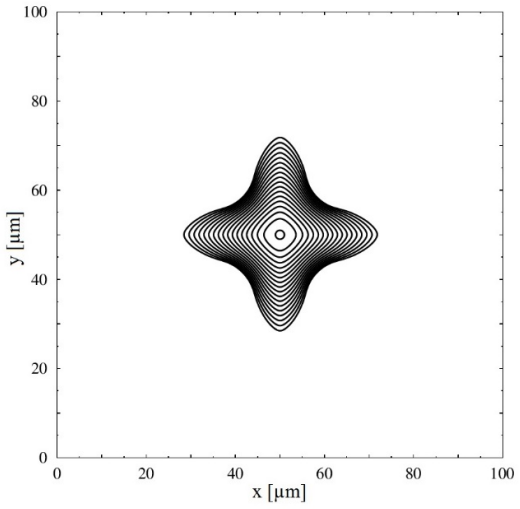

Figure IV-18: Interface evolution of four-fold symmetry. $\boldsymbol{r = 1\ \mu m}$. $\boldsymbol{\Delta T = 5\ K}$. $\boldsymbol{m_\gamma = m_v = 4}$. $\boldsymbol{\gamma = 0.05}$. $\boldsymbol{\theta_\gamma = \theta_v = 0}$. Boundary temperature $\boldsymbol{T_\infty - 1K}$. Interval time between interfaces 1 ms.

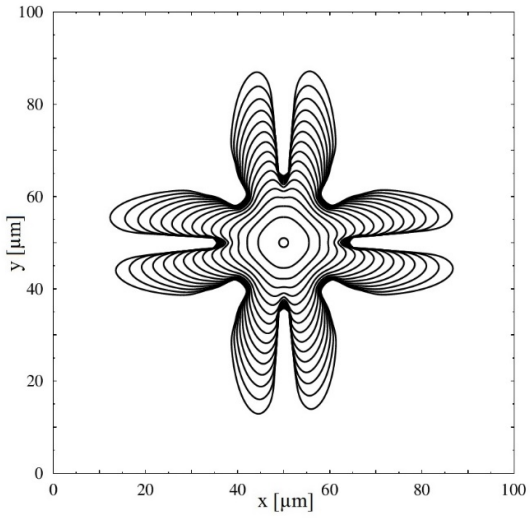

Figure IV-19: Interface evolution of four-fold symmetry. $\boldsymbol{r = 1\ \mu m}$. $\boldsymbol{\Delta T = 10\ K}$. $\boldsymbol{m_\gamma = m_v = 4}$. $\boldsymbol{\gamma = 0.025}$. $\boldsymbol{\theta_\gamma = \theta_v = 0}$. Boundary temperature $\boldsymbol{T_\infty - 1K}$. Interval time between interfaces 1 ms.

Globally, the obtained four-fold symmetrical interface has the same shape, but, with much less growth velocity. That is normally predicted, primary branches in that case are less developed and deviations at the interface providing these branches are weaker. Otherwise, although the produced interface is certainly unstable, but shows a lower level of morphological instability according to the involved supercooling degree.

IV.2.4.6. Effect of surface tension

By definition, surface tension tends to stabilize the interface evolution facing the effect of supercooling degree. In this sub-section, four-fold symmetry case is examined with isotropic surface tension $\gamma = 0.025$ (figure IV-19). Here, the result is completely different. Indeed, from early stages of computation, primary branches are slower toward the privileged directions of growth, to produce splitting phenomenon at each branch tip. In turn, these produced sub-branches grow quickly toward the privileged directions of growth, producing more unstable structure with more branches at the interface. Further, at more advanced stages, small protrusions tend to be produced on these sub-branches, introducing secondary-branches at the interface. That result shows the important role of surface tension to keep the interface stable facing the destabilizing effect of supercooling degree.

However, it is essential to test the interface behavior in somewhat more advanced stages to provide realistic dendritic phenomenon at the interface. This is done next.

IV.2.4.7. Interface evolution: tip-splitting and side-branching

The purposes of this sub-section is to demonstrate that the proposed method is able to deal with dendritic structures providing realistic features, and to describe dynamically in this case the evolution of the interface. Due to symmetry and time computation concerns, the computational domain is restricted to the positive quadrant. Further, a symmetry axis is imposed along the diagonal-axis of the domain to benefit from maximum possible space that could be given to the growing interface. In this case, numerical parameters are carefully chosen to provide realistic features of dendritic growth along the liquid-solid interface. An initial seed of radius $r = 1\ \mu m$ is imposed on the edge between the left and bottom domain boundaries. Initial temperature of supercooled liquid is $T_\infty = T_m - 8$. A domain of 100*100 μm^2 is considered with adiabatic conditions on the left and bottom boundaries, and a slightly smaller temperature elsewhere ($T_\infty - 1K$). Anisotropic parameters follow the case represented in figure IV-19 with different reference angle $\theta_\gamma = \theta_v = \pi/4$. The result is shown in figure IV-20. Figures IV-21, IV-22, and IV.23 represent the liquid phase temperature field at different time stages.

In figure IV-20, more advanced and realistic dendritic growth behavior can be clearly observed. From early computation stages (<30 ms), a dominating branch grows along the diagonal-axis according to the imposed reference angle in anisotropies expressions of surface tension and kinetic mobility. As shown in figure IV-21, liquid thermal field shows that, at 10 ms, local thermal gradient at the interface in the normal vector direction is homogeneous. Therefore, one can deduce that thermal gradient has no effect on the interface evolution to choose diagonal-axis as privileged growth direction, but only anisotropies effects which govern the evolution of the interface at these early stages.

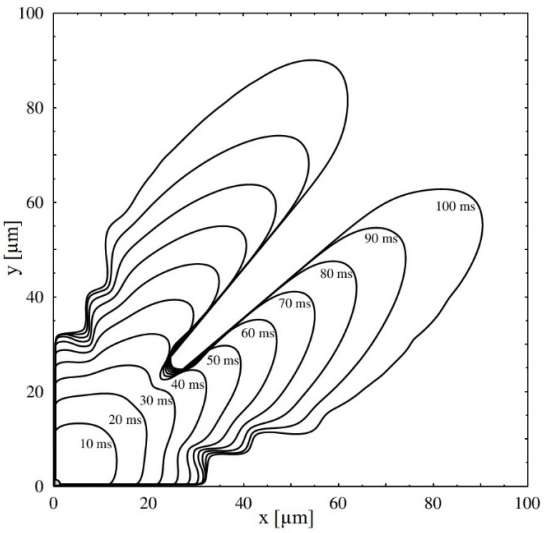

Figure IV-20: Interface evolution. $\boldsymbol{r = 1\ \mu m}$. $\boldsymbol{\Delta T = 8\ K}$. $\boldsymbol{m_\gamma = m_\upsilon = 4}$. $\boldsymbol{\gamma = 0.025}$. $\boldsymbol{\theta_\gamma = \theta_\upsilon = \frac{\pi}{4}}$. Boundary temperature $\boldsymbol{T_\infty - 1K}$ (right and top). Adiabatic boundaries (left and bottom). Interval time between interfaces 1 ms.

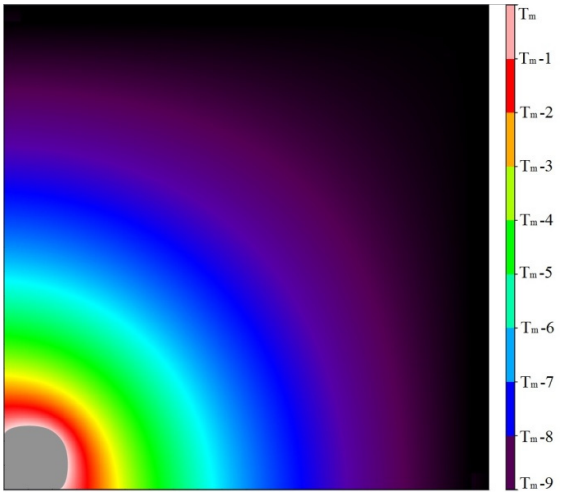

Figure IV-21: Liquid phase temperature field at 10 ms.

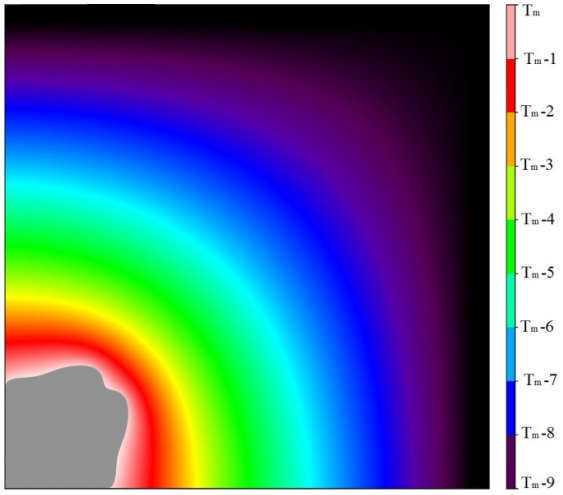

Figure IV-22: Liquid phase temperature field at 30 ms.

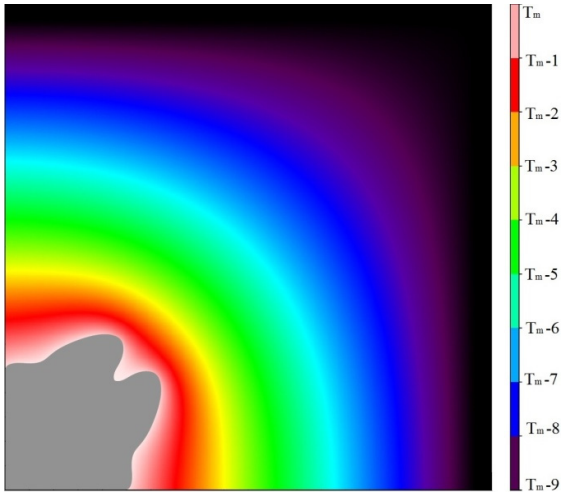

Figure IV-23: Liquid phase temperature field at 40 ms.

Further, at 30 ms, several deformations appear, at the tip and both extremities of the interface. At this stage, in figure IV-22, the homogeneous thermal gradient with liquid phase near the interface begins to break due to anisotropies effects, providing tip-splitting and small deformations at the interface both extremities (figure IV-20). At 40 ms, figure IV-23 presents an increase in liquid temperature in the vicinity of cavities at the branch-tip and interface sides (shown in pale pink). Increase in temperature prevents thereafter interface growing toward regions involving this temperature, amplifying the produced deformations and making then two large branches growing up and far from the nucleation center (figure IV-20). Furthermore, due to anisotropies effects, one can also observe predicted secondary branches along these two large

branches in somewhat more advanced stages of the evolution (>70 ms). These results involving both tip-splitting and secondary branches demonstrate the ability of the numerical code to show realistic features of dendritic growth and to study its characteristics.

IV.2.5. Conclusions

This paper deals with the solidification process of pure substances involved in several industrial applications. The interaction between thermal and anisotropies effects, which provides dendritic growth pattern, is described numerically in order to investigate what affects the dendrite evolution, and what is the influence of the thermal behavior on this growth. The study limits its scope to growth in a two-dimensional environment, free from natural convection in the upward direction.

The mathematical model is based on the heat diffusion equation in both phases, the heat balance at the solid-liquid interface, and the Gibbs-Thomson condition. The numerical method is based on an explicit front-tracking approach. It is embedding in a finite volume formulation in which an explicit first-order forward Euler time integration is used. The moving interface is represented by a moving set of maker points connected in a sequential order, which evolves over the global grid.

The numerical code behavior is first tested by use of the critical radius concept of homogeneous nucleation, and it is found to distinguish correctly whether the small germ has to grow up or down according to both its initial radius and supercooling degree. Then, the critical aspect of the interpolation of interface marker points velocity and local thermal gradients is checked by use a circular stable case of solidification, for which homogeneous velocities at the interface are produced. Agreement with the exact solution of Carslaw and Jaeger in this case is found. Two different anisotropies modes are simulated to produce appropriate crystal growth shapes involving both four-fold and six-fold materials. In addition, the effects of the variation of the orientation, the liquid initial temperature and the surface tension are provided for the four-fold crystal case. Finally, an advanced unstable case of solidification is simulated, for which the interface evolution is described in terms of different thermal and geometrical parameters. Results show that the code is able to deal with some particular cases of dendritic growth, providing realistic behavior as tip-splitting and secondary branches.

Upcoming works involve, in the one hand, the effect of non-homogeneous thermal gradient, which is imposed by the boundary conditions, on the symmetry and global shape of the crystal dendritic growth, and on the other hand, the design of a two-dimensional test bench in attempt to compare experimental visualization to numerical results obtained with the proposed method.

References

[1] Molinero V. *What determines the homogeneous freezing temperature of water?* AIP Conference Proceedings. AIP Publishing. 1527 (83): 82-88. (2013).

[2] Nistor R.A., Markland T.E., and Berne B.J. *Interface-limited growth of heterogeneously nucleated ice in supercooled water*. The journal of physical chemistry B. 118: 752-760. (2014).

[3] Karma A. Dendritic *Growth in Branching in Nature*: 365-402. Springer Berlin Heidelberg. (2001).

[4] Braga S.L., Milon J.J. *Visualization of dendritic ice growth in supercooled water inside cylindrical capsules*. International Journal of Heat and Mass Transfer, 55 (13): 3694-3703. (2012).

[5] Gilpin R.R. The effects of dendritic formation in water pipes. International journal of heat and mass transfer. 20: 693-699. (1976).

[6] Tirmizi S.H., and Gill W.N. *Effect of natural convection on growth velocity and morphology of dendritic ice crystals*. Journal of crystal growth. 85: 488-502. (1978).

[7] Jaafar M.A., Rousse D.R., Gibout S., and Bedecarrats J.P. *A review of dendritic growth during solidification: mathematical modeling and numerical simulations*. Renewable and Sustainable energy reviews. (Under Review).

[8] Roosen A.R., and Taylor J.E. *Modeling crystal growth in a diffusion field using fully faceted interfaces. Journal of computational physics*. 114: 113-128. (1994).

[9] Shyy W., Udaykumar H.S., and Liang S.J. *An interface tracking method applied to morphological evolution during phase change*. International journal of heat and mass transfer. 36 (7): 1833-1844. (1993).

[10] Juric D., and Tryggvason G. *A front-tracking method for dendritic solidification*. Journal of computational physics. 123: 127-148. (1996).

[11] Al-Rawahi N., Tryggvason G. *Numerical simulation of dendritic solidification with convection: two-dimensional geometry*. Journal of computational physics. 180: 471-496. (2002).

[12] Zhao P., Heinrich C., and Poirier D.R. *Fixed mesh front-tracking methodology for finite element simulations*. International journal of numerical methods in engineering. 61: 928-948. (2004).

[13] Voller V., and Cross M. *Accurate solutions of moving boundary problems using the enthalpy method*. International Journal of Heat and Mass Transfer. 24 (3) : 545-556. (1981).

[14] Voller V., and Cross M. *An explicit numerical method to track a moving phase change front*. International Journal of Heat and Mass Transfer. 26 (1): 147-150. (1983).

[15] Tacke K. and Harnisch A. *Finite difference enthalpy methods for dendritic growth*. Proceedings of the International Conference on Computational Modeling of Free and Moving Boundary Problems. (1991).

[16] Pal D., Bhattacharya J., Dutta P., and Chakraborty S. *An enthalpy model for simulation of dendritic growth*. Numerical Heat Transfer, Part B: Fundamentals. 50(1): 59-78. (2006).

[17] Voller V.R. *An enthalpy method for modeling dendritic growth in a binary alloy*. International Journal of Heat and Mass Transfer. 51 (3): 823-834. (2008).

[18] Sethian J.A., and Straint J. *Crystal growth and dendritic solidification*. Journal of Computational Physics. 98 (2): 231-253. (1992).

[19] Chen S., Merriman B., Osher S., and Smereka P. *A simple level set method for solving Stefan problems*. Journal of Computational Physics. 135 (1): 8-29. (1997).

[20] Kim Y.T., Goldenfeld N.D., and Dantzig J. *Computation of dendritic microstructures using a level set method*. Physical Review E. 62 (2): 2471. (2000).

[21] Gibou F., Fedkiw R.P., Cheng L. T., and Kang M. *A second-order-accurate symmetric discretization of the Poisson equation on irregular domains*. Journal of Computational Physics. 176 (1): 205-227. (2002).

[22] Fried M. A level set based finite element algorithm for the simulation of dendritic growth. Computing and Visualization in Science. 7 (2): 97-110. (2004).

[23] Yang Y., and Udaykumar H.S. *Sharp interface Cartesian grid method III: Solidification of pure materials and binary solutions*. Journal of Computational Physics. 210 (1): 55-74. (2005).

[24] Di Y., Li R. *Computation of dendritic growth with level set model using multi-mesh adaptive finite element method*. Journal of scientific computing. 39: 441-453. (2009).

[25] Theillard M., Gibou F., and Pollock T. *A sharp computational method for the simulation of the solidification of binary alloys*. Journal of scientific computing. 1-25. (2014).

[26] Kobayashi, R. *Modeling and numerical simulations of dendritic crystal growth*. Physica D: Nonlinear Phenomena. 63 (3): 410-423. (1993).

[27] Wang S. L., Sekerka R. F., Wheeler A. A., Murray B. T., Coriell S. R., Braun R. J., and McFadden G. B. *Thermodynamically-consistent phase-field models for solidification*. Physica D: Nonlinear Phenomena. 69 (1-2): 189-200. (1993).
[28] Wheeler A. A., Murray B. T., and Schaefer R. J. *Computation of dendrites using a phase field model*. Physica D: Nonlinear Phenomena. 66 (1): 243-262. (1993).
[29] Warren J. A., and Boettinger W. J. *Prediction of dendritic growth and microsegregation patterns in a binary alloy using the phase-field method*. Acta Metallurgica et Materialia. 43 (2): 689-703. (1995).
[30] Murray B. T., Wheeler A. A., and Glicksman M. E. *Simulations of experimentally observed dendritic growth behavior using a phase-field model*. Journal of Crystal Growth. 154 (3): 386-400. (1995).
[31] Do-Quang M., Villanueva W., Singer-Loginova I., and Amberg G. *Parallel adaptive computation of some time-dependent materials-related microstructural problems*. Bulletin of the Polish Academy of Sciences: Technical Sciences. 55 (2): 229-237. (2007).
[32] Wang H., Li R., and Tang T. *Efficient computation of dendritic growth with r-adaptive finite element methods*. Journal of Computational Physics. 227 (12): 5984-6000. (2008).
[33] Chen C. C., and Lan C. W. *Efficient adaptive three-dimensional phase-field simulation of dendritic crystal growth from various supercoolings using rescaling*. Journal of Crystal Growth. 311 (3): 702-706. (2009).
[34] Hu X., Li R., and Tang T. *A multi-mesh adaptive finite element approximation to phase field models*. Communications in Computational Physics. 5 (5): 1012-1029. (2009).
[35] Chang-Sheng Z., Li F., Zhi-Ping W., and Rong-Zhen X. *Numerical simulation of three-dimensional dendritic growth using phase-field method*. (2009).
[36] Tao L.N. *The Stefan problem with arbitrary initial and boundary conditions*. Quarterly of Applied Mathematics. 36 (3): 223-233. (1978).
[37] Lozano C.J., and Reemtsen R. *On a Stefan problem with an emerging free boundary*. Numerical Heat Transfer. 4 (2): 239-245. (1981).
[38] Carslaw H.S. and Jaeger J.C. *Conduction of heat in solids*. Oxford: Clarendon Press, 2nd ed. (1959).
[39] Mullins W.W., and Sekerka R.F. *Stability of a planar interface during solidification of a dilute binary alloy*. Journal of applied physics. 35(2): 444-451. (1964).
[40] Ivantsov G.P. *Temperature around a spheroidal, cylindrical and acicular crystal growing in a supercooled melt*. Dokl. Akad. Nauk. 58: 567-569. (1947).
[41] Almgren R. *Variational algorithms and pattern formation in dendritic solidification*. Journal of computational physics. 106(2): 337-354. (1993).
[42] Criscione A., Kintea D., Tuković Ž., Jakirlić S., Roisman I. V., and Tropea C. *Crystallization of supercooled water: A level-set-based modeling of the dendrite tip velocity*. International Journal of Heat and Mass Transfer. 66: 830-837. (2013).
[43] Shibkov A.A., Golovin Y.I., Zheltov M.A., Korolev A.A., and Leonov A.A. *Morphology diagram of nonequilibrium patterns of ice crystals growing in supercooled water*. Physica A: Statistical Mechanics and its Applications. 319: 65-79. (2003).
[44] Ben-Jacob E., Goldenfeld N.D., Langer J.S. and Schön G. Physical Review Letters. Vol. 51, no. 21: 1930. (1983).
[45] Goldenfeld N.D. *Dynamics of dendritic growth*. Journal of Power Sources. 26 (1): 121-128. (1989).

IV.3. Numerical investigation of thermal conditions effect on dendritic growth in pure substances using a front tracking method: Article 3

Mohamad Ali Jaafar [1,2], Stéphane Gibout [1], Jean-Pierre Bédécarrats [1], Daniel Rousse [2]

(1)Univ. Pau & Pays Adour - EA1932 - LATEP - Laboratoire de Thermique Energétique et Procédés, Rue Jules Ferry, BP7511 - PAU, F-64075, France
(2) t3e Industrial Research Group, École de technologie supérieure, Montréal (Qc), Canada

Abstract

The effect of non-homogeneous temperature field in a supercooled liquid on dendritic growth of pure substances is numerically investigated. The numerical method is based on a two-dimensional front tracking approach and a finite volume formulation. It has been found that the initial supercooling degree affects the size and the structure of the interface and that the macroscopic gradient (imposed by different temperatures at the domain boundaries) leads to an asymmetrical dendritic growth. The higher the macroscopic gradient is, the more visible the asymmetrical of dendritic growth is. The obtained quantitative results indicate that dendritic velocities depend only on the local supercooling degree. In this context, a local competition between the interface dynamics and the transfer rate of the associated latent heat in liquid phase is shown: when the interface grows rapidly, it moves to a region which is not yet influenced by the heat release, and then it keeps growing. Otherwise, when the interface movement is slow, it gets influenced by the heat release and then moves slower. Finally, it has been found that the variation of both total length of the interface and total solid phase are independent on the imposed macroscopic gradient, and that their ratio tends in all simulations to the same constant.

Keywords: Solidification process, Dendritic growth, Front tracking method.

IV.3.1. Introduction

Dendritic crystal growth is one of the most spontaneous and fascinating pattern formations, which is observed, for instance, in snowflakes formation phenomenon [1]. Dendritic structures are also commonly observed during metal and solution solidification, being present in all macroscopic castings ingots and welds [2]. Dendrites are crystals with a tree-like branching structure. That is why the term 'dendrite' originally comes from the Greek word 'dendron' which means tree [3]. While cooling the sample, the material may remain in its liquid state even at temperatures below the solid-liquid equilibrium temperature [4]. Such a state is metastable, and the liquid phase is called supercooled liquid. Once the metastability has been broken with the nucleation of solid, depending on supercooling degree (difference between equilibrium and

nucleation temperatures), dendrites may start to propagate within supercooled liquid raising its temperature to reach the equilibrium temperature. Then, the complete stable solidification occurs at this temperature. In supercooled mediums, dendrites are due to the competition between the destabilizing effect of supercooling and the stabilizing effects of, mainly, surface tension at the interface [5].

Dendritic pattern evolution has received much attention, mainly in metallurgy [5] and latent thermal storage domains [4]. On the one hand, dendrites constitute the initial microstructures of cast metals and alloys, so they strongly influence different properties of the finish obtained product. On the other hand, dendritic growth is the phase in which the temperature of the supercooled liquid returns to the equilibrium temperature. It is therefore studied in latent heat storage applications in which phase change materials are used. In addition, dynamic evolution of liquid-solid interface has a scientific potential in non-linear dynamics field to be simulated.

In this context, several experimental studies and numerical investigations deal with dendritic growth. As this paper deals with the numerical aspect of dendritic growth of pure substances, just selected experimental studies with water are reviewed. One of the first ice crystal visualizations came from Gilpin in 1976 [6]. He observed just after the nucleation at the top of a pipe which occurred at -3 °C, that dendrites started to propagate quickly within the supercooled liquid raising its temperature to 0 °C. Finally, he observed a stable annular front which came to solidify the whole section of the pipe. Later in 1987, a microscopic visualization was done by Tirmizi and Gill [7] to study in particularly the development of the dendrites. They showed that structures changed sequentially from disks, to perturbed-disks, to disk-dendrites, then to dendrites partially developed, and finally to dendrites completely developed. Recently in 2013 [8], visualization of crystallization inside a cylindrical capsule filled with water was carried out by Braga and Milon. They concluded mainly, by measuring temperature fields in the capsule, that crystal growth appears only in supercooled regions at nucleation instant, and that total blockage due to crystal growth occurs only with relatively high coolant temperature.

Modeling the mechanisms which result dendritic structures has been the objective over the last decades. The main difficulty in such problems is the fact that liquid-solid interface constitutes at the same time one of the problem boundaries and one of the problem unknowns. Such a problem is called moving boundary problem, for which analytical solutions are limited and numerical techniques are required. In the literature, two major classes of numerical methods dealing with dendritic solidification problem can be found, according to the way in which they handle and track the moving interface.

The first class is front tracking methods, which track the interface explicitly using a lower-dimension moving mesh. The sharp interface is represented by an independent deforming mesh which is reconstructed at each time step over the fixed background

describing the whole medium (liquid and solid phases). Roosen and Taylor [9], have showed, assuming some simplifying assumptions, that the use of front tracking approach is fast and easy to detect morphological changes. Later Shyy and al. [10] have got successfully dendritic phenomena such as tip-splitting and cusp formation. In 1996 Juric and Tryggvason [11] have described an explicit front tracking method to deal with complex dendritic solidification handling easily morphological changes under different conditions.

The second class of numerical methods is order parameter methods, which track the interface implicitly using an auxiliary variable. The interface is generally represented by a smooth zone described by the transition of the used variable between solid and phase values. The main numerical methods included in this category are phase-field model [12,13], level-set method [14,15], and enthalpy method [16,17]. For more Details see the review [18].

In contrast to order parameters methods, front-tracking methods use the unmodified energy equation with no need for an auxiliary variable to track the interface movement. Therefore, they require a relatively small computational capacity for quantitative studies. For these reasons mainly, a front tracking approach has been chosen for this study. The full description of the numerical method can be found in a previous study [19]. In the present paper particular cases are performed in order to investigate the effect of thermal conditions on the behavior of dendritic growth. The paper is divided in four main sections. The following section provides the complete mathematical formulation of the dendritic solidification problem. Then, the third section describes briefly the proposed numerical method. Finally, the fourth section presents and discusses simulation results investigating the thermal conditions effect on the interface evolution.

IV.3.2. Mathematical model

Generally, the whole domain can be divided into three regions: solid and liquid regions in which the temperature fields are described, and the interface separating phases at which boundary conditions have to be satisfied. However, the dependence of density on temperature in both phases is neglected, so that natural convection in liquid is neglected and only conduction heat transfer is taken into account. Furthermore, mass densities of liquid and solid phases are assumed to be equal and constant. However, discontinuities in other thermophysical properties between phases are considered, but they are all assumed to be independent of temperature. Consequently, dendritic growth problem involves first, the energy equation in both liquid and solid phases:

$$\rho . c_s . \frac{\partial T_s}{\partial t} = \vec{\nabla} \cdot \left(k_s \vec{\nabla} T_s \right) + \dot{Q}_s \qquad \text{solid phase region} \tag{IV-21}$$

$$\rho . c_l . \frac{\partial T_l}{\partial t} = \vec{\nabla} \cdot \left(k_l \vec{\nabla} T_l \right) + \dot{Q}_l \qquad \text{liquid phase region} \tag{IV-22}$$

where ρ is both liquid and solid density, c is the specific heat, and k is the thermal conductivity. $\dot{Q}$ is an energy source term due to liquid-solid interface movement. Subscripts s and l refer to solid and liquid phases, respectively.

Second, the Stefan condition (energy balance equation) at the interface which takes into account the released latent heat and the discontinuity of local gradients of temperature between interface and phases near it (figure IV-24):

$$\rho . L(T_f) . \mathbb{V}_n = (-\overrightarrow{\varphi_s} + \overrightarrow{\varphi_l})_P \cdot \vec{n} = \left(k_s \vec{\nabla} T_s - k_l \vec{\nabla} T_l\right)_P \cdot \vec{n} \quad \text{(IV-23)}$$

where $\mathbb{V}_n$ is the normal velocity of the interface, $\vec{n}$ the normal vector at the interface, and $L(T_f)$ the latent heat at the interface temperature T_f:

$$L(T_f) = L + (c_l - c_s)(T_f - T_m) \quad \text{(IV-24)}$$

with L the latent heat at T_m.

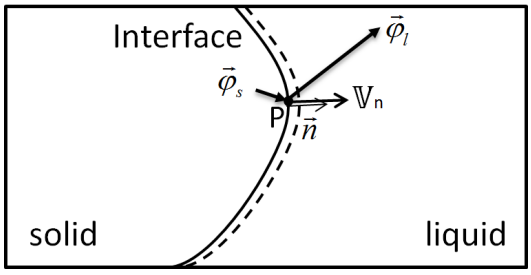

Figure IV-24: Interface separating solid and liquid regions.

Finally, the Gibbs-Thomson condition [11] at the interface, which has to be satisfied in order to evaluate the temperature of a curved interface:

$$T_f = T_m - T_m . \frac{\gamma(\theta) . \kappa}{\rho . L} - \frac{\mathbb{V}_n}{\upsilon(\theta)} - T_m . \frac{(c_l - c_s)}{L} . \left(T_f . ln\left(\frac{T_f}{T_m}\right) + Tm - T_f\right) \quad \text{(IV-25)}$$

where κ is twice of the interface mean local curvature, $\gamma(\theta)$ is the anisotropic surface tension, and $\upsilon(\theta)$ represents the anisotropic kinetic mobility. θ is the angle between normal vector at the interface and an arbitrary reference axis depending on the initial orientation of crystal germ.

IV.3.3. Numerical method

A two-dimensional front tracking method has been developed to simulate the interface evolution during dendritic solidification process in pure substances. This approach tracks the interface explicitly. It solves individually the heat equation in both phases in a fixed mesh, and reconstructs at each time step the representation of the interface which moves between phases. Front tracking method is coupled with a finite

volume method to discretize the energy partial differential equations in both liquid and solid phases, Eqs. (IV-21) and (IV-22). Herein, a regular mesh is used for dividing solid and liquid regions in elementary square volumes of unit thickness. On the other hand, an explicit first-order forward Euler method is employed to discretize time. The numerical resolution can be divided into two major parts: interface treatment and temperature fields resolution. In this section, the numerical method is briefly described, for more details, see [19].

IV.3.3.1. Interface treatment

The interface is then described by a set of moving marker points which are connected by a sequential order using linear interpolation to form one dimensional sharp mesh. The initial interface geometry is usually given by a list of points or by a functional form relating Cartesian variables. These points are uniformly distributed along the interface. Afterwards, to maintain a good resolution for the interface, characteristic minimum and maximum spacing limits are defined according to the fixed background dimensions. The interface representation is updated at each time step according to these limits (step I-1).

In order to solve the interface problem at each marker point, the required parameters must be evaluated (step I-2). The curvature and the normal vector orientation are found at each marker point, by constructing the unique circle which connects the point with its two neighbors. Normal vectors at the interface are always considered to be oriented toward the liquid phase.

Surface tension and kinetic mobility are chosen to be anisotropic, and given by the following functional expressions [11]:

$$\gamma(\theta) = \gamma.\left\{1 + A_\gamma\left[\frac{8}{3}.sin^4\left(\frac{1}{2}.m_\gamma.\left(\theta - \theta_\gamma\right)\right) - 1\right]\right\} \quad \text{(IV-26)}$$

$$\frac{1}{\upsilon(\theta)} = \left(\frac{1}{\upsilon}\right).\left\{1 + A_\upsilon\left[\frac{8}{3}.sin^4\left(\frac{1}{2}.m_\upsilon.(\theta - \theta_\upsilon)\right) - 1\right]\right\} \quad \text{(IV-27)}$$

where γ is the isotropic surface tension, υ is the isotropic kinetic mobility, A_γ and A_υ determine the magnitude of anisotropy of surface tension and kinetic mobility, respectively. m_γ and m_υ determine mode of symmetry of the crystal. θ_γ and θ_υ determine angle of symmetry axis with respect to x- axis.

The interface problem is then solved at each marker point in order to get temperature and velocity values (step I-3). These values are needed to determine both the elementary displacement of each marker point within the time step and the latent heat released by the marker point in both phases. The last step in the interface treatment is moving all marker points (step I-4).

IV.3.3.2. Medium treatment

Each grid cell is characterized by both geometrical and thermo-physical properties. Geometrical properties are centroid location, volume, as well as side exchange surfaces, while thermo-physical properties are density, thermal conductivity, and specific heat. In the proposed method, although density is constant, the other properties are not constant and may significantly change due to the evolution of the interface, dividing medium into liquid and solid phases. Consequently, at each time step, information must be transmitted between the moving representation of the interface and the stationary grid in order to update grid cells properties. In such a way, two virtual grids for phases are constructed over the stationary grid according to the actual position of the interface (step M-1). For that purpose, the numerical code has to be able to distinguish between two types of grid cells, regular grid cell without interface in which only one phase exists, and irregular grid cell with interface in which both phases coexist. The volumes of each phase in an irregular grid cell are calculated by assuming a polygon formed by the involved interface marker points and the edges of the grid cell.

Once medium grid properties are found adequately, temperature field of each phase is updated (step M-2). Based on the explicit finite volume scheme, the temperature of each elementary volume of each phase is updated through the time step taking into account both heat conductive flows exchanged with the surrounding cells and latent heat which is released by the interface if it takes place (eqs. (IV-21) and (IV-22)).

The time step is considered constant over the whole iterative procedure, and calculated according to both medium grid dimensions and maximum possible interface velocity, so that several time steps are needed for an interface point to pass through a grid cell.

IV.3.3.3. Numerical algorithm

The numerical code is written in C++ language using an object-oriented programming approach. The numerical algorithm proceeds iteratively through the main steps showed in figure IV-25.

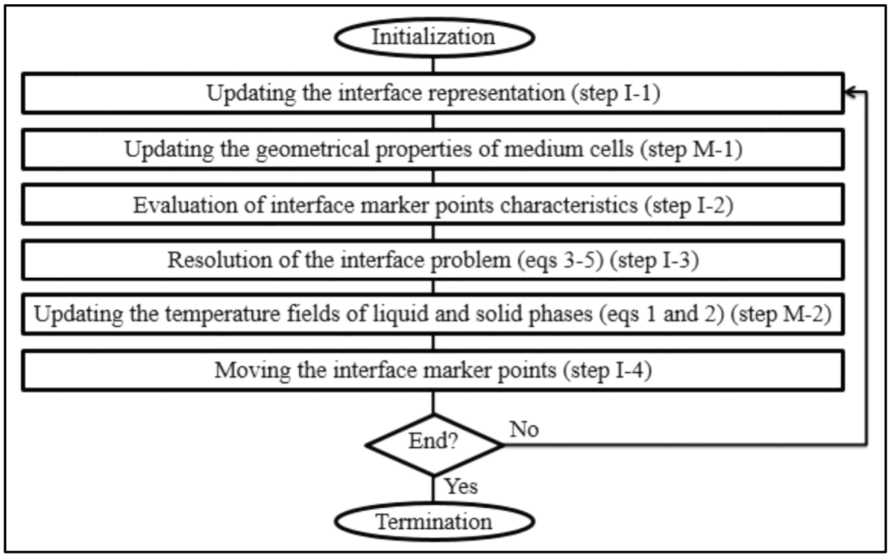

Figure IV-25: General numerical algorithm

IV.3.4. Results

In this section, numerical results are presented and discussed. The solidification is initiated by a circular solid germ (of 1 µm of radius) within the supercooled liquid in a rectangular domain (figure IV-26). Left and right boundaries are assumed to be adiabatic. Top T_t and bottom T_b temperatures are imposed in order to maintain a vertical macroscopic gradient over the whole domain ($T_t \leq T_b$). Initially, the solid temperature is assumed to be equal to the solid-liquid equilibrium temperature T_m. Four-fold anisotropic symmetry mode is considered for all computations (m_γ=m_υ=4). The reference axis is arbitrary chosen along the positive horizontal axis (θ_γ=θ_υ=0). Numerical cases are presented in two series: in the first one the vertical macroscopic thermal gradient is constant with different initial supercooling degrees at the central horizontal axis (cases 1, 2, 3, 4 and 5 in bold lines in figure IV-27), and in the second one different macroscopic thermal gradients are considered keeping the same initial supercooling degree at the central horizontal axis (cases 6, 7, 4, 8, 9, 10 and 11 in thin figure IV-27). Thermal conditions of all these cases are detailed in Table IV-1. It has to be noted that case 4 is involved in both series. For convenience, the macroscopic gradient is characterized by the temperature gap between bottom and top boundaries, and the central supercooling degree refers to the initial supercooling degree of liquid at the central horizontal axis passing through the initial germ center.

The obtained results are presented and discussed qualitatively and quantitatively in the following sub-sections. The qualitative analysis concerns the observed global shape and the involved topological phenomena during the interface evolution. For the quantitative analysis, positions, growth velocities, the dissymmetry of the dendrite, the total length of the interface and the total surface of solid phase are introduced and discussed. The nucleation is supposed to be occurred at the initial instant (0 s).

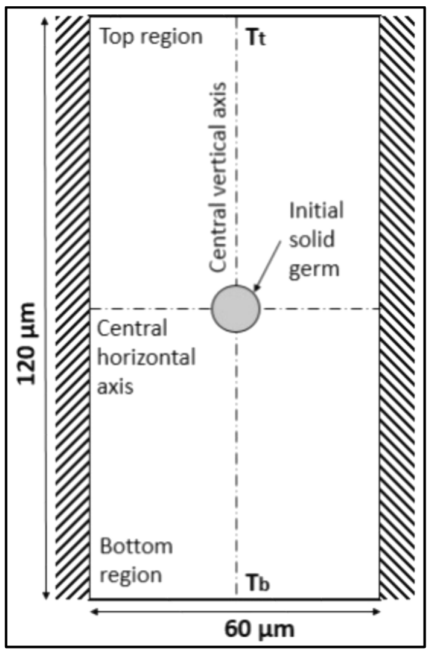

Figure IV-26: Schematic of the computational domain

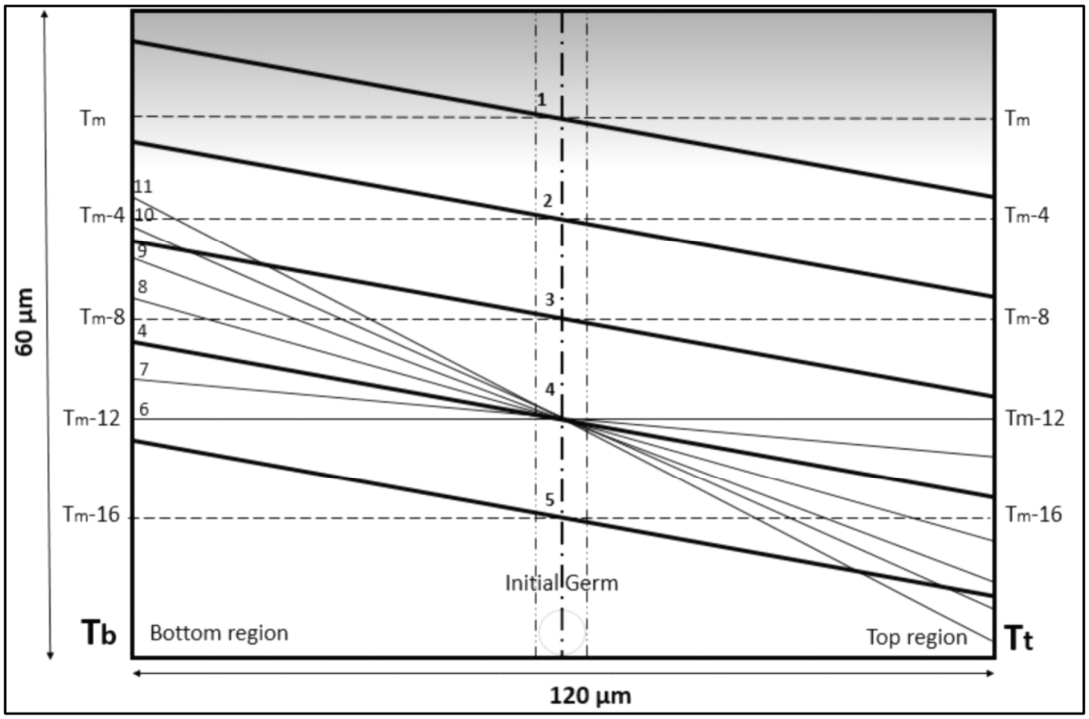

Figure IV-27: Linear temperature distribution in liquid. Bold lines (series 1): cases 1, 2, 3, 4, and 5. Thin lines (series 2): cases 6, 7, 8, 9, 10, and 11.

IV.3.4.1. Qualitative analysis

IV.3.4.1.1. Central supercooling degree effect

In this sub-section the central supercooling degree is investigated qualitatively. T_t and T_b are imposed in order to keep a constant macroscopic gradient but to lead to different temperatures at the central horizontal axis (series 1). These temperatures with respect to the equilibrium temperature T_m are represented in Table IV-1. The interface evolution for cases 1, 2, 3, 4 and 5 are represented, respectively, in figures IV-28, IV-29, IV-30, IV-31 and IV-32. The liquid temperature is decreased by 4 K between two consecutive cases.

Case	T_t	T_b	Central temperature	$T_b - T_t$	Figure
1	$T_m - 3$	$T_m + 3$	T_m	6	IV-28
2	$T_m - 7$	$T_m - 1$	$T_m - 4$	6	IV-29
3	$T_m - 11$	$T_m - 5$	$T_m - 8$	6	IV-30
4	$T_m - 15$	$T_m - 9$	$T_m - 12$	6	IV-31
5	$T_m - 19$	$T_m - 13$	$T_m - 16$	6	IV-32
6	$T_m - 12$	$T_m - 12$	$T_m - 12$	0	IV-33
7	$T_m - 13.5$	$T_m - 10.5$	$T_m - 12$	3	IV-34
8	$T_m - 16.5$	$T_m - 7.5$	$T_m - 12$	9	IV-35
9	$T_m - 18$	$T_m - 6$	$T_m - 12$	12	IV-36
10	$T_m - 19.5$	$T_m - 4.5$	$T_m - 12$	15	IV-37
11	$T_m - 21$	$T_m - 3$	$T_m - 12$	18	IV-38

Table IV-1: Thermal properties of cases in series 1 (1, 2, 3, 4 and 5) and in series 2 (6, 7, 4, 8, 9, 10 and 11) with respect to the liquid-solid equilibrium temperature.

First, we note that, at constant macroscopic gradient, the central supercooling degree affects not only the size of the interface but also its solid overall shape and the structure of branches. For case 1 (figure IV-28), the boundaries temperatures are chosen so that the central liquid temperature (at the central horizontal axis) is equal to the equilibrium one T_m; the top temperature is lower than T_m, and the temperature in the bottom region is higher than T_m. Only the top region of the liquid is therefore supercooled in this case. As observed in figure IV-28, the obtained interface only grows in the positive vertical direction, and it melts in the negative side. This is normal and predictable, liquid-solid transformation takes place only in regions of the liquid in which the temperature is lower than T_m at the nucleation instant.

Figure IV-29, represents the evolution stages of the solid germ when both top and bottom boundaries temperatures are lower than the equilibrium one, causing a supercooled liquid in the whole domain at the nucleation instant (case 2). In contrast to case 1, the interface grows in all directions, showing four privileged directions. This result affirms that supercooling is needed and essential for an interface to grow up. The obtained result is asymmetrical, and shows a more advanced interface in the positive vertical direction. That is due to the lower temperature (with respect to T_m) imposed at the top domain boundary. This shows that the vertical symmetry of a growing dendrite

is broken down by considering different thermal conditions at the domain boundaries. However, the obtained interface is symmetrical with respect to the central vertical axis due to the similar adiabatic conditions at the right and left boundaries.

Figure IV-30 represents case 3, in which much lower imposed temperatures on top and bottom boundaries are considered. The growing interface in this case is more developed in all directions, and clearly asymmetrical growing faster, from early stages, in the positive vertical direction. Furthermore, at 10 ms, the tip-splitting phenomenon is produced in this direction. At more advanced stages, protrusions at the interface tend also to be produced at the base of the positive vertical arms, introducing secondary branches. Thus, tip-splitting and side-branching phenomena are produced only in the positive vertical direction where relatively higher supercooling degree is taking place due to a sufficient low temperature imposed at the top boundary of the domain. The obtained result is important and illustrates the destabilizing effect of the supercooling phenomenon to produce more instable structures; stable and needle-like growth when it is relatively small, and branchfull dendritic growth when it is high enough.

For both last cases 4 and 5, in contrast to previous cases, the liquid is initially supercooled sufficiently, so that tip-splitting phenomenon is produced in all directions: top, bottom, right and left (figures IV-31 and IV-32). Indeed, the growing shape has eight arms, two arms in each direction. In both cases, the obtained shapes are non-homogeneous and asymmetrical with respect to the central horizontal axis. Indeed, the growing four arms in the top region of the domain are faster and more advanced than the four ones in the bottom region. That is due to the lower temperature imposed at the top domain boundary and therefore to the higher local thermal gradients near the interface which control the growing interface velocity. Once again, the obtained shape at all stages is symmetrical with respect to the central vertical axis because similar assumed conditions at both right and left boundaries. Adiabatic conditions don't allow heat dissipation toward the outside of the domain, and thus the released latent heat from the growing interface will be accumulated in regions near right and left boundaries. The released latent heat increases rapidly in these regions limiting the dendritic growth toward the horizontal directions. In addition, the horizontal arms have the tendency to grow along the vertical directions at advanced stages following the local thermal gradient which is more important in the vertical direction.

Recall that the liquid-solid transformation can take place only if the interface is able to release latent energy toward the surrounding environment which can occur only if the environment has a lower temperature than the interface one (slightly lower than the liquid-solid equilibrium temperature). As the purpose of the supercooling breakdown is to increase the liquid temperature to reach the equilibrium one, the dendritic pattern growth is probably a very effective mechanism at the beginning of crystallization, during which the length of the interface increases rapidly looking for supercooled liquid regions with lowest temperature in order to facilitate the energy exchange.

IV.3.4.1.2. Macroscopic gradient effect

In this sub-section the macroscopic gradient effect is investigated qualitatively, considering a constant central supercooling degree (series 2). The macroscopic gradient is imposed varying T_t and T_b in a manner that the central supercooling degree remains constant and equal to $T_m - 12$ (Table IV-1). This temperature is chosen low enough in order to produce tip-splitting phenomenon in all directions. Starting from case 6, for which there is no macroscopic gradient ($T_b - T_t = 0$), the temperature gap ($T_b - T_t$) is increased by 3 K. Recall that case 4 is involved also in this series.

A reference case is examined, for which there is no macroscopic gradient and the initial liquid temperature is assumed to be homogeneous (case 6). As observed in figure IV-33, the obtained shape is symmetrical with respect to both central vertical and horizontal axes. That is due to the similar imposed conditions, from one hand, at the top and bottom boundaries, and from the other hand, at the right and left boundaries. However, vertical arms are more developed and faster than horizontal arms. The limited growth in the horizontal direction is due to the adiabatic conditions at the right and left sides.

For the other cases in this series (7, 4, 8, 9, 10 and 11 in table IV-1) in which a macroscopic gradient is imposed, the interface evolution in time is represented in figures IV-34, IV-31, IV-35, IV-36, IV-37, and IV-38. The obtained shape is clearly asymmetrical showing more developed branches in the positive vertical direction. This means that the presence of the vertical macroscopic gradient produces an asymmetrical dendritic growth with respect to the central horizontal axis. Furthermore, one can deduce that the more the macroscopic gradient gets larger, the more the asymmetry is visible and noticeable by both vertical and horizontal branches. However, symmetry with respect to the central vertical axis is maintained in all cases. Therefore, different thermal conditions break generally the symmetry of a growing dendrite. That explains the non-perfectly symmetrical dendrites in Nature, where it is difficult to have similar thermal conditions surrounding the growing dendrite, and moreover, liquid flow may be involved improving heat transfer in one direction.

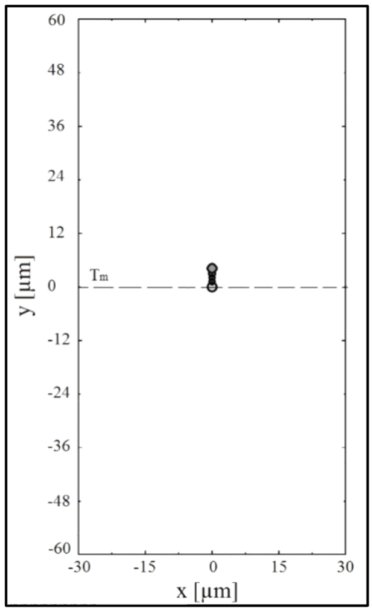

Figure IV-28: Interface evolution of case 1 with $\boldsymbol{T_t = T_m - 3}$ and $\boldsymbol{T_b = T_m + 3}$. Interval time between interfaces is 2 ms.

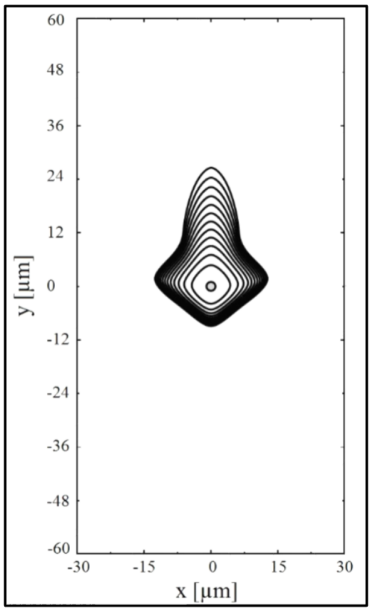

Figure IV-29: Interface evolution of case 2 with $\boldsymbol{T_t = T_m - 7}$ and $\boldsymbol{T_b = T_m - 1}$. Interval time between interfaces is 2 ms.

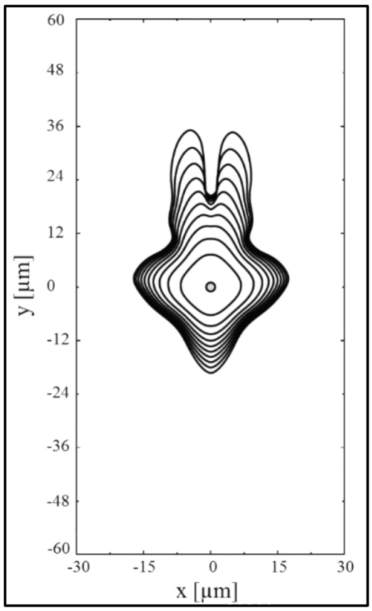

Figure IV-30: Interface evolution of case 3 with $\boldsymbol{T_t = T_m - 11}$ and $\boldsymbol{T_b = T_m - 5}$. Interval time between interfaces is 2 ms.

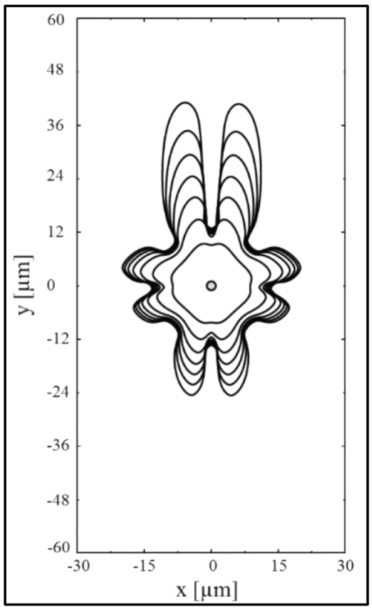

Figure IV-31: Interface evolution of case 4 with $\boldsymbol{T_t = T_m - 15}$ and $\boldsymbol{T_b = T_m - 9}$. Interval time between interfaces is 2 ms.

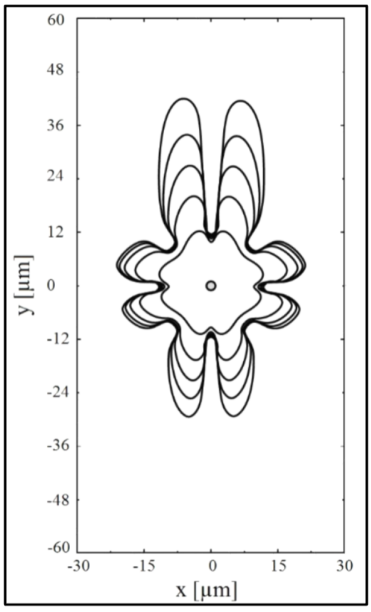

Figure IV-32: Interface evolution of case 5 with $\boldsymbol{T_t = T_m - 19}$ and $\boldsymbol{T_b = T_m - 13}$. Interval time between interfaces is 2 ms.

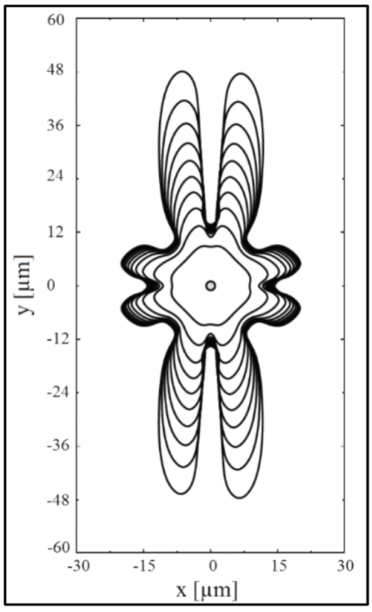

Figure IV-33: Interface evolution of case 6 with $\boldsymbol{T_t = T_m - 12}$ and $\boldsymbol{T_b = T_m - 12}$. Interval time between interfaces is 2 ms.

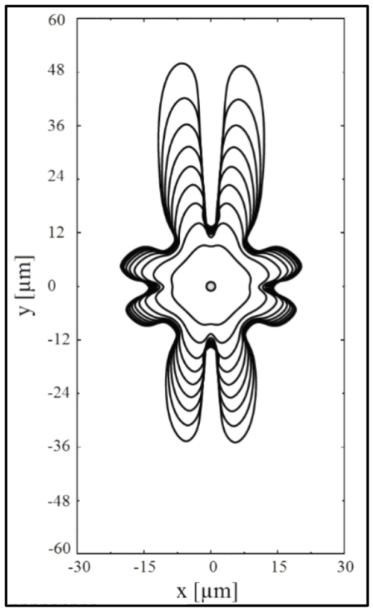

Figure IV-34: Interface evolution of case 7 with $\boldsymbol{T_t = T_m - 13.5}$ and $\boldsymbol{T_b = T_m - 10.5}$. Interval time between interfaces is 2 ms.

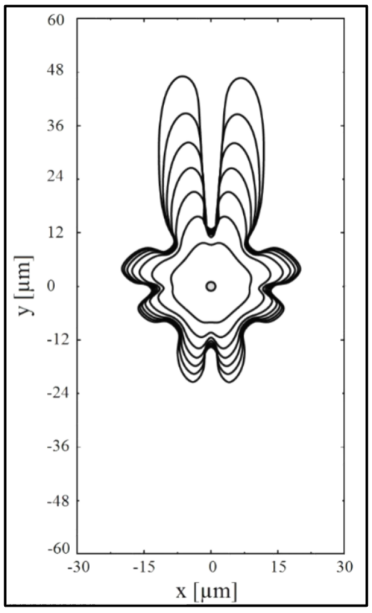

Figure IV-35: Interface evolution of case 8 with $\boldsymbol{T_t = T_m - 16.5}$ and $\boldsymbol{T_b = T_m - 7.5}$. Interval time between interfaces is 2 ms.

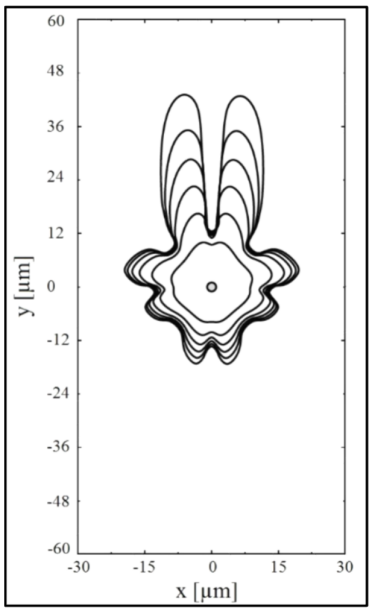

Figure IV-36: Interface evolution of case 9 with $\boldsymbol{T_t = T_m - 18}$ and $\boldsymbol{T_b = T_m - 6}$. Interval time between interfaces is 2 ms.

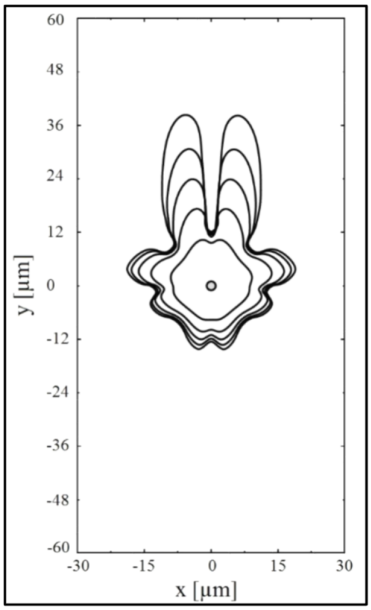

Figure IV-37: Interface evolution of case 10 with $\boldsymbol{T_t = T_m - 19.5}$ and $\boldsymbol{T_b = T_m - 4.5}$. Interval time between interfaces is 2 ms.

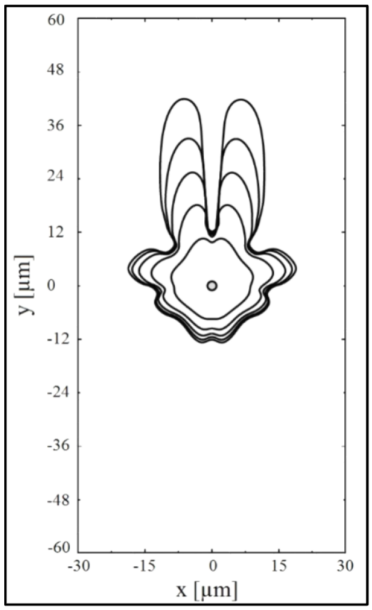

Figure IV-38: Interface evolution of case 11 with $\boldsymbol{T_t = T_m - 21}$ and $\boldsymbol{T_b = T_m - 3}$. Interval time between interfaces is 2 ms.

IV.3.4.2. Quantitative analysis

Here, thermal conditions effect on dendritic features is quantitatively investigated. In the following part, the studied parameters are defined and discussed in terms of both the central supercooling degree and the macroscopic thermal gradient. Noting that case 1 is not involved in this analysis. In all figures, cases of the first series (1, 2, 3, 4 and 5 in Table IV-1) and the second series (6, 7, 4, 8, 9, 10 and 11 in Table IV-1) are represented, respectively, in bold and thin curves.

IV.3.4.2.1. Interface dynamics

The interface dynamics is studied by tracking top-side and bottom-side vertical tips movement. Each tip is characterized by its position and velocity. The position is the distance measured vertically between the tip point and the central horizontal axis. In case of tip-split (two tips), it does not matter which tip position is considered because of the left-right symmetry. Based on positions data, velocities are evaluated by a central differencing scheme of the distance:

$$\mathbb{V}_{tip}^{i} = \frac{d_{tip}^{i+1} - d_{tip}^{i-1}}{2.\Delta t} \qquad \text{(IV-27)}$$

where d is the position, and i refers to the time step.

Positions curves are represented, for all cases, in figure IV-39. Positive positions and negative positions, describe respectively, the top-side and bottom-side tips movement, the limits being the top (+60 µm) and the bottom (-60 µm) boundaries. As observed in this figure, both tips have the tendency to go far from the nucleation center. However, for most cases (except case 6 for which there is no vertical macroscopic thermal gradient), all the computational time, positive positions are larger than negative positions. Thus, top-side tips are more developed than the bottom-side ones. That is obviously due to the vertical macroscopic thermal gradient, for which the top region is more supercooled than the bottom one. In addition, when the macroscopic thermal gradient gets more important, the gap between positive and negative positions gets larger (see section IV.3.4.2.5. vertical asymmetry).

Velocities of top-side and bottom-side tips are represented versus time, respectively, in figures IV-40 and IV-41. For the top-region (figure IV-40), the velocity varies in the same manner in time: at first stages, just after the supercooling breakdown, it falls down rapidly (transient phase), then it gets more or less stable passing through a minimum value, and finally it increases significantly at advanced stages when the interface approaches top boundary through which the released heat is dissipated outside the domain. This final phase explains the sudden increase of positive positions before the interface reaches the top boundary (around 40 µm in most curves in figure IV-39). As the minimum values are far from the first transient phase and not influenced by boundary condition, they are considered as nominal velocities and analyzed later.

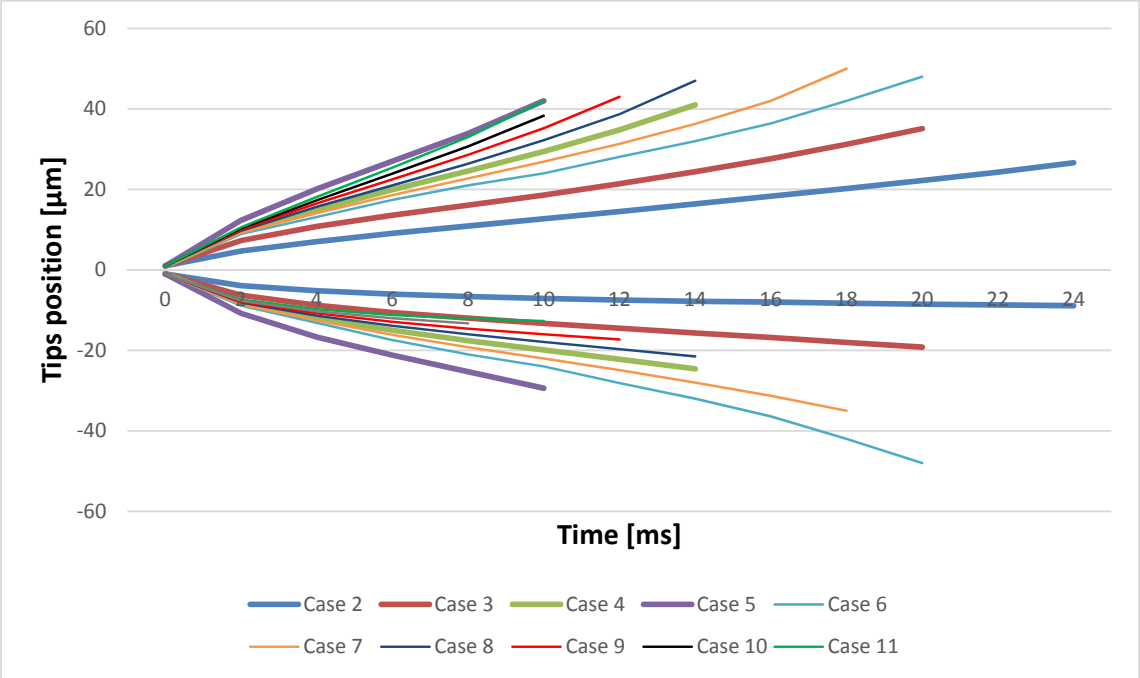

Figure IV-39: Tip-dendrites positions (µm) in function of time (ms). Positive positions for the top-region tips and negative positions for the bottom-region tips. Top and bottom limits are respectively 60 µm and -60 µm.

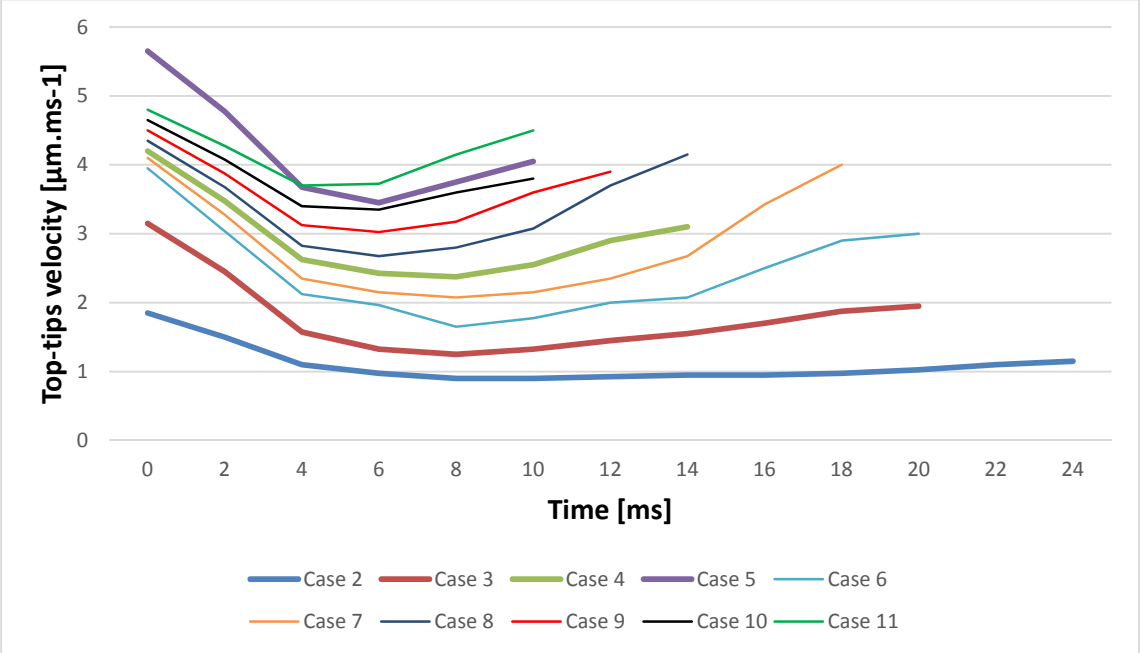

Figure IV-40: Top-region tips velocities (µm.ms^{-1}) in function of time (ms).

For the bottom-side (figure IV-41), the typical curve followed by top-side tips can be seen only for cases 6 and 7, for which the macroscopic gradient is quite small. However, for other cases, the interface is getting not able to increase its velocity at the final phase. That is due to the relatively high temperature imposed at the bottom boundary (with respect to T_m). It is worth noting here that, due to the supercooling lack

at advanced stages in some cases 2 and 11, the interface moves very slowly (velocity tends to zero).

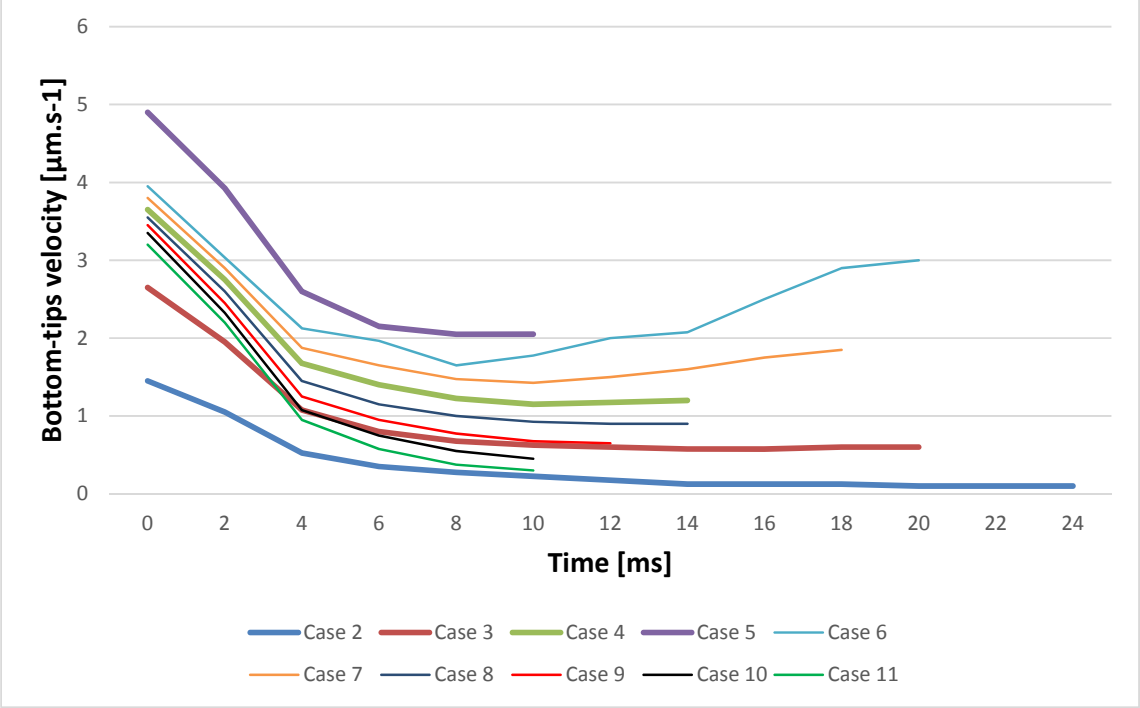

Figure IV-41: Bottom-region tips velocities (µm.ms^{-1}) in function of time (ms).

From eqt. IV-23, one can say that the dendritic rate depends only on the local thermal gradient at the interface. Velocity variation curves in both regions show that, neglecting the temperature variation in the solid phase, this gradient is the result of several parameters interaction. Although that these parameters include obviously the initial temperature field in liquid (determined by both macroscopic gradient and initial supercooling) and local interface temperature (which is calculated by the Gibbs-Thomson condition (eqt. IV-25) according mainly the curvature and anisotropic effects), it seems that there is a competition between interface dynamics and local latent heat transfer rate in liquid is always taking place. Indeed, when the interface propagates rapidly (with respect to the heat transfer rate), it moves to a new location where the associated latent heat is not sufficiently distributed yet. In the opposite situation, in which the interface is slower than the heat transfer rate, it moves to a new location which is preheated by the released latent heat, so that its propagation gets more constrained. This local continuous competition at the interface could be shown by two phenomena from the simulations.

The first one is the dendritic structure itself. Indeed, when anisotropic effects (at the same local supercooling) lead to a small protrusion at the interface along some privileged growth directions, this protrusion is quickly amplified and the growth of its surroundings is constrained. That is due, from one hand, to the dominating interface dynamics at the protrusion, which will be more and more acute, and on the other hand,

to the dominating transfer rate of the released latent heat at the surroundings. For case 11, for instance, figures IV-42, IV-43, and IV-44 represent the liquid temperature field at 0, 4, and 10 ms, respectively. In the top region, although that initial local gradient at the interface is almost homogeneous (figure IV-42), the interface shows, from early stages, two large arms growing faster than their surroundings (figure IV-43). That is due, at the beginning, to anisotropic effects which are then thermally amplified as the tips move to a new location with lower supercooling degree. Indeed, at 4 ms, figure IV-43 shows that the initial homogeneous gradient is broken in the top region so that tips can keep moving toward the supercooled region and their released latent heat constrain only their surroundings. The phenomenon is amplified as the interface grows, so that in figure IV-44 at 10 ms, the growth shows, on the one hand, a large cavity (top region) in which the temperature tends to the equilibrium temperature and the interface is completely stuck, and on the other hand, two tips, having sufficient local gradients making them still able to move forward.

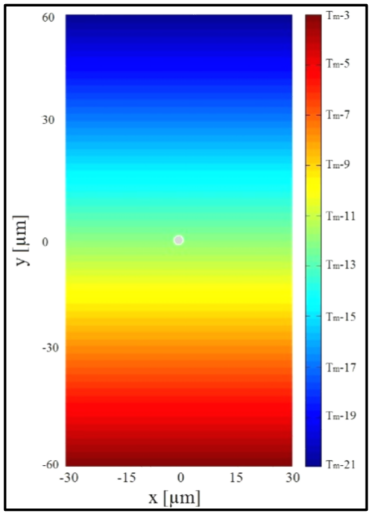

Figure IV-42: Temperature field of liquid phase (case 11) at the initial instant. The initial solid germ is situated at the domain center.

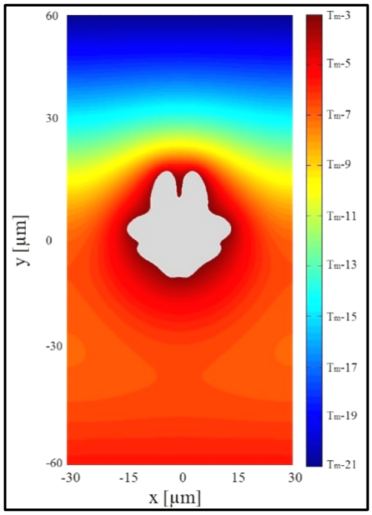

Figure IV-43: Temperature field of liquid phase (case 11) at 4 ms, with the involved solid-liquid interface.

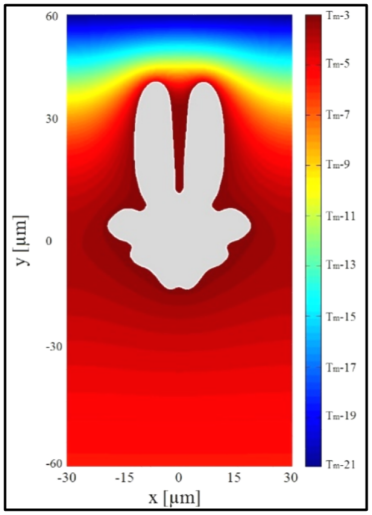

Figure IV-44: Temperature field of liquid phase (case 11) at 10 ms, with the involved solid-liquid interface.

The second phenomenon is the different dendrite-tip behavior in liquid regions with different supercooling degrees: in a sufficiently supercooled regions, the dendrite-tip propagation is rapid so that it cannot be constrained by the released latent heat associated to its movement, while in a liquid region having a relatively high temperature (near to the liquid-solid temperature), the dendrite-tip gets more and more affected and constrained by the released latent heat. In order to prove this, nominal velocities of cases in series 2, in both top (blue circular markers) and bottom (red circular markers) regions, are plotted in function of initial supercooling degree at the tip location (calculated at the instant of the nominal velocity for each case) in figure IV-45. One can realize that, first, the variation of dendritic rate has the same tendency of the Langer and

Muller-Krumbhaar theory [20], and second, that there are only two points involved in bottom-region (red markers) which do not follow the global tendency followed by the others in both regions. Indeed, these points have slightly lower velocities than those predicted by the global tendency. The points correspond to the bottom region in cases 9

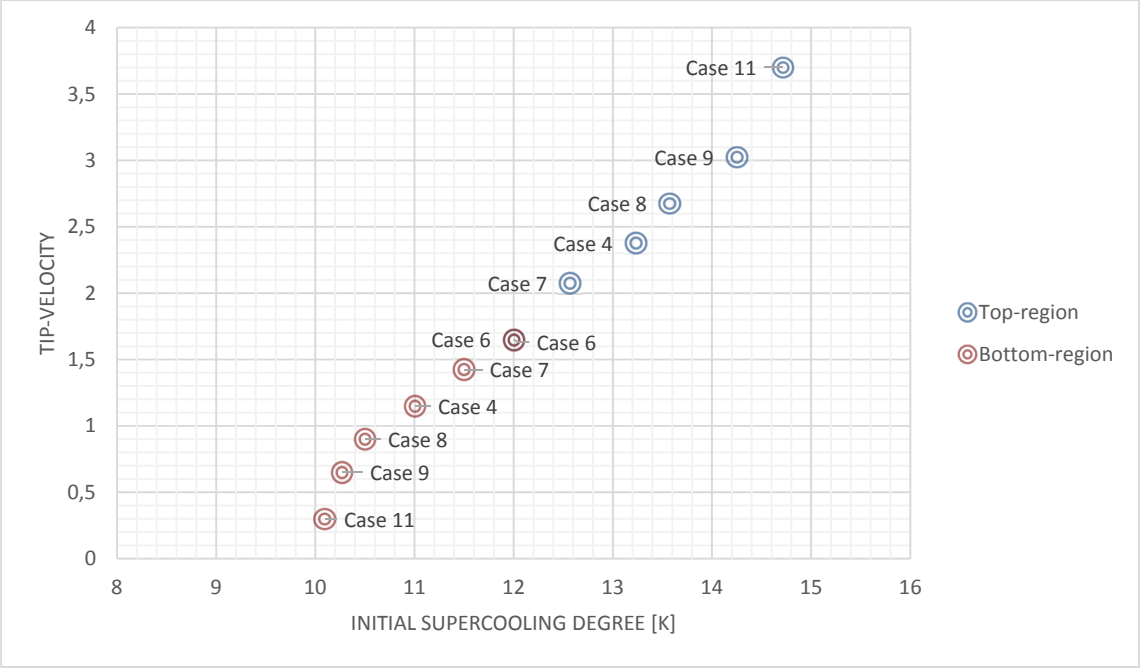

Figure IV-45: Nominal velocities at the dendrite-tip in both top (blue circular markers) and bottom-region (red circular markers) in function of the initial supercooling degree at the tip location.

and 11 for which the macroscopic gradient is relatively high, and the supercooling degrees at bottom boundaries are relatively low (Table IV-1). This means that the interface moves slowly in these regions and is, in contrast to other cases, affected and constrained by the associated released heat and then slower.

IV.3.4.2.2. Interface total length

Figure IV-46 represents the variation of the total length of the growing interface in time. It can be clearly observed that, many curves have almost the same variation of the total length in time but three are different (thin curves). The curves with the same slop have the same central supercooling degree (series 2: thin curves and curve of case 4), and the three others (series 1) have different central supercooling degree with the same imposed macroscopic gradient. This means that the variation of the interface length depends only on the central supercooling degree. Therefore, the dynamics of the interface creation is not affected by the macroscopic thermal gradient, but only by the central supercooling degree; larger slop is obtained with higher supercooling degree.

IV.3.4.2.3. Total solid surface

Figure IV-47 represents the variation of the total solid phase surface in time. Comparing the obtained curves and those in figure IV-46, one can realize that, for each

case, the total solid phase surface and the total length vary in time in the same manner. Indeed, the variation of solid phase surface is also only affected by the central supercooling degree; larger slop is obtained with higher supercooling degree.

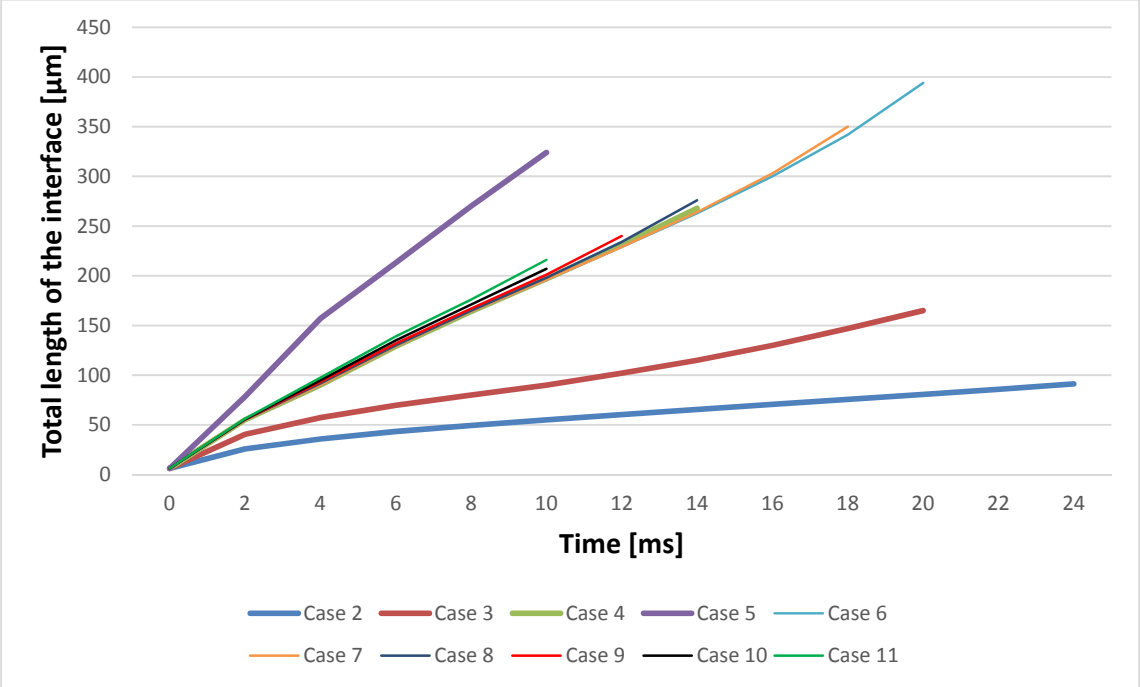

Figure IV-46: Variation of the total length of the interface (µm) in time (ms).

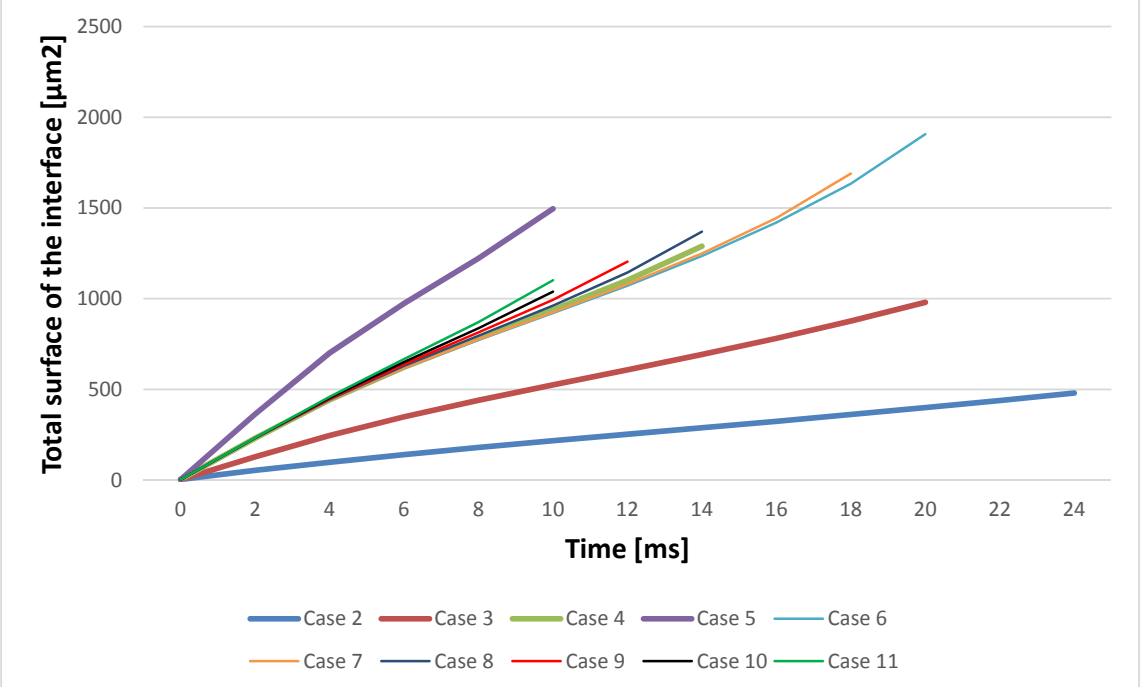

Figure IV-47: Variation of the total surface of the interface (μm^2) in time (ms).

In conclusion, when the supercooling degree is higher, the obtained growing interface is bigger (total length and total surface are larger). However, with a constant

central supercooling degree, in our simulations the growing interface has globally the same total length and total surface but with different geometries, depending on the imposed macroscopic thermal gradient. This means that, if the interface gets more developed in one direction (top-region), it gets less developed in the opposite one (bottom-region) in order to compensate length and surface gain. In the following sub-section, the ratio between the total length and total surface of the interface is investigated.

IV.3.4.2.4. Interface length and total solid surface ratio

In figure IV-48, the variation of the ratio of the interface length to the solid surface in function of time is represented. At the supercooling breakdown, the germ has an important tendency to increase its surface so that the ratio falls down rapidly. Then, for all cases (series 1 and 2), the ratio tends to a constant value around 0.2 (the average value). Therefore, the ratio length/surface does not depend either on the macroscopic gradient or on the central supercooling degree. However, this constant may depend on the geometrical and thermophysical conditions of the problem. In conclusion, the crystal reacts and evolves quickly, from first stages of computation, in order to reach a small constant value, regardless of the imposed thermal conditions. The different preliminary behavior of cases 2 and 3 (bold blue and red curves) may be explained by the absence of tip-splitting phenomenon on all directions.

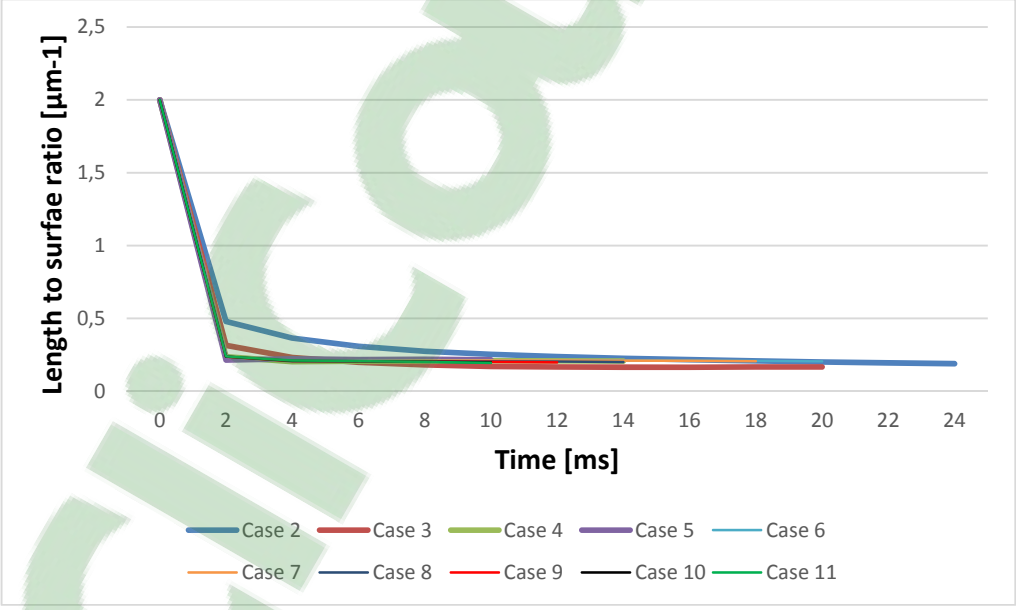

Figure IV-48: Variation of length to surface ratio (μm^{-1}) in time (ms).

IV.3.4.2.5. Vertical asymmetry

In this sub-section, the vertical asymmetry, which can be characterized by the absolute value of the ratio of the positive position to the negative one, is investigated in time (figure IV-49). For all cases, expect case 6, the asymmetry ratio decreases in time,

so that the top-side tips are faster than the bottom-side ones. That is due to the lower temperature imposed on the top boundary. In case 6, as the imposed temperatures on the top and bottom boundaries are equal, a symmetrical behavior is observed leading to a unity ratio for the whole computational time. However, for most of bold curves (cases in first series with a same macroscopic gradient), the asymmetry is almost constant. This means that the asymmetry is affected only by the macroscopic gradient and does not depend on the central supercooling degree. However, case 2 is the only case in first series that does not follow the same curve. That is due to the slower velocity in the bottom region tending to zero by lack of supercooling.

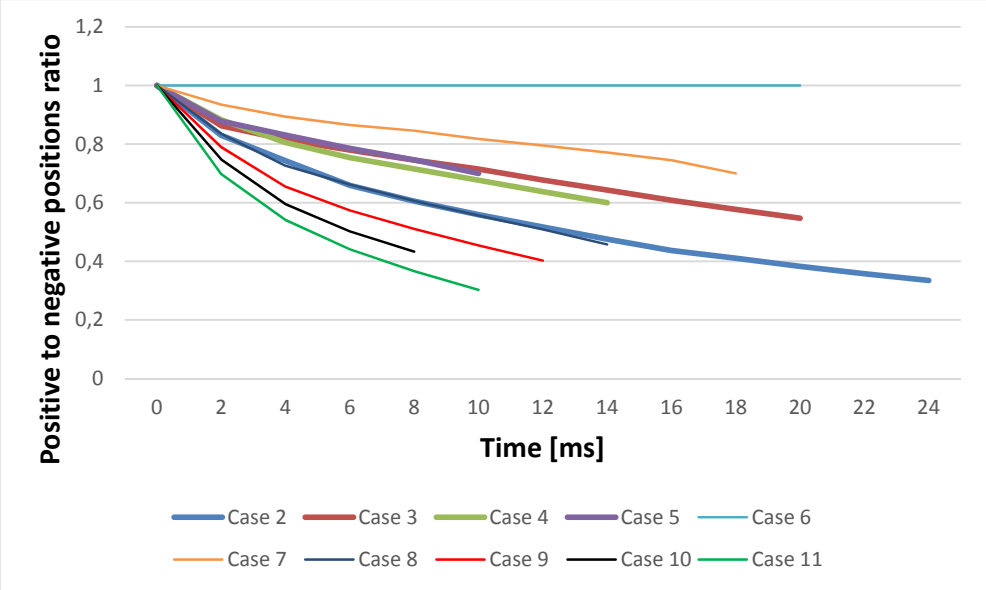

Figure IV-49: Variation of positive position to negative position ratio in time (ms).

IV.3.5. Conclusions

The effect of non-homogeneous temperature field in a supercooled liquid on dendritic growth of pure substances is numerically investigated. Neglecting the natural convection in the liquid phase, the mathematical model involves the heat diffusion equation to solve temperature fields in both phases. These fields are coupled with two boundary conditions at the solid-liquid interface: Gibbs-Thomson condition and the heat balance equation.

The numerical method is based on a two-dimensional front tracking approach. It is coupled by a finite volume formulation in which an explicit first-order Euler time integration is used. The numerical method [19] tracks the interface movement by a sequential set of marker points which evolves over a fixed Euler mesh representing the whole medium.

The behavior of dendritic growth is studied by imposing a small solid germ at the center of a rectangular domain, in which vertical macroscopic gradient is created by the imposed top and bottom boundaries temperatures. Right and left boundaries are assumed to be adiabatic. The effects of the macroscopic gradient and the initial central supercooling degree at the central horizontal axis are first qualitatively studied. On the one hand, the supercooling degree is found to affect not only the size of the interface but also its overall solid shape and the structure of branches. On the other hand, the macroscopic gradient leads to an asymmetrical dendritic growth; the higher the macroscopic gradient is, the more visible the asymmetrical of dendritic growth is.

Next, dendritic features are quantitatively investigated for different imposed temperatures on the top and the bottom domain boundaries. The obtained results indicate that dendritic velocities depend only on the local supercooling degree. It has been shown that there is a local competition between the interface dynamics and the transfer rate of the associated latent heat. When the interface grows rapidly (with respect to the heat transfer rate), it moves to a region in which the released latent heat is not sufficiently distributed yet, and then it keeps moving forward. In the opposed case, when the interface movement is slow, it moves to a region which is preheated by the associated latent heat, and then it gets constrained and slower.

It has been found that the variation of both total length of the interface and total solid phase surface is independent on the imposed macroscopic gradient, but only depends on the supercooling degree. Furthermore, the ratio of the total length and total surface tends in all simulations to the same constant which does not depend on either the supercooling degree or the macroscopic gradient.

References

[1] Ma, C.J. *A Preliminary Study on a Method for the Morphological and Quantitative Analyses of Individual Snow Crystals and Its Application for Field Measurement*. Asian Journal of Atmospheric Environment, 5(3): 196-203. (2011).

[2] Shuai, S., Guo, E., Zheng, Q., Wang, M., Jing, T. and Fu, Y. *Three-dimensional α-Mg dendritic morphology and branching structure transition in Mg-Zn alloys*. Materials Characterization. 118: 304-308. (2016).

[3] Karma A. *Dendritic Growth* in *Branching in Nature*: 365-402. Springer Berlin Heidelberg. (2001).

[4] Chen, S.L., Chen, C.L., Tin, C.C., Lee, T.S. and Ke, M.C. *An experimental investigation of cold storage in an encapsulated thermal storage tank*. Experimental Thermal and Fluid Science, 23(3): 133-144. (2000).

[5] Boettinger, W.J., Coriell, S.R., Greer, A.L., Karma, A., Kurz, W., Rappaz, M. and Trivedi, R. Solidification microstructures: recent developments, future directions. *Acta materialia*, *48*(1), pp.43-70. (2000).

[6] Gilpin R.R. *The effects of dendritic formation in water pipes.* International journal of heat and mass transfer. 20: 693-699. (1976).

[7] Tirmizi S.H., and Gill W.N. *Effect of natural convection on growth velocity and morphology of dendritic ice crystals.* Journal of crystal growth. 85: 488-502. (1978).

[8] Braga S.L., Milon J.J. *Visualization of dendritic ice growth in supercooled water inside cylindrical capsules*. International Journal of Heat and Mass Transfer, 55 (13): 3694-3703. (2012).

[9] Roosen A.R., and Taylor J.E. *Modeling crystal growth in a diffusion field using fully faceted interfaces.* Journal of computational physics. 114: 113-128. (1994).

[10] Shyy W., Udaykumar H.S., and Liang S.J. *An interface tracking method applied to morphological evolution during phase change.* International journal of heat and mass transfer. 36 (7): 1833-1844. (1993).

[11] Juric D., and Tryggvason G. *A front-tracking method for dendritic solidification.* Journal of computational physics. 123: 127-148. (1996).

[12] Kobayashi, R. *Modeling and numerical simulations of dendritic crystal growth*. Physica D: Nonlinear Phenomena. 63 (3): 410-423. (1993).

[13] Hu X., Li R., and Tang T. *A multi-mesh adaptive finite element approximation to phase field models*. Communications in Computational Physics. 5 (5): 1012-1029. (2009).

[14] Gibou F., Fedkiw R.P., Cheng L. T., and Kang M. *A second-order-accurate symmetric discretization of the Poisson equation on irregular domains*. Journal of Computational Physics. 176 (1): 205-227. (2002).

[15] Criscione A., Roisman I.V., Jakirlic S., and Tropea C. *Towards modeling of initial and final stages of supercooled water solidification.* International Journal of Thermal Sciences. 92: 150-161. (2015).

[16] Tacke K. and Harnisch A. *Finite difference enthalpy methods for dendritic growth.* Proceedings of the International Conference on Computational Modeling of Free and Moving Boundary Problems. (1991).

[17] Voller V.R. *An enthalpy method for modeling dendritic growth in a binary alloy*. International Journal of Heat and Mass Transfer. 51 (3): 823-834. (2008).

[18] Jaafar M.A., Rousse D.R., Gibout S., Bedecarrats J.P. *A review of dendritic growth during solidification: mathematical modeling and numerical simulations*. Renewable and Sustainable Energy Reviews. (Under Review).

[19] Jaafar M.A., Gibout S., Rousse D.R., Bedecarrats J.P. *Numerical study of dendritic growth using a double-mesh sharp-interface front tracking method*. Submitted in International Journal of Thermal Sciences.

[20] Langer J.S., Sekerka R.F., and Fujioka T. *Evidence for a universal law of dendritic growth rates*. Journal of Crystal Growth. 44: 414-418. (1978).

V. Conclusions et perspectives

L'objectif principal de ce doctorat était de modéliser et d'étudier la dynamique de la croissance dendritique des corps purs à la rupture de surfusion. Il a été fait dans le cadre d'une cotutelle internationale entre l'Université de Pau et des Pays de l'Adour (France) et l'École de Technologie Supérieure de Montréal (Canada). Le travail réalisé constitue la première étape d'un projet de recherche plus ambitieux. Les enjeux principaux sont d'étudier, expérimentalement et numériquement, les mécanismes physiques influençant l'évolution de l'interface liquide-solide lors de la croissance dendritique des Matériaux à Changement de Phase (MCP) afin d'optimiser le fonctionnement des procédés de stockage de l'énergie par chaleur latente. Bien que le doctorat comprenne deux aspects, numérique et expérimental, la majorité du travail s'est focalisée sur l'étude numérique et l'aspect expérimental s'est limité à la conception et au montage d'un banc d'essai par manque du temps.

Un banc d'essai expérimental a été monté, au Laboratoire de Thermique, Énergétique, et Procédés de l'Université de Pau et des Pays de l'Adour. Il permet de visualiser la phase dendritique lors de la cristallisation des MCP dans différentes conditions géométriques et thermiques. En effet, il est conçu de sorte que l'épaisseur de la couche liquide du MCP soit modifiable et que le gradient thermique au sein du liquide surfondu créé par le système de refroidissement soit contrôlé (voir Annexe A pour les détails).

Bien que la conception de ce dispositif ait permis l'identification des hypothèses sur lesquelles l'étude numérique est basée, aucun résultat expérimental significatif n'a été obtenu par manque de temps.

L'étude numérique sur laquelle ce doctorat s'est focalisé se base sur un code rédigé en interne en utilisant le langage C++ (programmation orientée objet). Ce code modélise l'évolution dynamique bidimensionnelle de l'interface liquide-solide lors de la cristallisation des corps purs en tenant compte de tous les effets thermodynamiques, géométriques et thermiques. Le modèle proposé traite les situations idéales de la croissance dendritique, dans lesquelles la variation de la masse volumique avec la température et au cours du changement de phase ainsi que la convection naturelle au sein du fluide sont négligées. La formulation mathématique se compose alors de l'équation de la conduction de la chaleur décrivant les champs de température dans les deux phases liquide et solide. Outre les conditions aux limites du domaine, ces champs doivent être couplés avec deux conditions à l'interface mobile : l'équation de Gibbs-Thomson avec laquelle la température à l'interface est calculée, et l'équation de la conservation de l'énergie traduisant les différents flux à l'interface.

La méthode numérique développée se base sur une approche de suivi explicite de l'interface (*front tracking approach*) à double maillage. Un maillage cartésien fixe « classique » est employé pour la résolution des équations de transfert thermique dans les zones liquide et solide, et un autre maillage mobile (ensemble des points discrets), complètement découplé du maillage cartésien, est employé pour situer l'interface. Ce

maillage est reconstruit d'une façon continue avec l'évolution de l'interface liquide-solide. Cette méthode est couplée, d'une part, avec une méthode de volumes finis d'ordre zéro, pour la discrétisation spatiale du système, et d'autre part, avec une méthode d'Euler explicite pour la résolution temporelle.

Dans un premier temps, la méthode numérique ainsi que les techniques numériques employées sont validées, d'une part, par le concept du rayon critique de la nucléation homogène, et d'autre part, par un cas de solidification circulaire stable, où les vitesses des points d'interface sont homogènes et l'interface reste stable et garde sa géométrie circulaire initiale. En plus, un bon accord avec la solution analytique de Carslaw and Jaeger (1959) pour des cas similaires a été trouvé. Deux modes différents d'anisotropie sont pris en compte pour modéliser les formes cristallines de symétries « *four-fold* » et « *six-fold* ». Les résultats obtenus sont similaires avec ceux présentés dans la littérature. Des études paramétriques classiques de la température initiale du liquide surfondu et de la tension superficielle sont proposées. La croissance dendritique est de plus en plus instable avec la diminution de la température initiale du liquide et la tension superficielle.

Dans un deuxième temps, l'effet d'un champ de température non-homogène au sein du liquide sur la croissance dendritique est étudié. Le gradient thermique macroscopique est imposé au niveau des deux frontières haute et basse alors que les frontières gauche et droite sont adiabatiques. Les résultats obtenus montrent une symétrie par rapport à l'axe central vertical et une dissymétrie par rapport à l'axe central horizontal. L'analyse de différents critères permet de conclure que les vitesses des têtes des branches ne sont liées qu'à la température locale (surfusion locale). Les résultats mettent ainsi en évidence un lien étroit entre la vitesse de propagation de l'interface et le transfert de chaleur local : lorsque la dendrite se propage rapidement (par rapport à la dynamique de propagation de la chaleur), elle se trouve dans une zone peu influencée par l'apport de chaleur, alors la dynamique de l'interface n'est pas freinée par la libération de l'énergie associée à son mouvement. Dans le cas opposé, où la vitesse de l'interface est plus lente, la dendrite se trouve dans une zone suffisamment réchauffée par l'énergie libérée et sa propagation est donc freinée. Ainsi, même si les effets d'anisotropie traduits par l'équation de Gibbs-Thomson ont une influence sur la morphologie de l'interface, il existe, dans certaines situations, une rétroaction thermique capable d'amplifier ces effets. On montre également que la variation de la longueur totale de l'interface et sa surface totale (surface de la phase solide) sont indépendantes du gradient macroscopique imposé par les conditions aux limites, mais seulement liées au degré de surfusion. De même le rapport de la longueur sur la surface tend vers une valeur asymptotique quasi-identique dans toutes nos simulations, et donc indépendante de la surfusion ou du gradient macroscopique imposé. Enfin, même si la surfusion a des effets sur la topologie des dendrites, il est montré que l'asymétrie d'une dendrite ne dépend que du gradient macroscopique thermique.

Plusieurs perspectives dans les prochaines étapes du projet peuvent faire suite aux travaux menés dans cette thèse.

Pour ce qui concerne le code numérique, une validation quantitative des résultats, allant au-delà des tendances, doit être faite pour des cas simples et stables. Ensuite, les changements topologiques plus précis ayant lieu au cours de la croissance dendritique doivent être modélisés, comme par exemple, le cas où deux interfaces se percutent. Enfin, une étape de la parallélisation, sur plusieurs processus ou plusieurs machines, du code numérique est requise afin d'obtenir des temps de calculs moins lents.

Des efforts doivent également être menés pour avancer le volet expérimental du projet. Les campagnes expérimentales ont plusieurs objectifs : (1) de valider le modèle et les hypothèses sur lesquelles le code numérique s'est basé, (2) de visualiser et d'étudier la croissance dendritique avec différents gradients thermiques.

Annexe A : Montage expérimental

Dispositif expérimental

L'objectif de l'étude expérimentale est d'étudier la création, la propagation, et le développement des dendrites croissant au sein d'un liquide surfondu en fonction des conditions thermiques imposées à ce liquide juste avant l'instant de la nucléation. Le dispositif et ses points forts sont décrits en détail dans cette annexe.

Un banc d'essai a donc été développé au laboratoire de thermique, énergétique, et procédés (LaTEP). Les figures (A-1) et (A-2) ci-dessous illustrent le dispositif expérimental et sa vue de face, respectivement. Il est constitué d'un tube cylindrique vertical (1) en plastique (PVC), de diamètre interne de 24 cm, et d'épaisseur de 0,5 cm, servant de support et accueillant l'ensemble des systèmes de mesure et de visualisation. À l'intérieur de ce tube deux disques de verre (2) sont placés horizontalement, entre lesquels le matériau à changement de phase (MCP) à étudier se trouve. L'épaisseur des deux disques est identique, et égale 10 mm. Cependant, le disque inférieur a un diamètre de 17 cm, plus grand que celui du disque supérieur qui est 15 cm. Le disque inférieur assure l'étanchéité avec le bas du tube, il empêche l'écoulement du liquide. Des modules Peltier (3) de même épaisseur (3,8 mm) sont posés sur le côté inférieur de ce disque, assurant ainsi le refroidissement du MCP. La géométrie et la puissance de ces modules Peltier peuvent être modifiées en fonction de l'objectif de l'expérience. Afin de permettre l'évacuation de la chaleur et donc d'assurer la performance du système de refroidissement, un dissipateur thermique à ailettes (4), de résistance thermique de 0,32 $K.W^{-1}$, est collé sur la face du bas des modules Peltier (voir figure (A-2)). Le disque supérieur est situé sur trois cales amovibles (5) reposant sur le disque inférieur. La dimension des cales détermine la distance séparant les deux disques et donc l'épaisseur du MCP utilisé. Cette épaisseur peut être alors également modifiée en fonction de l'objectif de l'expérience. Deux types de visualisation bidimensionnelle à l'aide d'une caméra sont envisagés : une visualisation par le dessus et une autre de côté. Un hublot (6) a été donc prévu dans le tube pour assurer la visualisation de côté correspondant à l'épaisseur du MCP entre les disques (voir les figures (A-1) et (A-2)).

Le matériau et l'épaisseur des deux disques constituaient une question principale. D'une part, il est indispensable que le disque supérieur soit transparent pour qu'il puisse permettre une visualisation de dessus en utilisant la caméra, située dans ce cas au-dessus de deux disques. Un disque en verre a donc été choisi. D'autre part, le matériau et l'épaisseur du disque inférieur sont des paramètres importants car l'efficacité et la performance du dispositif en dépendent. En effet, c'est par ce disque inférieur, séparant le MCP et le système de refroidissement (modules Peltier), que la chaleur peut être transférée. Pour cela, on a étudié, grâce au logiciel de dynamique des fluides (CFD) ANSYS Fluent, les échanges thermiques, entre le MCP en contact avec le côté supérieur de ce disque et les modules Peltier placés sur son côté inférieur, en fonction de sa conductivité thermique et son épaisseur. Les résultats indiquent qu'un disque en verre de 10 mm d'épaisseur répond aux attentes de notre étude expérimentale. En effet, il permet de conserver les gradients de température attendus sur sa face supérieure (en contact avec le MCP), imposés par les modules Peltier sur sa face inférieure.

La figure (A-1) indique deux paires d'orifices supérieures (7) et inférieures (8) dans le tube. Les orifices supérieurs servent à brancher le dispositif à une bouteille d'azote. Cette bouteille d'azote est utilisée pour remplir l'espace entre la caméra et les disques au début des expériences. Ceci permet d'éviter la présence d'air et la condensation de la vapeur d'eau sur le disque supérieur lors du refroidissement qui empêcherait la visualisation claire du phénomène de solidification. Les orifices inférieurs servent à remplir et à vider le MCP à tester au début et à la fin des expériences.

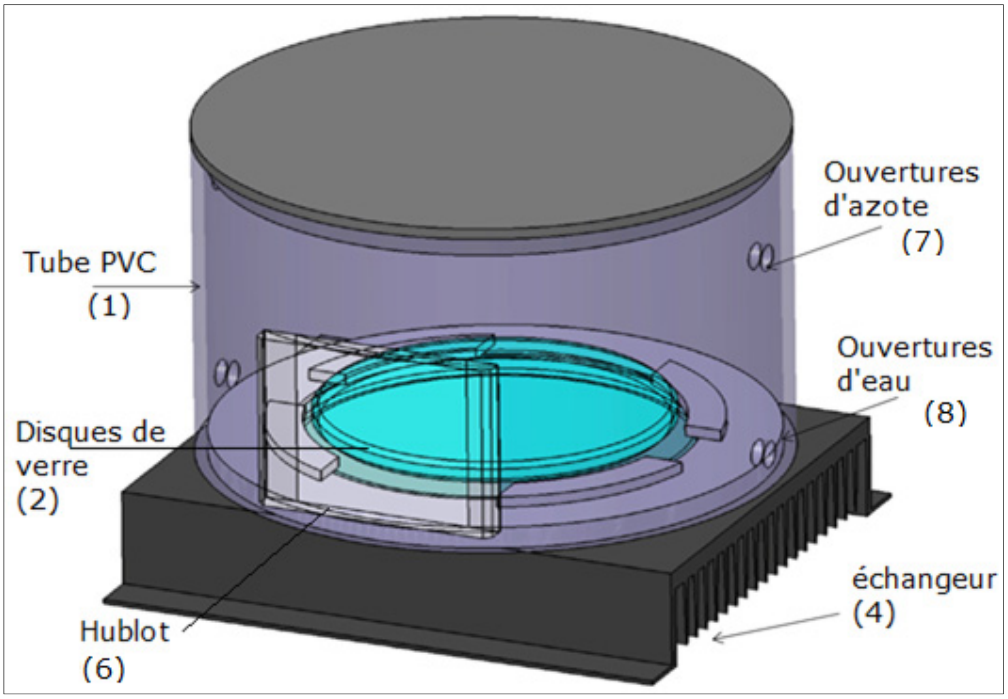

Enfin, pour mesurer l'évolution des températures, des thermocouples de type K de 0,2 mm de diamètre sont utilisés. Les thermocouples sont associés à une centrale de mesure de marque Fluke et de type Netdaq (précision de mesure de +/- 0,1 °C). Il faut noter qu'il faut être très précis lors du placement des thermocouples, pour qu'ils puissent mesurer la température du liquide à un endroit bien défini sans affecter la nucléation.

La hauteur des cales détermine l'épaisseur du MCP à étudier ; elle dépend, de l'objectif de l'expérience et du type de visualisation. Pour la visualisation de dessus, il faut éviter la propagation verticale des dendrites, difficile à observer dans ce cas. Cette propagation verticale peut être due à la convection naturelle créée par la différence de masse volumique au sein du MCP. Afin de pouvoir négliger ce phénomène, des petites cales très fines ont été prévues réduisant ainsi la couche de MCP entre les deux disques. Au contraire, pour la visualisation de côté, ces petites cales peuvent être remplacées par des cales de dimension plus grande pour laisser les dendrites libres de se propager verticalement. La possibilité d'utilisation des cales de dimensions variables qui assure la variété du type de propagation des dendrites constitue un point fort et original dans le

Figure A-1 : Schéma illustrant les éléments principaux du dispositif expérimental.

dispositif, parce qu'il permettra d'étudier expérimentalement et de valider les résultats numériques de plusieurs cas incluant ou négligeant l'effet du transfert thermique par convection naturelle sur la phase de la croissance dendritique en fonction de l'épaisseur

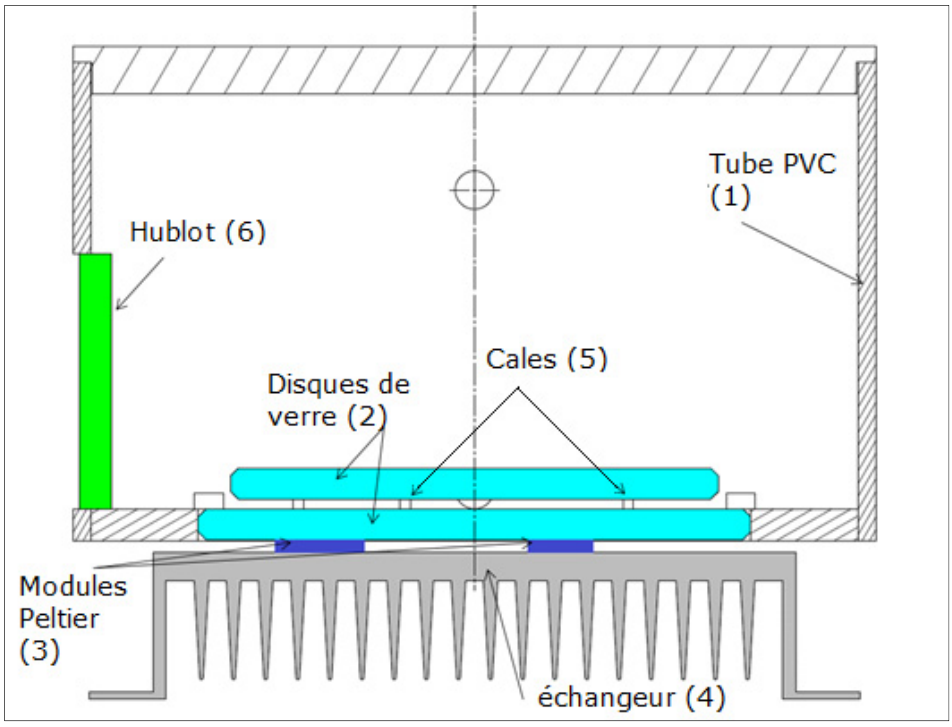

de l'échantillon à étudier.

Le deuxième point fort et original du dispositif est la variété de la géométrie et de la puissance des modules Peltier posés sur la face inférieure du disque en verre du bas assurant le refroidissement du MCP à étudier. En effet, le sens et la valeur du gradient de température sont respectivement contrôlés par la géométrie et la puissance (dimensions) des modules Peltier utilisés.

Dans la section suivante, une brève procédure expérimentale est proposée.

Procédure expérimentale

Toutes les procédures expérimentales à suivre pour visualiser la croissance dendritique dans un matériau surfondu sont semblables et peuvent être décrites de façon générale par les étapes suivantes :

- Mettre en place le système de refroidissement, la cellule contenant le MCP, et le système d'acquisition des températures.
- Refroidir le système jusqu'à la surfusion du liquide.
- La troisième étape peut être (1) d'attendre la nucléation spontanée du solide (nucléation homogène), ou bien (2) de perturber à l'instant souhaité le système pour la provoquer (nucléation hétérogène).
- Enfin, visualiser la propagation des dendrites.

Dans ce dispositif expérimental, il n'est pas facile d'introduire un germe solide ou de

Figure A-2 : Vue de face du dispositif.

perturber le liquide surfondu à un instant souhaité. Nous attendons donc, dans un premier temps, que la nucléation se fasse sans intervention extérieure. La procédure à suivre est alors la suivante :

- Choisir la géométrie et la puissance des modules Peltier selon le gradient de température souhaité.
- Choisir la dimension des cales selon l'objectif de l'expérience.
- Mettre la caméra en place en haut ou à côté du tube selon le type de visualisation prévue.
- Placer les modules Peltier, sur la face inférieure du disque inférieur, selon la géométrie définie.
- Remplir la cellule (entre les deux disques) de MCP à l'aide des orifices inférieurs et l'environnement d'azote à l'aide des orifices supérieurs.
- Refroidir le liquide en branchant les modules Peltier aux alimentations de table (générateurs électriques).
- Visualiser la phase de la croissance dendritique en notant principalement (1) la température de la nucléation, (2) la durée de la phase de la croissance dendritique, et (3) la direction de propagation des dendrites.

- Analyser les résultats en fonction du gradient de température initial et le profil de température instantané.

Pour une bonne compréhension de la phase dendritique cette procédure expérimentale sera lancée pour différents gradients de températures (contrôlés par la géométrie des modules Peltier), en incluant ou en négligeant l'effet de convection naturelle (selon l'épaisseur des cales, séparant les deux disques). De plus, pour obtenir des résultats pertinents, tenant compte du caractère stochastique des ruptures de surfusion (mentionné à la section II.1), la procédure sera répétée plusieurs fois pour les mêmes conditions. Un système d'acquisition est utilisé pour recevoir et traiter les résultats obtenus. Ce dernier est connecté à la caméra et à un ordinateur. Bien évidemment, un travail conséquent sera réalisé sur le traitement des images obtenues lors des visualisations.

État actuel du dispositif expérimental

La figure A-3 ci-dessous présente une photo du banc d'essai montrant le hublot et quelques cales situées à l'intérieur.

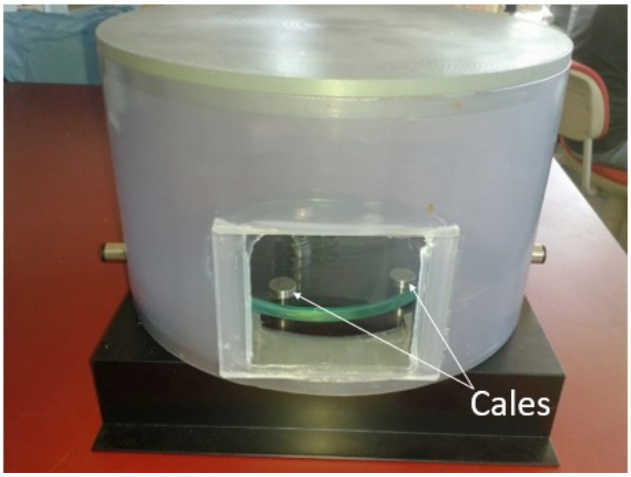

Figure A-3: Photo du banc d'essai (vue de côté).

Annexe B : Résultats numériques préliminaires

Cette annexe présente les résultats préliminaires du cas le plus simple où l'interface liquide-solide n'est pas considérée : conduction thermique sans et avec source de chaleur en régime transitoire. Ces essais numériques constituaient la base primaire du programme, dans laquelle l'interface mobile de solidification sera ensuite introduite.

Dans ce cas, le maillage reste régulier tout au long la période de calculs. Le bilan d'énergie peut être obtenu en ajoutant un terme de source à la somme des flux conductifs :

$$\rho.c.(\Delta x.\Delta y.\varepsilon).\left.\frac{dT_{m,n}}{dt}\right|_i = \emptyset_H^i + \emptyset_B^i + \emptyset_D^i + \emptyset_G^i + (\Delta x.\Delta y.\varepsilon).S_v \qquad \text{(B-1)}$$

Où S_v est la densité volumique de la source, exprimée en [W/m^3].

Les flux correspondant peuvent être approximés par les expressions suivantes :

- $\emptyset_G^i = k.\varepsilon.\Delta y.\frac{T_{m-1,n}^i - T_{m,n}^i}{\Delta x}$;
- $\emptyset_D^i = k.\varepsilon.\Delta y.\frac{T_{m+1,n}^i - T_{m,n}^i}{\Delta x}$;
- $\emptyset_H^i = k.\varepsilon.\Delta x.\frac{T_{m,n+1}^i - T_{m,n}^i}{\Delta y}$;
- $\emptyset_B^i = k.\varepsilon.\Delta x.\frac{T_{m,n-1}^i - T_{m,n}^i}{\Delta y}$;

En appliquant l'approximation d'Euler explicite pour la discrétisation temporelle, on obtient :

$$\rho.c.(\Delta x.\Delta y.\varepsilon).\left(\frac{T_{m,n}^{i+1}-T_{m,n}^{i}}{\Delta t}\right) = \emptyset_H^i + \emptyset_B^i + \emptyset_D^i + \emptyset_G^i + (\Delta x.\Delta y.\varepsilon).S_v \qquad \text{(B-2)}$$

En remplaçant les expressions approximatives des flux dans l'équation (B-2), on peut obtenir explicitement la distribution de la température à l'itération (*i+1*) par l'équation suivante :

$$T_{m,n}^{i+1} = T_{m,n}^{i} + \frac{\Delta t}{\rho.c.(\Delta x.\Delta y.\varepsilon)} \times \left(\sum \emptyset^i\right) + \frac{\Delta t}{\rho.c}.S_v \qquad \text{(B-3)}$$

En se basant sur l'équation (B-3), un code de conduction 2D programmé en langage C++ a été développé. Le code général permet de résoudre différents cas des conditions aux limites du problème de conduction avec ou sans source homogène.

Le code de base contient quatre fonctions principales :

- *load_parameters* : cette première fonction sert à charger les données d'un fichier externe.
- *create_tables* : Elle crée les matrices dynamiques contenant les valeurs de température du système.
- *calculs* : Dans cette fonction, la résolution du champ de température est exécutée. Elle contient trois boucles. La première boucle concerne les itérations du temps. La deuxième et la troisième concernent les discrétisations spatiales.
- *save_results* : Cette dernière fonction, sert à enregistrer l'évolution des résultats ainsi que les résultats à l'itération finale.

Ce code permet le choix des conditions aux limites pour chaque face limitant le domaine ; une face adiabatique ou température imposée. On discute ci-dessous d'une façon brève, les résultats finaux tirés de ce code pour les cas de conduction simples suivants:

1- Le premier cas n'inclut pas de source de chaleur. Les faces gauche et droite sont supposées adiabatiques ; une température non-nulle est imposée sur la face de haut (T=1) ; une température nulle est imposée sur la face de bas (T=0).

La figure (B-1) illustre les résultats obtenus pour ce cas très simple. Elle valide le code en montrant une solution linéaire après une période suffisante pour atteindre le régime stationnaire. Avec deux faces adiabatiques, la solution devient indépendante de la longueur donc unidimensionnelle. Ce faisant, une comparaison avec la solution analytique classique est facilitée.

Plusieurs tests sur la taille du maillage ont été effectués. Avec un résolveur explicite, il faut respecter le critère de convergence, assurant un pas de temps suffisamment petit, suivant :

$$\frac{\alpha.\Delta t}{(\Delta x)^2} \leq 0{,}25$$

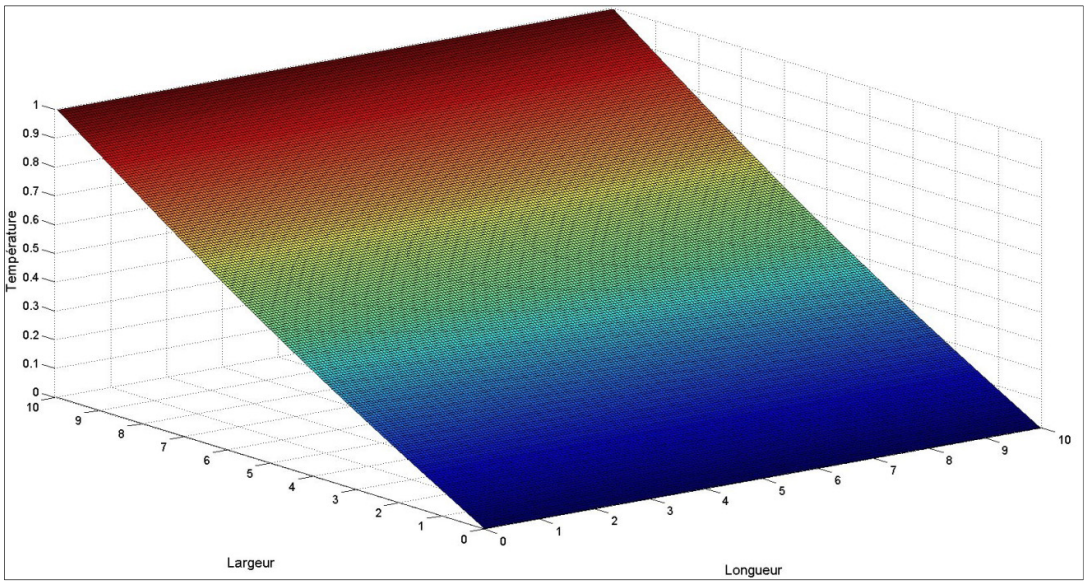

Figure B-1 : Résultats numériques de la conduction 2D du domaine cartésien sans source. Faces gauche et droite sont adiabatiques. Face haute : (T=1). Face bas : (T=0). M=N=200.

2- Dans le second cas, les conditions aux limites sont les mêmes que dans le cas 1. Cependant, il inclut une source de chaleur homogène également distribuée.

La figure (B-2) illustre les résultats obtenus pour le deuxième cas ; elle montre l'effet de la source homogène. Encore ici, ces résultats valident la correcte implantation de la formulation mathématique incluant le terme source.

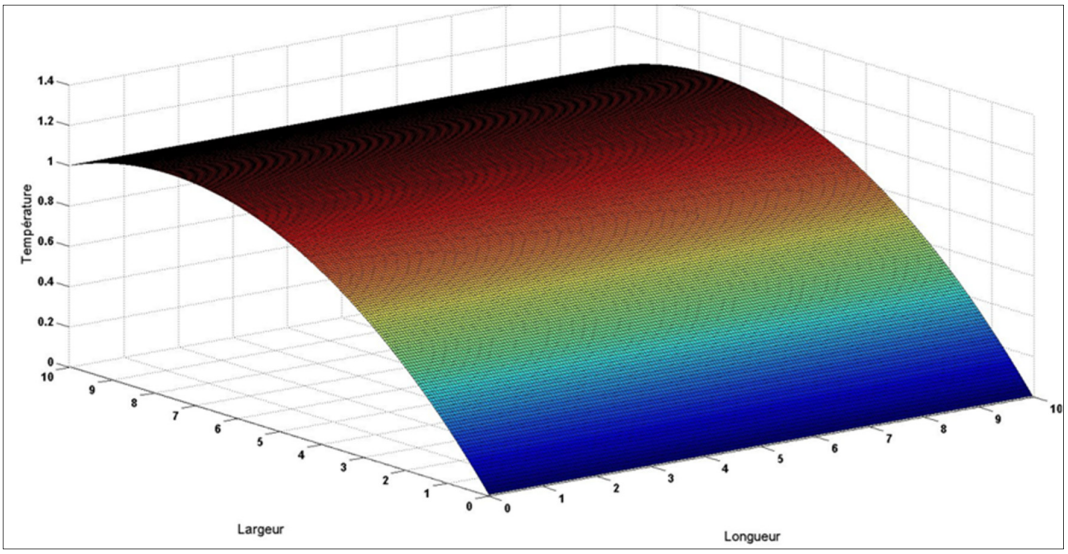

Figure B-2 : Résultats numériques de la conduction 2D du domaine cartésien avec source (S_v=10 W.m^{-3}). Faces gauche et droite sont adiabatiques. Face haute : (T=1). Face bas : (T=0). M=N=200.

3- Ce troisième cas présente une solution non-linéaire : la source de chaleur est supposée nulle ; une température non-nulle est imposée sur la face de haut (T=1) ; et une température nulle est imposée les faces gauche, droite, et bas (T=0).

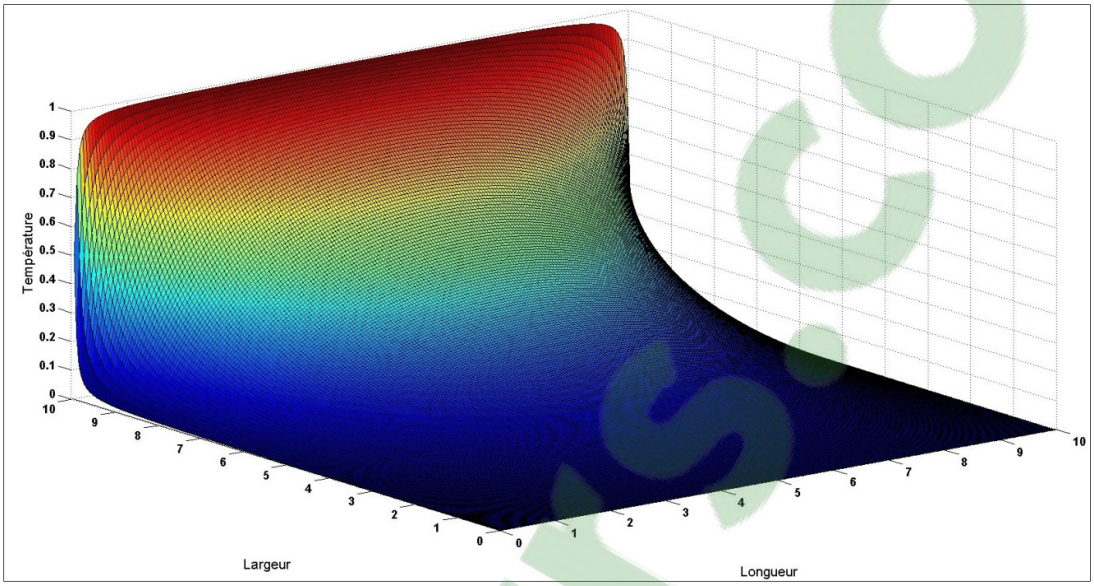

Figure B-3 : Résultats numériques de la conduction 2D du domaine cartésien sans source. Faces gauche, droite et bas : Température imposée T=0 ; Face haut (T=1). M=N=200.

La figure (B-3) présente la solution de ce cas : elle n'est pas linéaire. Ce problème est un problème classique de la littérature sur le transfert thermique en deux dimensions. Il fut résolu de manière analytique par Fourier et est inclus les livres de transferts thermiques depuis 1959 (Carslaw, H.S., et Jaeger, J.C., 1959). La solution numérique issue du code proposé a été validée en calculant, pour chaque nœud du maillage, l'erreur entre la solution numérique correspondante et celle que l'on trouve dans la littérature.

La figure (B-4) présente la variation de la valeur moyenne de l'erreur en fonction de la taille du maillage (M=N) : une décroissance de l'erreur numérique avec le raffinement du maillage.

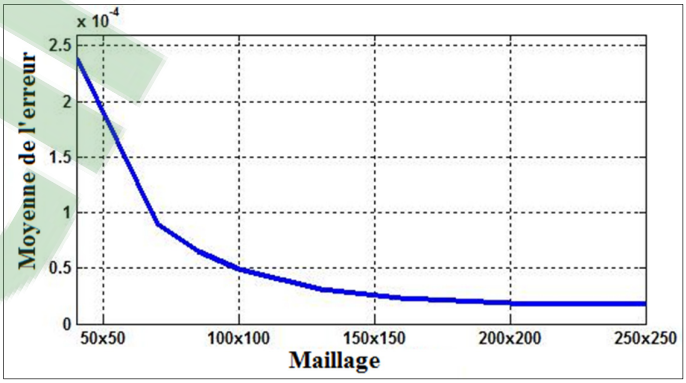

Figure B-4 : Variation de la valeur moyenne de l'erreur numérique en fonction de la taille du maillage (M=N).

L’évolution de la température dans ce troisième cas est présentée sur la figure (B-5). On choisit pour cela, un maillage moins fin (M=N=30).

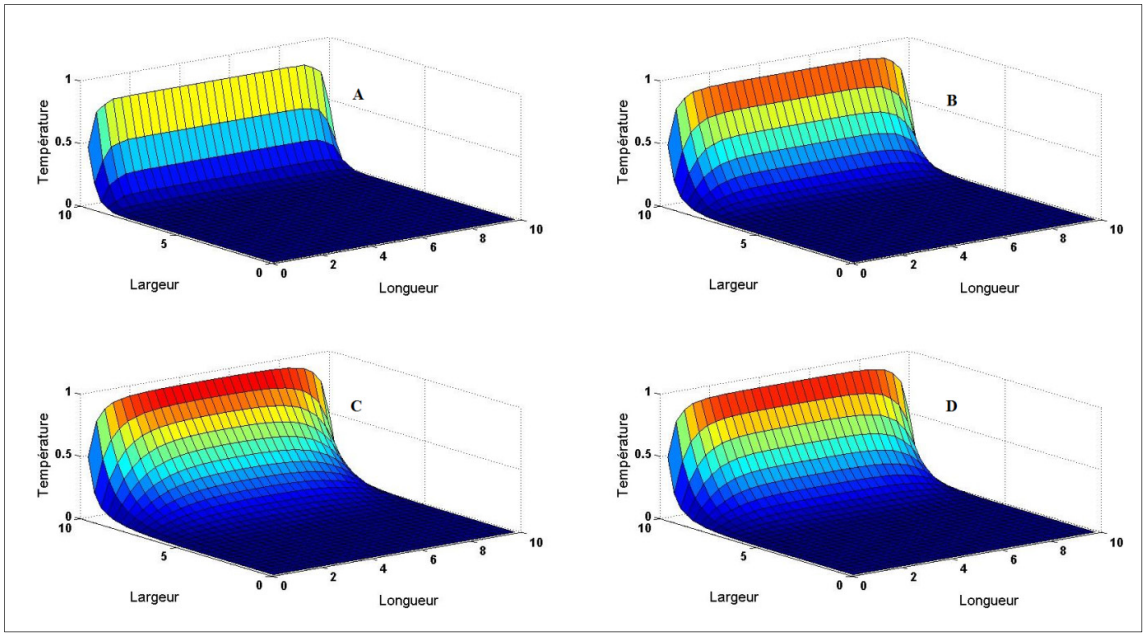

Figure B-5 : Evolution des résultats numériques de la conduction 2D du domaine cartésien sans source. Face gauche et droite sont adiabatiques. Face haute : (T=1). Face bas : (T=0). M=N=30.

Références bibliographiques

Abraham, F.F. (1968). A reexamination of homogeneous nucleation theory. Thermodynamics aspects. Journal of the Atmospheric Sciences, 25: 47-53.

Aguerd, M. (1984). Contribution à l'étude de la nucléation spontanée et induite des phases aqueuses dispersées. Thèse de doctorat, Pau.

Akyurt, M., Zaki, G., Habeebullah, B. (2001). Freezing phenomena in ice-water systems. Energy conversion and Management. 43: 1773-1789.

Babin, L. (1966). Contribution à l'étude de la surfusion des solutions salines aqueuses. Thèse de doctorat, Bordeaux.

Bales, C., Gantenbein, P., Jaenig, D., Kerskes, H., Van Essen, M. Weber, R. (2008). Chemical and sorption storage: The over view, B7-Task 32.

Becker, R., Doring, W. (1935). Kinetische Behandlung der Keimbildung in ubersattigen Dampfen. Annalen der Physik, 24 : 719-752.

Bédécarrats, J.P. (1993). Etude des transformations des matériaux à changements de phases encapsulés destinés au stockage du froid. Thèse de doctorat, Pau.

Benmansour, A., Hamdan, M.A. (2001). Simulation du Stockage de l'Energie Thermique dans un Lit Fixe de Sphères Contenant un Matériau à Changement de Phase. Rev. Energ. Ren. Vol. 4: 125-134

Bigg, E.K. (1953). The supercooling of water. Proceedings of the Physical Society. Lond. Ser. B66: 688-694.

Binsbergen, F.L. (1973). Heterogeneous nucleation in the crystallization of polyolefins. III – Theory and mechanism, Journal of polymer Science, 11: 117-135.

Braga, S.L., Milon Guzman, J.J., Pacheco, H.G.J. (2008). A study of cooling rate of the supercooled water inside of cylindrical capsules. International journal of Refrigeration, 32: 953-959.

Braga S.L., Milon, J.J. (2012). Visualization of dendritic ice growth in supercooled water inside cylindrical capsules. International Journal of Heat and Mass Transfer, 55: 3694-3703.

Broto, F. (1979). Etude de la cristallisation monotherme de l'eau et de l'eau lourde surfondues à l'état dispersé. Thèse de doctorat, Pau.

Cai, Y., Zong, X., Zhang, J., Du, J., Dong, Z., Wei, Q., Zhao, Y., Chen, Q., Fong, H. (2014). The Improvement of Thermal Stability and Conductivity via Incorporation of Carbon Nanofibers into Electrospun Ultrafine Composite Fibers of Lauric Acid/Polyamide 6 Phase Change Materials for Thermal Energy Storage. International Journal of Green Energy, 11 (8): 861-875.

Carslaw, H.S., Jaeger, J.C. Conduction of Heat in Solids. Oxford University Press. London. 1959.

Carte, A.E. (1956). The freezing of water droplets. Proceedgins of the Physical Society. Lond. Ser. B69: 1028-1037.

Chen, S.L., Wang, P.P., Lee, T.S. (1998). An experimental investigation of nucleation probability of supercooled water inside cylindrical capsules. Experimental Thermal and Fluid Science, 18 : 299-306.

Chen, S.L., Chen, C.L. (1999). Effect of nucleation agents on the freezing probability of supercooled water inside capsules. HVAC & Research, Vol. 5, No. 4.

Chen, S.L., Lee, T.S. (1997). A study of supercooling phenomenon and freezing probability of water inside horizontal cylinders. International Journal of Heat and Mass Transfer, Vol. 41: 769-783.

Chikama, H., Shibata, H., Emi, T., Suzuki, M. (1996). "In-situ" Real Time Observation of Planar to Cellular and Cellular to Dendritic Transition of Crystals Growing in Fe–C Alloy Melts. Materials Transactions, JIM 37.4: 620-626.

Clausse, D., Dumas, J.P., Meijerp, H.E., Broto, F. (1987). Effects of thermal treatment on nucleation phenomena: experiences and model. Journal of dispersion Science and Technology, 8.

Clausse, D., Dumas, J.P., Broto, F. (June 1985). Effects of thermal treatment on nucleation phenomena: experiences and model. In 5Th Conference on colloids and Interface Science, volume 8: 1-28, Postdam, USA.

Clausse, D. (1983). Contribution à l'étude de la surfusion et de la sursaturation des solutions aqueuses de chlorure d'ammonium. Thèse de doctorat, Pau.

Combes, B. (1982). Etude de changements de phases d'hydrates salins macroscopiques et dispersés. Application au stockage thermique basse température. Thèse de doctorat de 3eme cycle, Pau.

Debenedetti, P. (1996). Metastable liquides, Concepts and Principles. Princeton Academics Press.

Defray, R., Prigogine, I. (1951). Tension superficielle et adsorption. Dunod, Paris.

Dufour, L., Defay, R. (1963). Thermodynamics of clouds. Academic Press.

Dumas, J.P. (1976). Etude de la rupture de métastabilité et du polymorphisme des corps organiques. Thèse de doctorat, Pau.

Dumas J.P. (2002). Stockage du froid par chaleur latent. Techniques de l'ingénieur, traité Génie énergétique.

Dutil Y., Rousse D.R., Ben Salah N., Lassue S., Zalewski L. (2011). A review on phase-change materials: Mathematical modeling and simulations. Renewable and Sustainable Energy Reviews, Vol. 15: 112-130.

Fahrenheit, D.G. (1724). Experimenta & observationes de congelatione aquæ in vacuo factæ. Philosophical Transactions 33: 78-84.

Faucheux, M., Muller, G., Havet, M., LeBail, A. (2006). Influence of surface roughness on the supercooling degree: Case of selected water/ethanol solutions frozen on aluminum surfaces. International Journal of Refrigeration, 29: 1218-1224.

Fernandez, Al., Martinez, M., Segarra, M., Martorell, I., Cabeza, LF. (2010). Selection of materials with potential in sensible thermal energy storage. Solar energy Materials and Solar Cells, 94: 1723-1729.

Fletcher, N. H. (1987). The chemical physics of ice (Cambridge Univ. Press, Cambridge) Chap. 4.

Font, J., Muntassell, J., Navarro, J., Tamarit, J., LLoveras, J. (1986). Transitions solide-solide pour le stockage d'énergie. Journée de Calorimétrie, d'Analyse Thermique (et de thermodynamique chimique), J.C.A.T. FERRARE, Vol. 1 : 314-317.

Gibbs, J.W. (1948). Collected works, Vol. I, Thermodynamics, Yale University Press, New Haven.

Gibout, S. (2001). Méthodes inverses de calcul appliquées à l'étude des transferts thermiques lors de la cristallisation de liquides dispersés surfondus. Thèse de doctorat, Pau.

Gilpin, R. R. (1976). The effects of dendritic ice formation in water pipes. International Journal of Heat Mass Transfer. 20: 693-699.

Gilpin, R. R. (1977). The effect of cooling rate on the formation of dendritic ice in a pipe with no main flow. Journal of Heat Transfer. 99: 419-424.

Glicksman, M. E. (2011). Mechanism of dendritic branching. Metallurgical and Materials Transactions A, 43(2): 391-404.

Gonda, T., Nakahara, H. (1995). Formation of side branches of dendritic ice crystals grown from vapor. Journal of Crystal Growth. 160: 162-166.

Heneghan, A.F., Wilson, P.W., Haymet, A.D.J. (2002). Heterogeneous nucleation of supercooled water, and the effect of an added catalyst.

Huang, S.C. and Glicksman, M.E. (1981). Fundamentals of dendritic solidification – (i). Steady-state tip growth; (ii). Development of sidebranch structure. Acta Metall. 29: 701-734.

Istria, S., Castaing-Lasvignottes, J., Neveu, P. (1996). Energetic analysis, application field and performance of a new thermpchemical sorption cycle: the mulisalt system. Applied Thermal Engineerign, 16: 875-889.

Jia, L., Peng, L., Chen, Y., Mo, S., Li, X. (2014). Improving the supercooling degree of titanium dioxide nanofluids with sodium dodecylsulfate. Applied Energy. Vol. 124 : 248-255.

Khalifa, A., Tan, L., Date, A., Akbarzadeh, A. (2014). A numerical and experimental study of solidification around axially finned heat pipes for high temperature latent heat thermal energy storage units. Applied thermal Engineering. Vol. 70: 609–619.

Koo, K-K., Ananth, R., Gill, W.N. (1991). Tip splitting in dendritic growth of ice crystals. Physical Review A. 44: 3782-3790.

Kordesch, K. (1980). Electrochemical Energy Storage. In Energy Storage: 8-34. Editor Silverman, J. British Library Cataloguing in Publication Data. University of Maryland, USA.

Lafrague, C. (1952). Limites en stabilité de l'eau surfondue étudiées en vue d'application à la physique des nuages. Thèse de doctorat, Paris.

Lemercier, M. (1975). Contribution à l'étude de la surfusion de l'étain. Thèse de doctorat de 3éme cycle, Pau.

Lere-Porte, M. (1970). Contribution à l'étude de surfusion de l'eau lourde. Thèse de doctorat, Pau.

Li, X., Chen, Y., Huang, H., Mai, Y.W. and Zhou, L. (2016). Electrospun Carbon-based Nanostructured Electrodes for Advanced Energy Storage-A Review. Energy Storage Materials.

Milon Guzman, J.J., Braga, S.L. (2005). Supercooling water in cylindrical capsules. International Journal of Thermophysics, Vol. 26, No. 6.

Molinero, V. (2013). What determines the homogeneous freezing temperature of water?. Nucleation and atmospheric Aerosols. AIP Conf. Proc. 1527, 83-88.

Monge, P. (1968). Contribution à l'étude de la surfusion du mercure. Thèse de doctorat, Bordeaux.

Mugnier, D., Goetz, V. (2001) Energy storage comparison of sorption systems for cooling and refrigeration. In solar Energy, 71: 47-55.

Mullin, J.W. (2001). Crystallization. British library cataloguing in publication data. ISBN 0 7506 4833 3.

Okawa, S., Saito, A., minami, R. (2000). The solidification phenomenon of the supercooled water containing solid particles. International Journal of Regrigeration 24: 108-117.

Ouchi, K. (1954). Freezing mechanism of supercooled water. Science Rep. Tohuku University, Ser. 5, Geophys., 6, 43.

Paksoy, H.O. (2007). Thermal Energy Storage for Sustainable Energy Consumption. Fundamentals, Case Studies and Design. Published by Springer. Cukurova University, Adana, Turkey.

Perepezko, J.H., Rasmussen, D.H. (1979). Solidification of highly undercooled liquid metals and alloys. Proc. 17th Aerospace Sci. Meet., New Orleans.

Pruppacher, H.R. (1973). Electrofreezing of supercooled water. National Science Foundation under grant No. GA-32814. Vol. 104 : 623-634.

Ribeiro, J. (2007). Contribution à l'étude thermique et dynamique de la cristallisation de l'eau surfondue. Thèse de doctorat, Pau.

Rocha, O. L., Siqueira, C. A., Garcia, A. (2003). Cellular/dendritic transition during unsteady-state unidirectional solidification of Sn–Pb alloys. Materials Science and Engineering. A, 347(1): 59-69.

Saito, A., Utaka, Y., Okawa, S. (1989). Fundamental research on the supercooling phenomenon on heat transfer surfaces – investigation of an effect of characteristics of surface and cooling rate on a freezing temperature of supercooled water. Int. J. Heat Mass Transfer, Vol. 33: 1697-1709.

Saito, A., Okawa, S. (1994). Fundamental research on initiation of freezing of supercooled water on heat transfer surface. Proc. of 10th Int. Heat Transf. Conf. 1994; 4 [7-FM-22]: 121-126.

Schulz, G. (1948). Der EinfluB von Fremdkorpern auf die Unterkuhlungs-fahigkeit des Wassers. Meteorol. Rundschau. Meteorol Rundschau. 1 : 237.

Sifrini, I. (1983). Phénomènes de cristallisation dans des solutions salines aqueuses à l'état dispersé et sous formes de gouttes (ø ≈ 1 mm). Thèse de doctorat, Pau.

Soares N., Costa J.J., Gaspar A.R., Santos P. (2013). Review of passive PCM latent heat thermal energy storage systems buildings' energy efficiency. Energy and Buildings. Vol. 59: 82-103.

Stan, C.A., Schneider, G.F., Shevkoplyas, S.S., Hashimoto, M., Ibanescu, M., Wiley, B.J., Whitesides, G.M. (2009). A microfluidic apparatus for the study of ice nucleation in supercooled water drops. The Royal Society of Chemistry.

Stys, Z.S. (1980). Mechanical Energy Storage. In Energy Storage: 60-80. Editor Silverman, J. British Library Cataloguing in Publication Data. University of Maryland, USA.

Tang, X., Li, W., Zhang, X., Shi, H. (2014). Fabrication and characterization of microencapsulated phase change material with low supercooling for thermal energy storage. Energy. Vol. 68: 160-166.

Tirmizi, S. H., Gill, W. N. (1978). Effect of natural convection on growth velocity and morphology of dendritic ice crystals. Journal of crystal growth. 85: 488-502.

Turnbull, D., Vonnegut, B. (1952). Nucleation catalysis. Ind. Eng. Chem. 44: 1292-1298.

Vail, G., Stansbury, R.J. (1966). Time dependent characteristics of the heterogeneous Nucleation of Ice. Can. Journal Physics, 44: 477-502.

Viskanta, R., Bathelt, A.G., Hale, N.W.Jr (1983). Latent heat-of-fusion energy storage: experiments on heat transfer during solid-liquid phase change. Alternative energy sources III, Vol. 1: 279-304.

Volmer, H., Weber, A. (1925). Z. Physik. Chem.: 277-301.

Volmer, M. (1939). Kinetic der Phasenbildung, Steinkopff, Leipzig.

Vonnegut, B., (1947). Nucleation of ice formation by Silver Iodide. Journal applied Physics, 18: 593-595.

Wall, E. (1942). Material zur Frage der Eiskeimbildung in der Atmosphare. Meteorol. Z. 59:109.

Weickman, H.K. (1942). Experimentelle Untersuchungen zur Bildung von Eis und Wasser an Keimen bei tiefen Temperaturen und ihre Folgerungen bezuglich des Wachstums der atmospharischen Eiskristalle. Zentral wiss. Berichtswesen Forschungsber: 1730.

Weickman, H.K. (1951). A theory of the formation of ice crystals. Arch. Met. Geoph. Biokl. A. Bd. IV, Zentralanstalt-Festschrift. 21: 309-323.

Wolk, J., Wyslouzil, B.E., Strey, R. (2013). Homogeneous nucleation of water: from vapor to supercooled droplets to ice. Nucleation and Atmospheric Aerosols, AIP Conf. Proc. 1527, 55-62.

Xans, P. (1970). Contribution à l'étude de la surfusion et de la sursaturation de solutions salines aqueuses. Thèse de doctorat, Pau.

Xans, P., Barnaud, G. (1975). Etude des conditions de rupture spontanée des états de surfusion de l'eau et de l'eau lourde en volume de 5 mm3 et de quelques µm3 en fonction de la pression (P<1100 bars). C.R. Acad. Sci. Paris, b, 280, 25.

Xans, P., Saint-Guirons, H., Dumas, J.P. (1979). Etude par A.T.D. sous haute pression et basse température des changements d'états de corps dispersés. 7eme conférence int. AIRADT sur les hautes pressions, LE GREUSOT.

Yoon, J.I., Moon, C.G, Kim, E., Son, Y.S., Kim, J.D., Kato, T. (2000). Experimental study on freezing of water with supercooled region in a horizontal cylinder. Applied Thermal Engineering 21: 657-668.

Yot, P.G., Vanduyfhuys, L., Alvarez, E., Rodriguez, J., Itié, J.P., Fabry, P., Guillou, N., Devic, T., Beurroies, I., Llewellyn, P.L. and Van Speybroeck, V (2016). Mechanical energy storage performance of an aluminum fumarate metal–organic framework. Chemical Science, 7(1): 446-450.

Zanganeh, G., Commeerford, M., Haselbacher, A., Pedretti, A., Steinfeld, A. (2014). Stabilization of the outflow temperature of a packed-bed thermal energy storage by combining rocks with phase change materials. Applied thermal Engineering. Vol. 70: 316–320.

Zhao, J.M. and Zhang, Z.M., 2015. Electromagnetic energy storage and power dissipation in nanostructures. Journal of Quantitative Spectroscopy and Radiative Transfer, 151: 49-57.